DOCTORAL THESIS

Affective state and emotion inducing imagery classification for brain-computer interfaces

Author
Bigirimana, Alain Desire

AFFECTIVE STATE AND EMOTION INDUCING IMAGERY CLASSIFICATION FOR BRAIN-COMPUTER INTERFACES

Alain Desire Bigirimana, BSc, MSc

Faculty of Computing, Engineering and the Built Environment

Ulster University

This dissertation is submitted for the degree of Doctor of Philosophy

July 2020

Dedicated to my dear parents, little brothers and sisters, aunts, and uncles who always have offered me encouragement and support in all my endeavours

DECLARATION

This dissertation is the result of my own work and includes nothing, which is the outcome of work done in collaboration except where specifically indicated in the text. It has not been previously submitted, in part or whole, to any university of institution for any degree, diploma, or other qualification.

Signed: _____

Date: _____

Alain Desire Bigirimana, BSc, MSc

Ulster University

ABSTRACT

The ongoing effort in brain-computer interface (BCI) research has established that factors such as fatigue level, spatial ability, and affective state (i.e., emotions, moods, and stress responses) among others influence the BCI performance. Furthermore, while there has been significant progress in BCI deployment, studies indicate that a non-negligible proportion of users are unable to intentionally modulate their brain signal to control a motor imagery based BCI. The research presented in this thesis aims to augment BCI with affective state. There is a growing body of literature for affective state classification using brain signals. Identifying the user's affective state should enable calibration of the BCI system for optimal performance. The research in this thesis investigates a novel BCI control strategy, emotion-inducing imagery (EII) which involves imagining fictional or recalling mnemonic emotional events. The research in this thesis was carried out through offline dataset analysis and a series of online experiments which resulted in five main contributions paving the way for BCI augmentation with affective state.

In the **first contribution**, the research in thesis proposes a hybrid method of independent components analysis (ICA) and wavelet transform for the pre-processing of electroencephalogram (EEG) and magnetoencephalogram (MEG) data for affective state classification and demonstrates that this method enhances affective state classification. For the **second contribution**, the research introduces EII as a potential alternative BCI control strategy and presents evidence that EIIs are associated with distinct neural correlates. For the **third contribution**, the work in this thesis resulted in evidence that MI outperforms EII for the majority of the participants, however, the research also presented evidence that some users can consistently achieve higher performance with EII than with MI demonstrating that EII might be a viable alternative imagery for some users. In the **fourth contribution**, the research showed that different EEG rhythms during the period prior to using BCI and the classification accuracies across participants during EII-BCI or MI-BCI use are significantly correlated. Finally, for the **fifth contribution**, the research established that a signal processing framework combining neural-time-series-prediction-pre-processing (NTSPP), filter bank common spatial patterns (FBCSP), and hemispheric asymmetry (ASYM) leads to higher performance than the individual framework in terms of classification accuracy.

ACKNOWLEDGEMENTS

I would like to acknowledge Dr Nazmul Siddique and Prof Damien Coyle for their unparalleled guidance and research skill development opportunities they provided me at Ulster University. I would like to acknowledge my selfless wife Paulette for her endless support. I am grateful for the kindness of the staff and students at the Intelligent Systems Research Centre. I would like to acknowledge people who participated in my research experiments.

TABLE OF CONTENTS

LIST OF FIGURES

LIST OF TABLES

LIST OF APPENDICES

LIST OF ABBREVIATIONS AND ACRONYMS

AI:	Artificial Intelligence
ALS:	Amyotrophic lateral sclerosis
ANN:	Artificial neural network
AUC:	Area under curve
BCI:	Brain-computer interface
Bits/min:	Bits per minute
CA:	Classification accuracy
CAR:	Common average reference
CNS:	Central Nervous System
CPU:	Central processing unit
CSP:	Common spatial pattern
CT:	Classification time
DAC:	Digital-to-analogue conversion
DAQ:	Data acquisition
DC:	Direct current
DEAP:	Database for Emotion Analysis Using Physiological Signals
DFNN:	Dynamic Fuzzy Neural Network
ECoG:	Electrocorticogram
EEG:	Electroencephalogram
EMG:	Electromyogram
EOG:	Electrooculogram
EPSP:	Excitatory post synaptic potential
ERD:	Event-related desynchronisation
ERP:	Event-related potential
ERS:	Event-related synchronisation

FBCSP:	Filter bank common spatial pattern
FFT:	Fast Fourier transform
FIR:	Finite impulse response
FP:	False positive
GA:	Genetic algorithm
GUI:	General User interface
HMM:	Hidden Markov model
ICA:	Independent component analysis
iEEG:	Intracranial EEG
IPSP:	Inhibitory post synaptic potential
ITR:	Information transfer rate
k-NN:	k-nearest neighbour
LDA:	Linear discriminant analysis
MEG:	Magnetoencephalogram
MEMD:	Multivariate empirical mode decomposition
MI:	Mutual information
MLP:	Multilayer perceptron
MSE:	Mean squared error
NN:	Neural network
NTSPP:	Neural time-series prediction pre-processing
PCA:	Principle component analysis
PNS:	Peripheral Nervous System
PSD:	Power spectral density
QDA:	Quadratic discriminant analysis
R&D:	Research and development
RMSE:	Root mean squared error
ROC:	Receiver operator curve

SNR:	Signal-to-noise ratio
SOFNN:	Self-organising fuzzy neural network
SSVEP:	Steady-state visual evoked potential
STFT:	Short time Fourier transform
SVM:	Support vector machine
t-f:	Time-frequency
TSD:	Time-varying signed distance
VEP:	Visual evoked potential

CHAPTER 1

1 INTRODUCTION

1.1 Introduction

In the past 2 decades significant evidence has been presented to demonstrate that people can operate brain-computer interface (BCI) systems. BCI applications include neurogaming (Ahn et al., 2014) (Coyle et al., 2016) (Beveridge et al., 2019), neuromuscular rehabilitation (Bundy et al., 2017) (Biasiucci et al., 2018) (Rathee et al., 2019) and assistive technologies (Stawicki et al., 2016), (Abiyev et al., 2016) (Tang et al., 2018) (Vidaurre et al., 2016) (Tariq et al., 2018) among many others. BCI offers an alternative communication channel as opposed to traditional neuromuscular or hormonal paths of signalling from the central nervous system (CNS). In traditional communication channels, based on current understanding, CNS (which comprises the brain and spinal cord) processes sensory information from outside environment or within the body conveyed by the peripheral nervous system (PNS) and produces responses appropriate to the needs of the body, a response delivered to the appropriate body part/organs by the peripheral nervous system (PNS). CNS electrophysiological signalling refers to observed phenomena (e.g., neuronal action potentials, synaptic potentials, neurotransmitter releases, and neuronal oxygen consumption) when processing sensory information. The electrophysiological signals can be measured in a variety of ways including electroencephalogram (EEG) and magnetoencephalogram (MEG). In a BCI system, the measured brain activity is translated into an artificial output (Wolpaw and Winter Wolpaw, 2012).

The BCI may offer an alternative means of communication to people and people with physically disabilities such as those suffering from severe head trauma, cerebral palsy (CP), and Amyotrophic Lateral Sclerosis (ALS). The CP is defined as "*a group of permanent disorders of the development of movement and posture, causing activity limitations that are attributed to non-progressive disturbances that occurred in the developing foetal or infant brain*" (Armstrong, 2007). CP prevalence ranges from 1.49 to 4 per 1000 live births (Cans, 2007) (Reid et al., 2016). In most of the cases, additional problems accompany the CP motor disorders, like epilepsy, further musculoskeletal problems, and disturbances of sensation, perception, cognition, behaviours, and communication. ALS is a neurons disorder where neurons are unable to activate the muscle (Kiernan et al., 2011). The late stage of ALS may lead to complete paralysis and 'locked-in-syndrome' where the brain is functioning but the patient has no way to communicate due to complete paralysis. ALS patients can be given a

way to communicate without movement using real-time BCI as in (Speier et al., 2017). Apart from being used as an alternative means of communication, real-time BCI setup can be used in the rehabilitation program of patients suffering from neuromuscular disorders, as in (Wolpaw et al., 2000) (Fetz, 2007) (Blankertz et al., 2007) (Prasad et al., 2010) (Zhu et al., 2010) (Bundy et al., 2017) (Biasiucci et al., 2018) (Rathee et al., 2019).

The popular BCIs offering an alternative communication channel include sensorimotor (SMR)-based BCIs and evoked-potential based BCIs. In sensorimotor-based BCI, also known as motor imagery-based BCI, the user imagines moving his/her limbs, and the brain activity at the motor processing area of the brain is translated into communication content by the use of signal processing algorithms and appropriate feedback. For the evoked-potential-based BCI, instead of the user actively imagining limbs' movements, he/she is presented with visual/auditory stimuli or somatosensory signalling and the brain activity at brain's areas processing the visual stimuli (areas of occipital and parietal cortex), auditory stimuli (areas of temporal cortex) or activity at the somatosensory cortex for somatosensory signalling is translated into communication content. Studies have shown that users can communicate using a P-300 speller BCI (Donchin et al., 2000) (Krusienski et al., 2008) (Guger et al., 2009) (Speller, 2015) (Nguyen et al., 2018) (Cao et al., 2019), or select different commands in evoked-potential-based BCI games (Marshall et al., 2013) (Chumerin et al., 2013) (Marshall et al., 2015b) (Beveridge et al., 2019).

Whilst SMR- and ERP-based BCIs have been deployed and show significant promise, there are still many shortcomings and issues to be resolved to ensure robust communication. The BCI users and people developing signal processing frameworks to accurately translate brain signals into control signal face some challenges. Most of these challenges arise from the non-stationarity and low signal to noise ratio of electrophysiological signalling, and the limitations and variations in BCI users' capacity to intentionally modulate and learn to voluntarily control these signals. Modulating sensorimotor rhythms by motor imagery to achieve reasonable control accuracy (i.e., 70% for binary communication task (Vidaurre and Blankertz, 2010)) poses a challenge for over 30% of BCI users (Blankertz et al., 2010) (Ahn et al., 2013b). For this reason, it is important to explore other mental tasks or user states that may offer alternative strategies for BCI users and enable BCI developers to know how to adapt the translation algorithms for particular user states. This thesis focuses on exploring new tasks for BCI users.

The research of this thesis investigates non-invasively recorded brain activity (EEG and MEG) associated with emotions for BCI augmentation. Brain activity associated with emotions is studied in two ways: passive emotion monitoring and active emotion monitoring. In passive emotion monitoring, the user/participant passively attends to emotional stimuli, and associated brain activity is classified into various emotional states. On the other hand, in the active emotion monitoring, the user/participant actively self-induces emotion. Researchers have reported that different emotions are associated with different brain processes (Davidson et al., 1990) (Davidson, 1992) (Canli, 1999) (Dalgleish, 2004) (Kroupi et al., 2011) (Hamann, 2012) (Reznik and Allen, 2018), and this difference observed in brain processes can be exploited in classifying brain activity for different emotions induced by emotion-charged stimuli, as in (Petrantonakis and Hadjileontiadis, 2010) (Petrantonakis and Hadjileontiadis, 2012) (Liu et al., 2018a).Furthermore, some studies (Chanel et al., 2009) (Makeig et al., 2011) (Sitaram et al., 2011) (Iacoviello et al., 2015) have shown that it is possible to achieve classification accuracy greater than 70% in binary classification of self-induced emotions.

Building on this, the research in this thesis investigates emotion-inducing imagery as a novel control approach for BCI. The remainder of this chapter provides further rationale for this direction of research, describes the aims and objectives of the research, the hypothesis tested and overall structure of the thesis

1.2 Rationale

Even though BCI is useful for people with very limited or no means of communication, e.g., people with locked-in syndrome, there are limited control strategy options available to BCI users. In addition, some BCI strategies, e.g., motor imagery, are challenging for some users and require training (Blankertz et al., 2010) (Ahn et al., 2013b), and other strategies (evoked potentials) often require gaze control and are dependent on external stimuli. Furthermore, a non-negligible portion of users are unable to learn to control a motor imagery (MI)-based BCI (Blankertz et al., 2010) (Ahn et al., 2013b) within a limited duration of training, thus there is a necessity to investigate alternative imagery strategies for such users.

Different alternative imagery strategies that have been used to control BCIs include emotion inducing imagery (EII) (Makeig et al., 2011) (Chanel et al., 2009) (Iacoviello et al., 2015) (Sitaram et al., 2011), mental singing (Stangl et al., 2013), mental arithmetic (Power et al., 2011), mental rotation, word association, auditory imagery, mental subtraction, and spatial navigation (Friedrich et al., 2012). In some cases, alternative imagery strategies outperformed motor imagery, e.g., Curran and

colleagues reported easier to carry out and higher classification performance with spatial navigation and auditory imagery compared to motor imagery (Curran et al., 2004). In the work reported in this thesis, the viability of EII as a potential BCI control strategy is investigated. The EII strategy has potential because the associated tasks can be constructed from the user's natural experience, and this is likely to make it easier for the BCI users to adopt these tasks. In addition, electrophysiological correlates of emotion are well studied and there is good knowledge of the spectral and spatial patterns of brain activity associated with emotions

In additional to investigating alternative imagery strategies, there is a need for further investigation of factors for BCI performance. The researchers have been investigating influential factors for the BCI performance including the user's emotional state, mood, motivation, and fatigue level. In an ongoing effort to identify optimal conditions or users' profiles associated with good performance of BCI, some studies report that people with the learned ability to intentionally alter brain states, e.g., people who practice meditation, generally perform well with BCI (Eskandari and Erfanian, 2008) (Tan et al., 2014a) (Liang and Shastri, 2018) (Tan et al., 2019), and people with spatial abilities generally perform well with mental imagery based BCI (Jeunet et al., 2015). Within this framework of investigating optimal condition for good BCI performance, the relationship of brain state pre-BCI use period and the performance of EII- and MI-based BCI across several recording sessions is analysed in this thesis. As the brain state during pre-BCI use is likely to be associated with a particular affective state, affective state recognition is needed so that the relationship between affective state during Pre-BCI use and BCI performance could be established. Furthermore, the work in this thesis, contribute to the affective state recognition framework by assessing the effect of different pre-processing methods on the emotions' classification performance.

1.3 Aims and Objectives

There are many factors that influence BCI performance, and these factors mainly fall under these categories: the user's mental state, user's ability to modulate brain activity, paradigm setup, and the signal processing methods adopted. Contributing to the ongoing effort to identify the optimal conditions for BCIs development in the BCI research community, the work in this thesis aims to augment BCI by developing a better understanding of how accurately emotional states and emotion related imagery can be classified . The objectives leading to this aim include looking at passive emotion monitoring and active emotion monitoring.

- **Passive emotion monitoring**: the user's emotional state is changed by some external stimuli but not intentionally by the user. Identifying the emotional state of the user is part of

determining the user's mental state, the factor affecting the BCI performance. The establishment of the user's emotional state should allow to identify the relationship between emotional state and the BCI performance. There are several studies on brain activity-based emotion classification, (as reviewed in the chapter 2), thus the first of objective of the thesis is as follows:

- ***Objective 1***: The quality of the signals used in a BCI is important, but it can challenging and time consuming to properly clean these signals. The first objective is to assess how automated independent component analysis based pre-processing method affects the classification of EEG data associated with different emotions. The associated work is reported in chapter 3.

- **Active emotion monitoring**: The user's emotional state is intentionally changed. If the user can intentionally produce brain activity associated with some emotions, this can be exploited as a mean of BCI communication. To the best of the author's knowledge, there are not more than 5 studies involving active emotion monitoring (Chanel et al., 2009) (Sitaram et al., 2011) (Makeig et al., 2011) (Iacoviello et al., 2015), and all of these studies are one session-based studies. This thesis's work carries out active emotion monitoring studies with the following objectives:
  - ***Objective 2***: assess the difference in the brain signals associated with different emotion-inducing imagery tasks. The associated work is reported in chapter 4.
  - ***Objective 3***: identify the best BCI framework for emotion-inducing imagery. The associated work is reported in chapter 5.
  - ***Objective 4***: comparison of emotion-inducing imagery performance to motor imagery performance. The associated work is reported in chapter 4 and chapter 5.
  - ***Objective 5***: identify the relationship between brain state prior to BCI use and the performance of emotion-inducing imagery. The associated work is reported in chapter 5.

1.4 Thesis' Outline

The following section present an outline of the thesis:

- ***Chapter 1*** introduces the thesis and the rationale for the research proposed. The aims and objectives of the thesis as well as the outline of the thesis are also presented.

- ***Chapter 2*** presents a literature review of brain-computer interface (BCI) systems development and brain activity-based emotion classification. Different stages of BCI development including data acquisition, pre-processing, features extractions and selection, features classification, and post-processing are outlined. Different brain activity dynamics exploited in BCIs are outlined. The chapter 2 also reviews the trend for data acquisition modalities used in the last two decades' brain activity-based studies of emotions. The current feature extraction and classification methods for emotion classification studies are outlined. Besides the data acquisition trends, different features extraction methods used in emotion classification studies are outlined.

- ***Chapter 3*** presents an assessment of different methods for removing artefacts from EEG data. Four methods are presented and evaluated: band-pass filtering, manual independent component analysis (ICA), artefact detection based on joint spatial and temporal characteristics (ADJUST), and the automated hybrid ICA-wavelet transform method (ICA-W). ICA is statistical based method which consists of separating the brain activity recorded on scalp into contributing source signals, referred to as components. When removing the artefacts from EEG with ICA, the components representing the artefacts should be removed and then the remaining components are recombined into cleaned EEG. In manual ICA, the artefactual components are identified by visual inspection which is time consuming and requires a high level of expertise. In ADJUST, the artefactual components are automatically identified by using some statistical measures. Due to a limitation in the number of components produced by ICA, the source separation is not optimal, because removing artefactual components removes some residual neural activity contained in those components. In ICA-W, wavelet-based decomposition is used to identify the artefactual portion of the component and remove only that portion instead of the entire component. EEG signals from a database for emotion analysis using physiological signals (DEAP) (Koelstra et al., 2012) are used to assess how these artefacts removal methods affect the classification accuracy of emotion classes in the dataset. The DEAP dataset was recorded in a passive emotion monitoring paradigm using emotional video clips.

- ***Chapter 4*** presents emotion-inducing imagery (EII) as a novel potential alternative BCI control strategy for motor imagery (MI). During EII, which is an active emotion monitoring, the participant is asked to recall happy and events or imagine happy and sad events. The data recording followed the standard motor imagery paradigm, and the features extraction method was based common spatial patterns (CSP). Two studies are presented; one looks at the

classification performance of EII using EEG and MEEG data, and it also looks at the difference in the brain activity for happy and sad imageries across the participants. The second study establishes preliminary comparison between classification performance of EII and performance of MI. Each participant participated in a calibration run and an online feedback run. A linear discriminant analysis (LDA) classifier is trained on CSP-based features from calibration runs and applied on the online run to drive the feedback. EII performance is not significantly different from MI performance in this preliminary comparison study.

- ***Chapter 5*** presents a comprehensive comparison between the performance of emotion-inducing imagery (EII) and performance of motor imagery as BCI control strategies. EII and MI are compared in multiple EEG data recording sessions, and each session contains a calibration run and feedback run for both EII and MI. EII and MI are compared across different signal-processing frameworks: neural-time-series-prediction-pre-processing (NTSPP), filter bank common spatial patterns (FBCSP), hemispheric asymmetry (ASYM), combination of NTSPP and FBCSP, and combination of all the three (NTSPP, FBCSP, and ASYM). The relationship between brain state prior to engaging in the feedback run and the performance for the feedback run for EII and MI is studied. The MI classification performance was significantly higher than EII performance across participants.
- ***Chapter 6*** presents the concluding summary. It also outlines the main contributions of the research, recommendations for future research based on the research undertaken and knowledge acquired from studies presented in this thesis.

CHAPTER 2

2 BCI SYSTEMS & BRAIN ACTIVITY-BASED EMOTION CLASSIFICATION STUDIES

2.1 Introduction

There have been a growing literature of brain-computer interfaces (BCIs) studies and emotion classification studies utilising recorded brain signals. There are different techniques for measuring brain activity. The measuring techniques used in BCI include recording the neuronal electrical signals (direct measurement) as electroencephalogram (EEG) or magnetoencephalogram (MEG) and assessing brain's metabolism (indirect measurement) such as in the case of functional magnetic resonance imaging (fMRI) and functional near-infrared spectroscopy (fNIRS). Depending on where the EEG sensors are placed, we can distinguish invasive and non-invasive EEG. The sensors are often placed on the scalp (non-invasive EEG). Invasive EEG, often referred to as intracranial EEG (iEEG), is used in some studies. Intracranial EEG types include the electrocorticogram (ECoG) measuring the electrical signals at the cortical level with subdural strips or grids of special EEG sensors placed on the cortex. In addition to ECoG, iEEG types include stereo-EEG which measures the local activity at targeted cortical area and deep brain structure using depth electrodes (Parvizi and Kastner, 2018). In the case of MEG, the brain electrical signals are measured non-invasively by recording the generated magnetic activity using a special magnetic field scanning machine. The invasive measurements offer a high spatial resolution which is useful in some clinical cases such as in epilepsy pre-surgical evaluation (Zumsteg and Wieser, 2000).

The direct measurement of brain activity is exploited in BCI to provide an alternative communication pathway by interpreting recorded brain signals. So, in this chapter, procedures used in BCIs are reviewed, and associated important BCI methods and BCIs performance evaluation approaches are highlighted. Furthermore, brain-activity based emotions studies are reviewed, and relevant electrophysiological features for emotion classification are highlighted. A few studies have attempted to use emotions in the context of BCIs previously (Makeig et al., 2011) (Sourina et al., 2012) ; these studies are reviewed in more depth in this chapter.

2.2 Brain-Computer Interfaces

In the last two decades, we have seen a growing number of studies in brain-computer interfaces (BCIs) driven by evidences showing that people can learn to modulate their brain activity and by advancing computing technologies. In BCI, the person's brain activity is recorded, and using signal processing and machine learning methods, the changes in brain activity are detected and translated into a command/communication signals. This interface offers an alternative communication channel as opposed to traditional neuromuscular paths for CNS. The most recent complete definition for BCI state: *"A BCI is a system that measures CNS activity and converts it into artificial output that replaces, restores, enhances, supplements, or improves natural CNS output and thereby changes the ongoing interactions between the CNS and its external or internal environment*" (Wolpaw and Winter Wolpaw, 2012). *CNS activity* (or brain signal) refers to observed phenomena (e.g., neuronal action potentials, synaptic potentials, neurotransmitter releases, and neuronal oxygen consumption) when processing sensory information. BCI interfaces are primarily beneficial to people without or with defected communication channel (e.g., locked-in patients), but its applications also include entertainment (e.g. BCI games) (Ahn et al., 2014) (Coyle et al., 2016) (Beveridge et al., 2019), rehabilitation (Bundy et al., 2017) (Biasiucci et al., 2018) (Rathee et al., 2019) and assistive technologies (e.g., mobile robots (Stawicki et al., 2016), wheelchairs (Abiyev et al., 2016) (Tang et al., 2018), limb prosthesis (Vidaurre et al., 2016) (Tariq et al., 2018)).

EEG data offer a high temporal resolution (in order of milliseconds) and EEG recording systems are portable and relatively inexpensive. MEG data offer the same high temporal resolution as EEG and higher spatial resolution than EEG (Proudfoot et al., 2014), but due to the high cost and non-portability of MEG systems, EEG systems are the preferred modality for most BCI systems. This chapter and subsequent chapters focus more on non-invasive EEG-, MEG-based BCIs studies, but there are some references to studies based on other neuroimaging modalities throughout this and other chapters.

2.2.1 Brain structure

The central nervous system (CNS) is comprised of brain and spinal cord. The brain is of interest here as the work in the thesis explores directly measured brain activity. The brain and the spinal cord are surrounded and protected by three layers of tissues, known as meninges. The first meningeal layer directly on the surface (of the brain and spinal cord) is *pia mater*. The second layer is the *arachnoid mater*, and the outer layer is the *dura mater*. The main brain structures are brainstem, cerebellum,

thalamus, hypothalamus, pineal gland, and cerebrum (Felten et al., 2016). Some of these structures are illustrated in Figure 2-1.

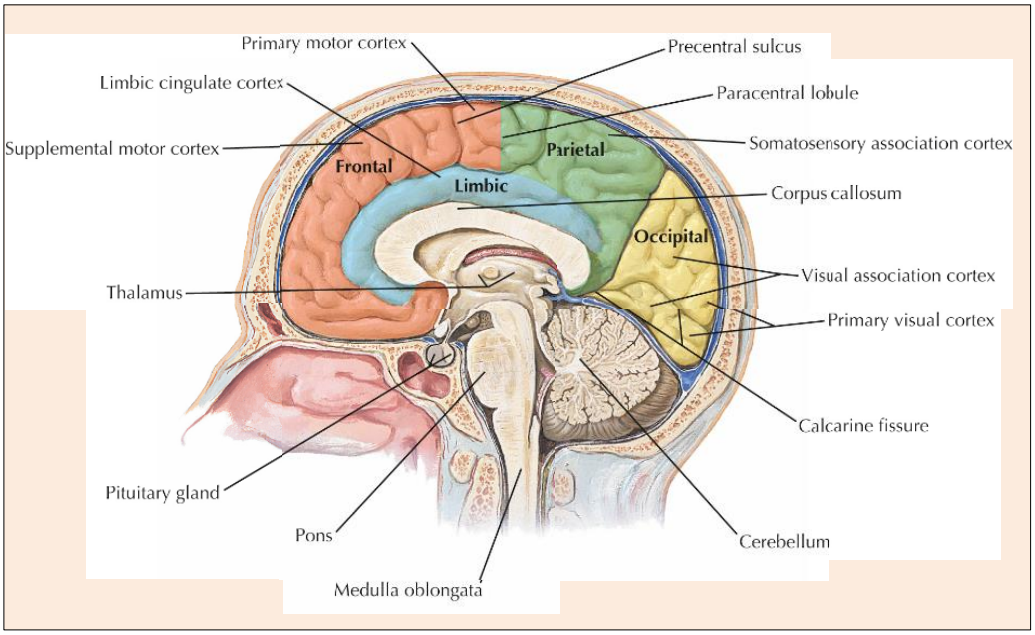

Figure 2-1. Midsagittal view of the brain's lobes and functional areas (figure adapted based on illustration from (Felten et al., 2016))

- ***Brainstem*** connects the brain to the spinal cord and is a relay centre for cerebellum and cerebrum. The brainstem is subdivided into three regions: medulla oblongata, pons, and mesencephalon which is further subdivided into tectum and cerebral peduncles.
- ***Cerebellum*** is located posterior to brainstem under the cerebrum. The cerebellum coordinates motor movements, especially complex motor activities, and maintains posture and balance.
- ***Thalamus*** acts as a relay centre for sensory inputs from peripheral nervous system and the corresponding processing centres of the cerebrum.
- ***Hypothalamus*** is located superior to the pituitary gland and inferior to the thalamus. The hypothalamus acts as the control centre for neuroendocrine functions (Felten et al., 2016).
- ***Pineal gland*** is also referred to as the epithalamus. The pineal gland secrets melatonin which help regulating the body's internal clock.
- ***Cerebrum*** is the largest structure of the brain, and it is composed of left and right hemispheres joined by the corpus callosum. The surface of cerebrum has several convolutions allowing to fit an extensive surface into a small volume. The surface hump (gyrus), fold (sulcus) of the

cerebral cortex, cortical grey and white matter are illustrated in Figure 2-2. The cerebrum's surface is a layer of gray matter and is referred to as cerebral cortex. Each cerebral hemisphere is subdivided into cortical lobes: frontal, temporal, parietal, and occipital lobes. The insula forms the fifth cortical lobe, however this can only be seen by opening the sylvian fissure which separates the temporal lobe below from the parietal and frontal lobes above. The four visible cerebral lobes are shown in Figure 2-3.

- ***Frontal lobe*** is involved in processing/coordinating/regulating brain functions including:
  - Personality behaviour and emotions
  - Speech (Broca's area)
  - Concentration and self-awareness
  - Problem solving and planning
- ***Temporal lobe*** is involved in processing/coordinating/regulating brain functions including:
  - Memory, sequencing
  - Hearing, understanding language
- Parietal lobe is involved in processing/coordinating/regulating brain functions including:
  - Visual and spatial perception
  - Interpreting language, words
  - Sensing pain, touch, and temperature
  - Interpreting information from motor, visual , and auditory sensory
- ***Occipital lobe*** is involved in processing/coordinating/regulating brain functions including:
  - Interpreting colour, light, and movement (vision)
- ***Limbic system*** contains the cingulate gyrus, hypothalamus (not part of the cerebrum), amygdala and hippocampus. The limbic system acts as the centre for emotional reactions, memory, and learning.

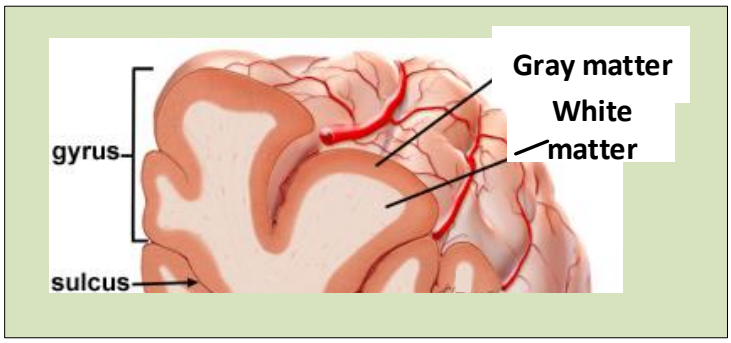

Figure 2-2. A portion of the cerebral cortex illustrating the gyrus and sulcus

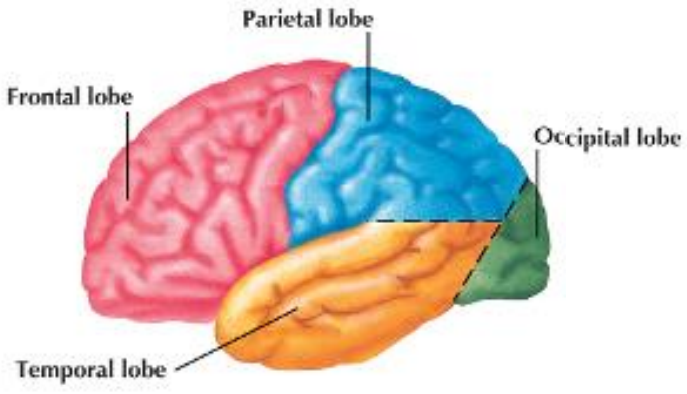

Figure 2-3. Lateral view of the brain's lobes

2.2.2 Brain electrical activity: EEG and MEG

At the cellular level, the brain contains two types of cells: neurons (nerve cells) and glial cells. The glial cells protect, support, and provide maintenance to neurons. The neurons transmit nerve signals. A neuron is illustrated in Figure 2-4. The neuron is made of de cell body (soma), dendrites, and axon which may branch in more than 500,000 axon terminals (Felten et al., 2016). The soma processes the incoming signal to determine if it is to be transmitted. The incoming stimulus is converted into electrical signal by the primary sensory neurons which is then carried into the CNS. In the brain, the neuronal activity is stimulated by chemical activity at the synapse. Electrical potentials, action potentials (APs), allow an electrical signal to be transmitted and trigger neurotransmitter release through excitatory-secretion coupling (at the synapse). The APs usually start at the initial segment of axons, and this happens when temporal and spatial summation of excitatory postsynaptic potentials (EPSPs), referred to as stimulus in Figure 2-5 (but not shown) cause sufficient excitation (depolarization) to open Sodium ions (Na^+) channels.

The measured MEG and scalp EEG, non-invasive EEG, present a portion of electrical activity resulting from a large population of activated neurons in the brain. An electrical field is generated all over the brain surface and the scalp when different cortical areas are activated as in Figure 2-6 to process sensory information or mental processes, and the scalp EEG portion ranges from 5-100μV. Since the recorded EEG resulted from various cortical areas, there is a challenge to decode what information is conveyed by it. Most of these BCIs are based on characteristics reflected in EEG in different brain oscillations during or after some internal (mental task) or external event (stimulus presentation).

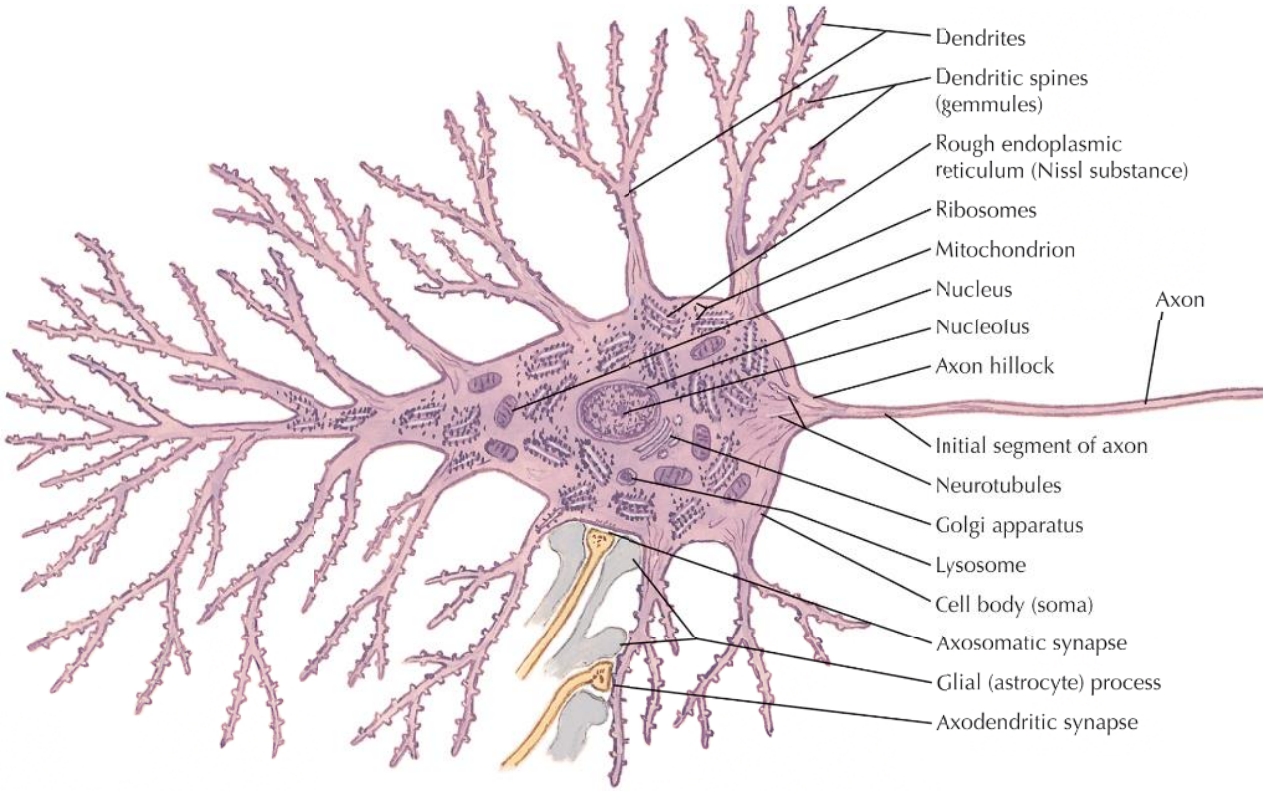

Figure 2-4. A neuron illustration (figure adapted based on illustration from (Felten et al., 2016)), a pyramidal cell is used in this illustration.

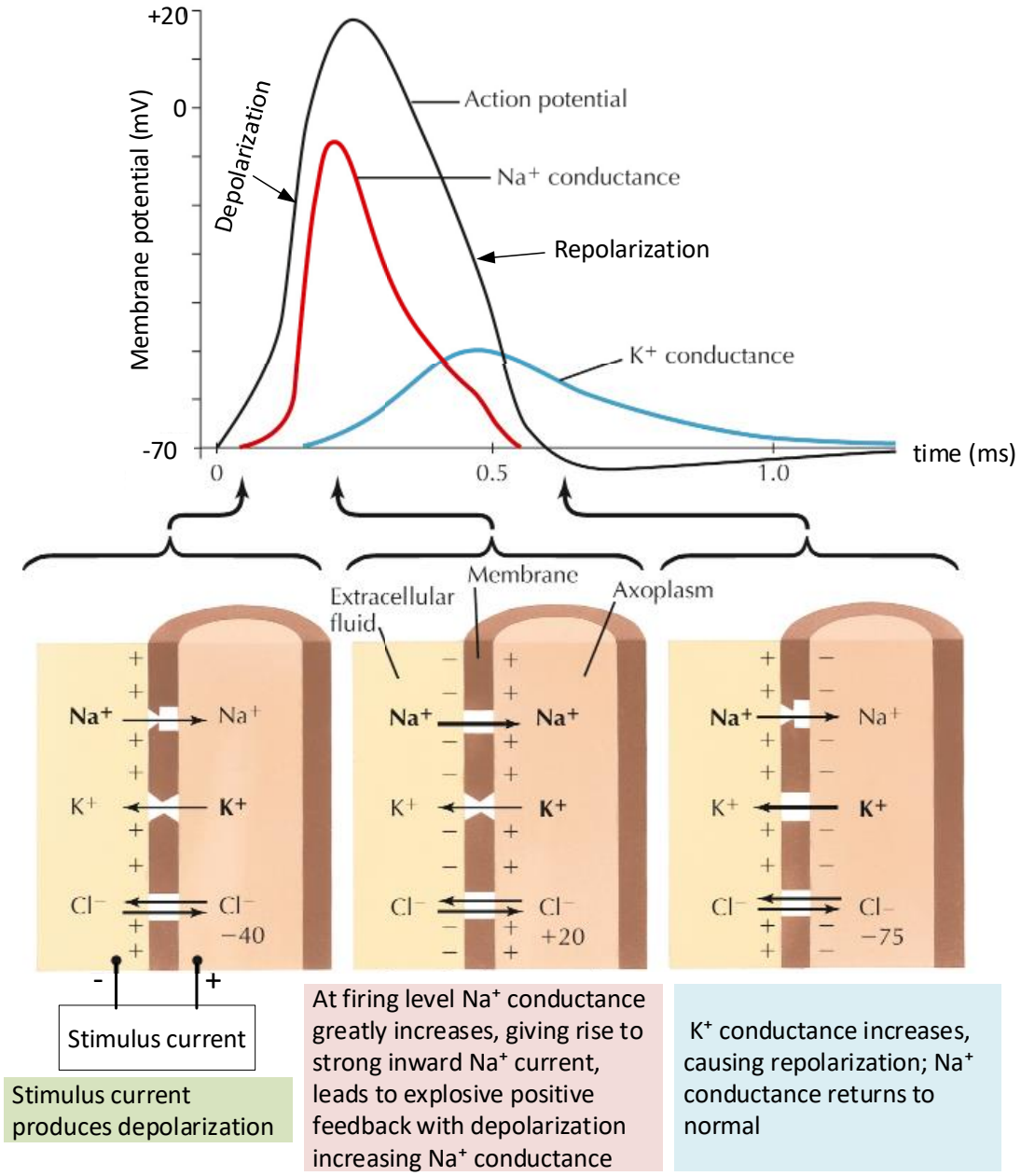

Figure 2-5. Action potential mechanism (figure adapted from illustration in (Felten et al., 2016)), cross-membrane movements of Potassium ions (K^+), Sodium ions (Na^+), and Chloride ions (Cl^-) are shown by directional arrows.

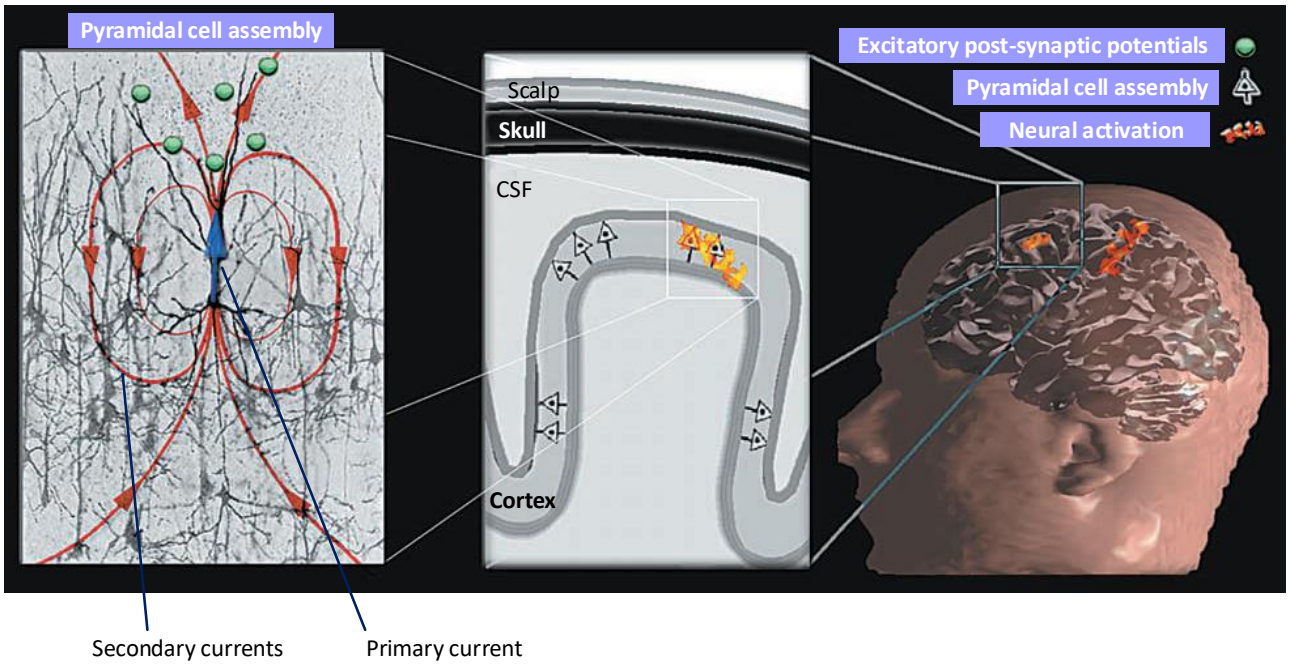

Figure 2-6. Generation of recorded MEG/EEG signals. In the left portion: at the micro-level, the neural activity shown as the primary and secondary currents (in blue and red respectively). In the middle portion of the figure: show a macro-assemblies of the cortical pyramidal cells. When a large population is simultaneously activated the individual currents from different pyramidal cells are superimposed creating a current flow that produces measureable EEG and MEG signals. This figure was adapted from the illustration from (Baillet et al., 2001).

2.2.2.1 Brain oscillations

The recorded brain-activity, EEG or MEG data, contains different brain rhythms: delta, theta, alpha, *Mu*, beta, and gamma frequencies. These rhythms have been associated with brain functions, processes and neural disorders.

- ***Delta Rhythms*** (0.5-4Hz): these rhythms are usually observable in deep sleep and have also been associated with some pathologies (Koutroumanidis et al., 2004). Klados and Colleagues have reported delta power increase when their participants were presented with arousing stimulus (Klados et al., 2009). Delta rhythms have been also used in limbs movement trajectory decoding (Bradberry et al., 2010) (Paek et al., 2014).
- ***Theta Rhythms*** (4-7Hz): these rhythms are known to be present in sleeping adults and can be observed in awake children. A significant presence of theta rhythms in awake adults suggests brain abnormality case. For emotion, some studies found increase in frontal theta band power in arousing stimulus presentation (Balconi and Pozzoli, 2009) and increase in frontal theta

rhythms activity when a participant is listening to a high valence music stimulus (Lin et al., 2010b).

- ***Alpha Rhythms*** (8-13Hz): these rhythms are prominently present in wake but relaxed adults, especially when the eyes are closed. The decrease in alpha activity under visual stimulus usually correlates with mental process activation (alpha ERD), whereas the increased activity (ERS) correlates with some process inhibition (Klimesch et al. , 2007) or cortical areas at rest. Alpha asymmetries, mostly in the frontal area, have been reported (Coan and Allen, 2004; Davidson et al., 1990) in response to different emotional stimuli.
- ***Beta Rhythms*** (13-30Hz): these rhythms are usually seen in the frontal and central scalp areas and have smaller amplitudes compared to alpha rhythms. The central beta rhythms are associated with mu-rhythms (about 10HZ) which is related to motor cortex. An increase in temporal beta activity is observed in positive emotions, but not in the case of negative emotions (Cole and Ray, 1985).
- ***Mu-rhythms*** (around 10Hz): these rhythms are associated with motor related processing, in the motor cortex.
- ***Gamma Rhythms*** (>30Hz): these oscillations are associated with several cognitive processes. Their association to varied processes makes it harder to decode the mental state. Gamma oscillations are closely linked to emotional memory (Headley and Paré, 2013).

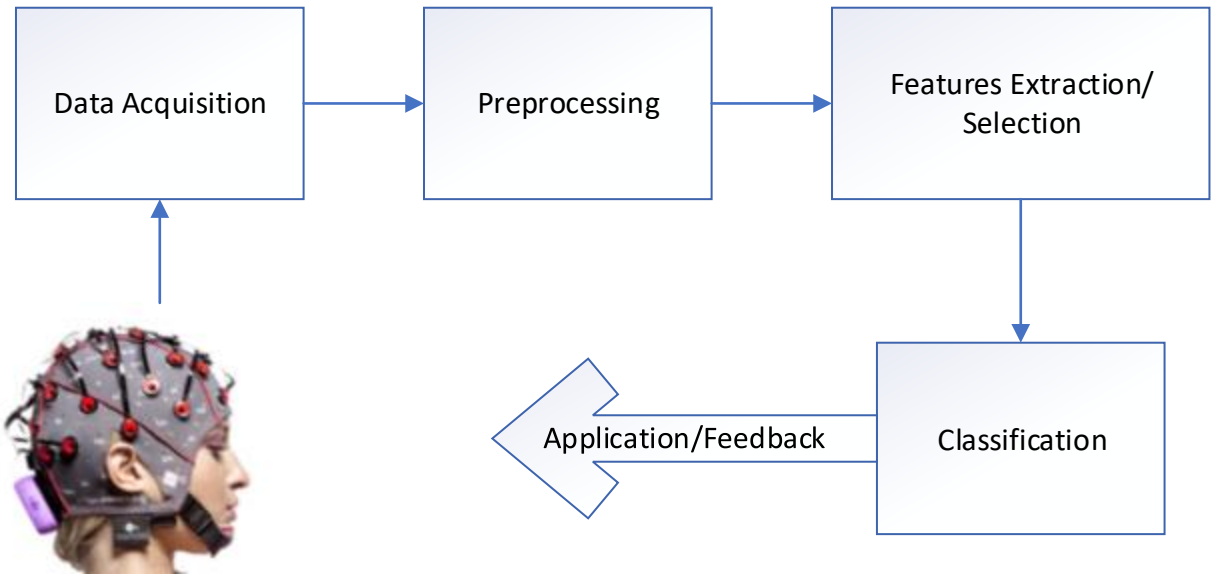

Figure 2-7. The standard EEG-based BCI processing loop

2.2.3 BCI systems

The analysis of the neural activity data recorded in a BCI setup varies depending on the approach or paradigm used in the BCI setup. Considering the user, we can have brain-activity associated with active and passive engagement with the setup, and considering the stimulus, we can have self-induced and stimulus-evoked brain-activity. Combining the user's volition and the stimulus, the BCI approaches may include the following cases:

i. The user attends to the stimulus presented, examples include visually-evoked potential (VEP) and event-related potential (ERP) studies.

ii. The BCI does not rely on the user being engaged in any specific task or attending to a specific stimulus, e.g., workload monitoring as in (Estepp and Christensen, 2015).

iii. The user actively shifts the gaze to a given position/target, e.g., motion-onset visually-evoked potentials (MVEP)-based BCI (Beveridge et al., 2015) (Marshall et al., 2015a)and steady-state visually-evoked potentials (SSVEP)-based BCI.

iv. The user actively (voluntarily) engages into a mental activity, e.g., motor imagery based BCI, in which the user imagines the limbs' movements as in (Prasad et al., 2010). The BCI approaches based on the user voluntarily modulating his/her brain signals are (and have been) of significant interest because they offer an alternative communication channel that only depends on the ability of the user to modulate the brain activity (assuming that appropriate signal processing are utilized in the BCI setup). The BCI approaches in this case are also known as independent BCIs (Wolpaw et al., 2002) or active BCI. The primary targeted users for active BCIs are people with severe neuromuscular disabilities who even cannot get reliable eye-blinks and patients with locked-in syndrome.

The BCIs development process in all the four cases follows closely the BCI processing stages shown in Figure 2-7. After acquiring the brain-activity data, the data processing phase includes pre-processing, feature extraction, feature selection, classification, and the classification output may be used as input to an application and/or provide a feedback to the participant to enable learning. In the following sections, we are going to look at several popular data processing methods, features extraction techniques, features selection methods, and classification models used in BCI systems.

TABLE 2-1. NOISE AND ARTEFACTS & METHODS TO REDUCE THEM FROM THE DATA

Noise or artefact	Comment on artefact	Noise reduction method
ECG	Mainly found around 1.2Hz	Frequency filtering, BSS
EOG	Mainly found below 4Hz	BSS, adaptive filters, Wavelet decomposition
EMG	Mainly found above 20Hz	BSS, Wavelet decomposition
50/60Hz line noise	Found around 50 or 60Hz depending on the electrical system used in the recording	Notch filters

2.2.3.1 Pre-processing

The objectives of pre-processing step is to increase the signal-to-noise-ratio (SNR) of the brain-activity data by reducing the noise and artefacts. The recorded EEG or MEG data for a targeted task are often contaminated with noise and artefacts including 50/60Hz power line noise, noise due to electrode shifting, artefacts associated to heart activity, electrocardiography (ECG), eye movements or blinking, electrooculography (EOG), muscle activity, electromyography (EMG), and cognitive processes (van Boxtel, 2001) (Nicolas-Alonso and Gomez-Gil, 2012). The TABLE 2-1 shows some of the methods used for artefacts and noise reduction from EEG. These methods include values-thresholding, frequency filtering, and complex techniques such as independent components analysis (ICA) (Nicolas-Alonso and Gomez-Gil, 2012).

The EOG can be filtered out through the adaptive filter (Sanei and Chambers, 2007) by estimating the noise (or artefact) as shown in Figure 2-8. Offline pre-processing usually utilises blind sources separation (BSS), such as ICA to remove artefacts from EEG or MEG, by unmixing the data into independent sources, independent components signals, and then components representing artefacts are set to zero. The remaining components signals are remixed for the cleaned EEG signal. Castellanos and Makarov raised concerns that ICA may introduce power spectral underestimation and coherence of cortical areas overestimation, and they proposed a method that utilizes ICA and wavelet transform to reject artefacts from EEG data. (Castellanos and Makarov, 2006). The artefacts removal based on ICA-wavelet transform method was further investigated in one of the author' studies (Bigirimana et al., 2016). This study compares the effects of pre-processing the EEG with ICA-wavelet method versus regular ICA method or frequency filtering on the classification performance of emotion classes. The findings from the author's investigation suggests that ICA-wavelet method performs better than compared methods (details are reported in chapter 3).

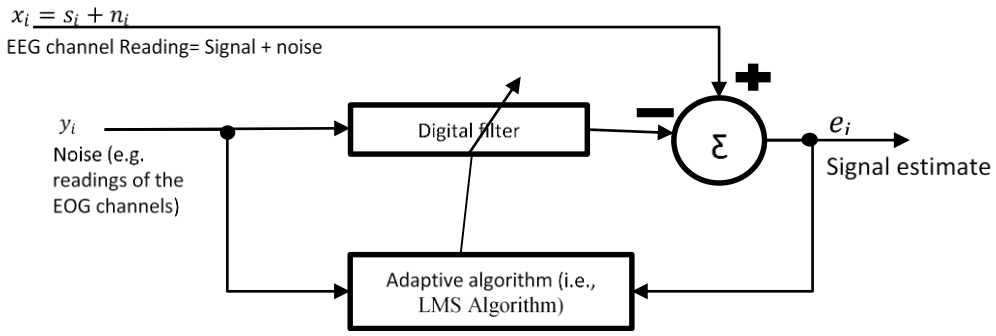

Figure 2-8. Adaptive noise canceller, the clean signal estimate is found by estimating the noise, then this noise estimate is subtracted from the EEG channel reading. The coefficients of the digital filter are adapted to the changes in the readings by using the clean signal estimate back into the adaptive algorithm, and the preferred algorithm is the least mean squares algorithm (Sanei and Chambers, 2007).

2.2.3.2 Feature extraction methods

Once the brain activity data are cleaned, characteristics associated with brain activities are extracted for further analysis. For the BCI setup that relies on the user actively engaging into mental tasks, the features extraction exploits the relevant features for the brain activity associated to each of the mental tasks the user is asked to carry out. For this, the mental tasks with distinctive neural correlates are used in such BCI setups. For example imageries for left hand versus right hand movement are used in most motor imagery-based BCIs because of the known difference between the neural correlates for the two imagery tasks. Each of the two imagery is normally associated with increased contralateral activity and decreased ipsilateral activity in the motor cortex. Such differences are extracted as event-related (de)synchronization (ERD/S), (Pfurtscheller, 1992). Often, the spatial filters are used to make even more evident the differences between motor imageries, e.g., the common spatial patterns (CSP)-based method is commonly used in motor imagery-based BCI to increase separability between classes. Furthermore, the features of interest in BCI are also extracted as frequency-domain features through frequency content analysis using Fourier transform-based methods such as fast Fourier transform (FFT), periodogram, and Welch method (Palaniappan, 2010). Besides, the frequency content based features, the time-domain features are also extracted. The time-domain features are often extracted as statistical measures of the signal or other temporal behaviours such as event-related potentials (ERPs). Methods looking at both temporal and frequency resolutions have been applied in the literature, and these include wavelet decomposition (Murugappan et al., 2009b), ERD/S, and short-time Fourier transform (STFT) (Coyle et al., 2005). The following sections describe some of these feature extraction methods.

2.2.3.2.1 Event-related potentials

The stimulus presented to a BCI user/ participant is associated with changes into EEG, namely event-related potentials (ERPs), event-related field (ERF) in the case of MEG. These changes are presented as an increase in negative or positive peak amplitude in EEG at some specific time points post the stimulus presentation. Usually the notation using the letter 'N' and 'P' together with a number to indicate the negative or positive going and associated latency, e.g., P300 is the positive peak occurring about 300ms post stimulus onset (in some studies the P300 component is reported to occur between 350 and 600ms post stimulus onset). Due to lower SNR of EEG/MEG and noise, to successfully extract the ERP components, several single trial ERPs of the same type need to be averaged together. This averaging attenuates the non-stimulus-evoked potentials which vary from trial to trial as they are not phase locked.

The types of ERP components of interest depend on the type of stimulus used. The stimuli types include auditory, somatosensory (e.g., median nerve stimulation), and visual stimuli. In the case of auditory stimuli, the interest usually involves looking at ERPs responses to changes in frequency, intensity, duration of the stimulus, also referred to as mismatched negativity (MMN) paradigm. The rare stimulus evoke larger MMN component (this is a negative peak occurring around 200ms post stimulus onset) in anterior areas (Näätänen et al., 2004; Pakarinen et al., 2007). When visual stimuli are being presented to the participants, the resulting ERPs are referred to as visually-evoked potentials (VEP). Research has shown that the amplitude of the P300 component recorded on the parietal-occipital area is higher for the target than non-target visual stimulus where the target is rarer than the non-target (Sutter, 1992) (Luck, 2005). The normal latencies for recordings done on the midline over the primary visual cortex are: 70ms for N1, 100ms for P1, and 140ms for N2 when stimulus like alternating checkboard flashing (at 2Hz) patterns is used (Felten et al., 2016).

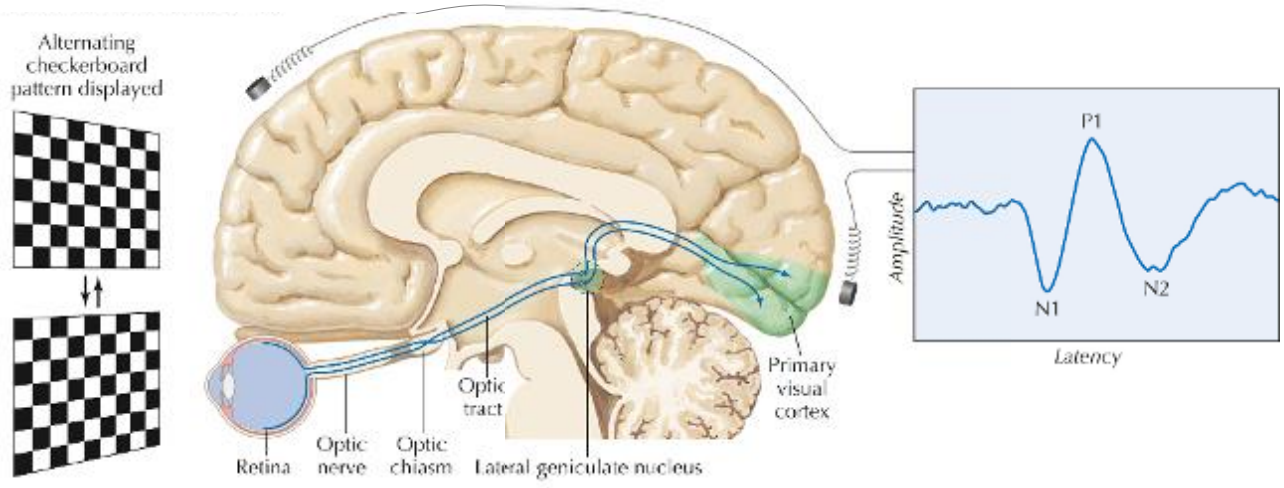

Figure 2-9.Visual evoked potential with alternating flashing checkboard (figure adapted based on illustration from (Felten et al., 2016))

The ERP-based BCIs allow the user/participant to communicate by passively attending stimuli provided, and this communication can have a relatively high information transfer rate (ITR). In a steady state visually-evoked potentials (SSVEP)-based BCI – this uses constant light in targets and non-target at specified frequency, a participant can select a letter from a keyboard-like matrix characters by shifting the gaze to the targeted character. The discrimination of the relevant ERP components is generally fast and accurate. For example in a 6 by 6 matrix of characters P300 speller, the achieved online accuracy is often above 90% (Krusienski et al., 2008), and disabled participants (wheelchair bound paraplegia) can achieve an ITR of about 3.2 bits per minute at an accuracy of 95% (the BCI performance evaluation is described in 2.2.4). Average ITR of 60.2 bits per minutes was reported with accuracy of 81.0% in online SSVEP BCI (Lin et al., 2016), and Nagel and Spüler recently achieved an average ITR of 122.7 bits/min with average accuracy of 99.3% in an online setup of a 4 × 8 matrix-keyboard VEP-based BCI speller (Nagel and Spüler, 2019).

The general process of extracting the SSVEP features consist of isolating the different frequencies of interest, frequencies at which the light is flickering for targets and non-targets buttons, and their adjacent frequencies. The frequencies of interest for ERP components are often less than 30Hz, and are extracted by filtering the signal with band-pass of 0.01-30Hz (Intriligator and Polich, 1994). The extracted features are often the amplitude and latency for ERP component. In some studies, high frequencies are also used in the flickering of stimuli (Zhu et al., 2010). There are other varied ways to setup VEPs, such as the motion-onset VEP in which a light moves across target and non-targets, and code modulated VEPs in which target flickers according to its associated modulation code (Liu et al., 2018b).

2.2.3.2.2 Event-related desynchronization/synchronization

In contrast to the ERP features which look at the time-domain evolution of neural responses to stimuli, event-related desynchronization or synchronization (ERD/ERS) looks at time-frequency of the neural responses (Pfurtscheller and Lopes Da Silva, 1999) (Durka et al., 2001). ERD is the decrease in amplitude of the EEG response with respect to the reference amplitude of the background EEG in a specific frequency band, and this can be associated with decrease in synchronization of the neuronal population generating the EEG being recorded (Pfurtscheller and Aranibar, 1977). On the other hand, ERS is the increase of the power amplitude with respect to the reference power in specific frequency

band (Pfurtscheller, 1992). The ERD/ERS observations are generally computed in the following steps (Pfurtscheller and Lopes Da Silva, 1999):

i. Bandpass filtering the event related trials in specified frequency band;

ii. Compute the power samples by squaring the amplitude of each sample;

iii. Averaging the power samples, then

iv. Smooth the average by an appropriate number of samples

The ERD/ERS observations in a given frequency band at some instant of time are expressed in terms of percentage of power increase and decrease respectively and are computed as: $\text{ERD\%} = \frac{\text{A-R}}{\text{R}} * 100$, where A is the power in the specified frequency band at some instant of time after the event (or during the event); R is the baseline power. (Pfurtscheller and Lopes Da Silva, 1999).

The are other variations of ERD/ERS computation including event-related spectral perturbation (ERSP) (Makeig, 1993), inter-trial variation (ITV) (Kalcher and Pfurtscheller, 1995), task-related power increase (TRPI), task-related power decrease (TRPD) (Gerloff et al., 1998), and temporal-spectral evolution (TSE) (Salmelin et al., 1995). The ITV is obtained by filtering the data into a specified frequency band, followed by calculating sample-to-sample inter-trial variance, and then averaging the variance over a specified time window. In BCIs, the characteristics of ERD/ERS dynamics are usually extracted using spatial filters such as common spatial patterns (CSP) and filter bank CSP (FBCSP).

2.2.3.2.3 Common spatial patterns and Filter bank common spatial patterns

The common spatial patterns (CSP) method is used to maximize the ratio of class-conditional variances of EEG or MEG sources. To isolate the dynamics of interest, the EEG (or MEG) data are first filtered in a specific frequency band, and CSP is applied by pooled estimates of the covariance matrices, Σ_1 and Σ_2, for data belonging to two classes, as follows:

$$\sum_c = \frac{1}{I_c} \sum_{i=1}^{I_c} X_i X_i^t \ (c \in \{1,2\}), \qquad (2\text{-}1)$$

where I_c is the number of trials for class c, and X_i are the $M \times N$ matrices containing the i^{th} windowed segment of trial i; N is the window length, and M is the number of EEG channels.

The two covariance matrices, Σ_1 and Σ_2, are simultaneously diagonalized such that the Eigenvalues sum to 1. This is achieved by calculating the generalized eigenvectors W:

$$\sum_1 W = (\sum_1 + \sum_2) W D, \qquad (2\text{-}2)$$

where the diagonal matrix *D* contains the eigenvalues of Σ_1 , and the column vectors of *W* are the filters (i.e. spatial patterns) for the CSP projections. With this projection matrix the decomposition mapping, *E*, of the windowed trials *X* is given as:

$$E = WX. \qquad (2\text{-}3)$$

Features, $\bar{\omega}$, are derived from the log-variance of pre-processed/surrogate signals, *E*, within a selected *k* s (usually 2 s for MI-based BCI) sliding window:

$$\bar{\omega} = log(\, var(\, E)). \qquad (2\text{-}4)$$

There are some variations of CSP methods based on regularisation applied on the estimates for covariance matrix and or on the expression in (2-2). In the comparison of classic CSP and CSP with regularization methods (Lotte and Cuntai, 2011) showed that Tikhonov regularisation (Morozov, 1966) resulted into a high performing CSP in compared CSP methods. Furthermore, CSP can be extended to extract features from multiple frequency bands. In this case, CSP is repeated for different frequency bands creating a filter bank CSP (FBCSP). The projection map in FBCSP, i.e. CSP filters, is computed for each frequency band, and features are extracted from surrogate signals in each frequency band. Depending on the number of CSP filters used, the dimensionality of the features vector can be high in FBCSP framework, a feature selection might be needed to reduce this high dimensionality. Some features selection methods used in BCI are described in the following section.

2.2.3.3 Features selection

The dimension of extracted features is often high and often with redundant information. The main task of feature selection is to reduce the dimension of the features matrix by selecting the relevant features and discarding the non-relevant ones. Methods used to rank and select relevant features generally fall into filters or wrapper methods. Filter methods statistically interact with extracted features using methods such as the ReliefF algorithm (Peker et al., 2015), minimal-redundancy-maximal-relevance (mRMR) (Erfanian et al., 2011), and effect-size methods (Jenke et al., 2014). In mRMR, the goal is to find the features which are the most relevant to the targeted class, and this relevance can be measured using mutual information estimation. The mutual information *MI* is computed using the expression (2-5):

$$MI(x;y) = \iint p(x,y) log \frac{p(x,y)}{p(x)\,p(y)} dxdy \qquad (2\text{-}5)$$

where, x, y are random variables with their probabilities and joint probability density functions being $p(x), p(y)$, and $p(x, y)$respectively. The wrapper on the other hand, applies a classifier on the features

and uses the classifier's outputs in ranking and selecting the features , e.g. a genetic algorithm (GA) (Nicolas-Alonso and Gomez-Gil, 2012). In some instance, one or two of these methods are combined to improve the performance (Peng et al., 2005).

2.2.3.4 Classification

The extracted/selected EEG/MEG features are mapped into corresponding classes or categories. This features-mapping task is often accomplished in two steps: training the classifier and applying the trained classifier to classify unseen data or in an online setup. Most of BCI studies have utilised standard classifiers used in machine learning problems. These classifiers include Fisher's linear discriminant analysis (LDA), Support Vector Machine (SVM), k-nearest neighbour (KNN), Mahalanobis distance (MD), and in some instance neural networks (NN). Beside the standard classifiers, there are emerging new classification frameworks for EEG/MEG data including convolution neural networks (CNNs), random forest, and Riemannian geometry classifier (RGC).

LDA establishes linear discriminating hyperplanes between features that maximize the classes' separability; the class is determining by where its features are located with respect to the hyperplanes. The hyperplane is a projection which maximizes the distance between classes' features while minimizing the intra-class variance (Lotte et al., 2007). In multiclass problems, each class is isolated from the others through the one-versus the rest scheme. The LDA can achieve high classes' separability with low computational burden, making it more attractive in BCI. However due to the fact that EEG is highly non-linear, in situation where overlapping or very similar features, LDA may be an unsuitable choice of classifier (Coyle, 2005).

In its simple form, SVM classifier uses linear decision boundaries to establish a hyperplane that gives the maximal distance between boundary training points (support vectors) of different classes. This SVM is often identified as linear SVM. It is possible to have SVM with non-linear decision boundaries, non-linear SVM, by remapping the extracted features into a space that allows maximum distance between support vectors. The remapping is achieved through the use of kernel function where in the test phase (after training), the SVM classifier follows the following expression (Burges, 1998):

$$c = \sum_i a_i k\left(s_i, f\right) + b \qquad (2\text{-}6)$$

where k is the kernel function, α_i the weights, and s_i the support vectors. The features vector f is classified in the first group if $c \geq 0$, and in the second group otherwise. In the case of linear SVM, the kernel is a linear function. SVM is known to perform well and does not suffer from the overtraining

or dimensionality issues usually found in LDA classifier. However, computations might take longer in SVM compared to LDA.

Beside LDA and SVM, Neural Networks are also used in brain signals classification as in (Khosrowabadi et al., 2011) (Zheng et al., 2015). NNs are neuron-inspired methods, where artificial neuron models make the decision boundaries. One of the popular NN classifier is Multilayer Perceptron (MLP). MLP is built into input layer, many hidden layers (or just one hidden layer), and output layer utilizing sigmoid transfer functions (Jain et al., 2000). The other NN classifiers include radial basis function based (RBF) neural network (NN). The RBFNN has one or more layers of neurons utilizing Gaussian transfer functions. The Neural network classifiers are sensitive to overtraining and do take long to train, but can achieve good results in situation where features are only separable using nonlinear decision boundaries (Khosrowabadi et al., 2014).

K-Nearest Neighbour (k-NN) establishes k groupings (from k classes' features) during training and any features vector is then classified depending on the nearest grouping considering the Euclidean distance:

$$d\left(x, trn\right) = \sqrt{\sum_{i}^{n}\left(x_i - trn_i\right)^2} \qquad (2\text{-}7)$$

where, x is the features vector (of n features) to be classified, and trn is (one training) features vector. In the case of relatively sufficiently high k and low dimensional features sets, k-NN offers interesting results, as in (Khosrowabadi et al., 2010) (Murugappan et al., 2010). Another nearest classifier found in emotion-BCI literature is the Mahalanobis distance (MD). MD classifier classifies the features vector to the nearest mean of the covariance matrices of considered classes during training (Babiloni et al., 2001):

$$d_{md}\left(x\right) = \sqrt{\left(x - tr_l\right)^T C^{-1}\left(x - tr_l\right)} \qquad (2\text{-}8)$$

where, tr_l is the mean of the covariance matrix computed during training for the class l. C is the estimated full covariance matrix, and the T is the transpose operator.

In some of the studies, the classification framework is constructed by considering output from several individual classifiers. One of the example of such ensemble classifiers is the random forest which is made of several decision trees. Input features of EEG/MEG data are subdivided into training and test subsets for each decision tree using bootstrapping sample technique. A standard classifier (e.g., SVM) is then trained and validated for each decision tree. The overall performance is given by the average

of performance of all decision trees. In case of discrete output as in Figure 2-10, the overall output is given by the majority voting decision.

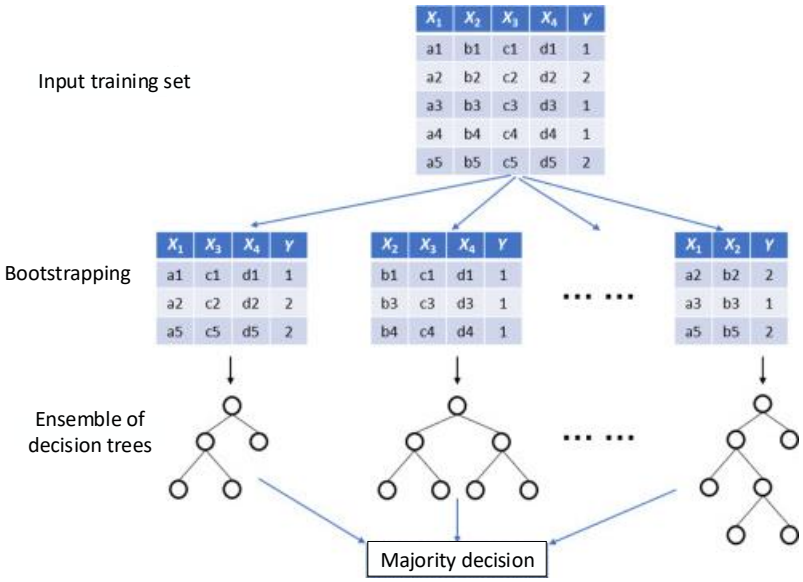

Figure 2-10. An illustration of implementation of random forest classifier. In this example the dataset has four features (X_1, X_2, X_3, and X_4) and two classes (Y = 1 and 2).

There is ongoing effort to apply promising deep learning methods used in computer vision technologies such as the CNN into BCI. CNN is variations of MLP. CNN structures include the convolution layer containing convolution kernels used to compute feature maps and a pooling layer aiming to achieve shift-invariance by subsampling the feature maps (Gu et al., 2018). High accuracies has been achieved in BCI with CNNs framework, e.g., in (Tang et al., 2017). Apart from deep learning methods, Riemannian geometry classifier (RGC) has been recently introduced in BCI (Yger et al., 2017) (Lotte et al., 2018). In RGC framework, the data is mapped onto a geometrical space which allows to directly carry out classification.

2.2.3.5 Application and feedback

The output of the classifier is interpreted to suit the application of the BCI in question and to generate appropriate feedback to the user. In most BCI systems, the feedback is offered as a display on the screen (e.g., game character reacting to the user's command), on-screen command/character selection (e.g., selecting a character in a VEP based speller), or activation of some devices (e.g., moving wheelchair or prosthetic limbs). The provided feedback can help the user learn to control or modulate his/her mental state and keeps the user engaged (Wolpaw et al., 2000) (Fetz, 2007), important for helping to effectively control the application.

The feedback provided may be continuous and real-time, or discrete (Wolpaw et al., 2000). The simple form of continuous feedback can be provided as a cursor movement on the screen, on the other hand the discrete feedback is usually presented as activation or selection of buttons on the screen. In BCIs, the control signal for continuous feedback is generated from successive classification's outputs. By carrying out classification every 100ms, the resulting feedback looks continuous to human eye. Most researchers use the feedback control signal in the form of the time-varying signed distance (TSD) (Pfurtscheller et al., 2000) (Schlögl et al., 2002) (Coyle et al., 2009). For each sample point in TSD signal, the magnitude of this distance is the classifier's confidence. The confidence is the distance from class hyperplane. The sign of the TSD indicates the class label.

The classifier, trained to distinguish between different classes, may be biased toward one class than the other. A post classification analysis step is usually used in BCI to create a de-biased and smooth TSD signal (Coyle et al., 2011). The de-biased TSD is obtain by continuously removing the mean of classification outputs from the last few trials. The length of the de-biasing window is subject dependant, but Coyle and colleagues found that a window of 30 to 35s long gives good results in the BCI setup used (Coyle et al., 2011). Another ways of de-biasing the classifier is to use an adaptive classifier framework, in which the classifier weights are updated as the new data becomes available (Lotte et al., 2018).

2.2.4 BCI system performance assessment

In the previous sections, various features extraction methods and classifiers were described, and now this section discusses measures used to assess BCI systems based on those methods. In order to be able to track the increase or decrease in the performance of a BCI system with respect to other related BCI systems, various measures are used to assess the performance of the BCI system. The most used measures include classification accuracy (CA), which is the percentage of correctly classified items, and information transfer rate (ITR) which considers both the CA and response (classifier output) speed of the system (Wolpaw et al., 1998). The ideal system should have a high CA in real-time, however, in most of BCI applications, e.g., in case of choosing an answer, switching on a device for example, the real-time response might not be the most important, but the accuracy might be crucial in the situation.

2.2.4.1 Classification measure

The classification accuracy (CA) is the percentage of correctly classified samples. The classification results are usually reported into a confusion matrix which allows to compute the accuracy (A), true

and false positive rate and, true and false negative rate. An example of a confusion matrix is show in TABLE 2-2 for a two-class (e.g., positive = *right hand and negative = left hand movement imageries*) classification problem. The content in the given confusion matrix example are:

- *TP = true positives* is the number of samples of class *'positive'* correctly classified
- *FN = false negatives* is the of samples of class '*positive*' classified as '*negative'*
- *FP = false positives* is the of samples of class '*negative'* classified as '*positive'*
- *TN = true negatives* is the number of samples of class *negative* correctly classified

TABLE 2-2. AN EXAMPLE FOR A CONFUSION MATRIX FOR A TWO-CLASS CLASSIFICATION

	Output classes	
Actual classes	positive	negative
positive	TP	FN
negative	FP	TN

Furthermore, various classification measures can be computed from the information given in the confusion matrix as follow:

- *Accuracy* (A) is the ration of correctly classified samples and is given by (2-9):

$$A = \frac{TP + TN}{TP + FN + FP + FN} \qquad (2\text{-}9)$$

- The *true positive rate* (TPR) is associated with *TP* in the confusion matrix, and this is the ratio expressing of how many of the samples from the positive class which are correctly classified (classified as positive). The TPR is also known as *recall* or as *sensitivity* measure, and it is computed by the expression in (2-10). The TPR, the recall, should be high in a good classification model. Another measure usually used is the *precision* measure which is a ratio expressing how many samples correctly classified out of the total samples classified as positive class, and it is given by the expression in (2-11). The *precision* should be high in good classification model. The recall and precision can be combined into one measure referred to as F1 score, a harmonic mean of *recall* and *precision* computed by (2-12), to allow comparison between different classification models. The search for optimal classification model should maximize the F1 score.

$$TPR = \frac{TP}{TP + FN} \qquad (2\text{-}10)$$

$$recall = \frac{TP}{TP + FP} \qquad (2\text{-}11)$$

$$F_1 = 2 \times \frac{precision \times recall}{precision + recall} \qquad (2\text{-}12)$$

– The *false positive rate* (FPR) is the ratio of sample from class *negative* classified as class *positive*, and it is computed by (2-13):

$$FPR = \frac{FP}{FP + TN} \qquad (2\text{-}13)$$

– The *true negative rate* (TNR) rate is the ratio expressing number of samples from class *negative* correctly classified. The TNR is also referred to as *specificity* measure, and it is computed by (2-14).

$$specificity = \frac{TN}{FP + TN} \qquad (2\text{-}14)$$

Other measures for classification include the receiver operating characteristic (ROC) curve which is a plot TPR versus FPR. This curve allows to optimize the classification model against a given threshold, a threshold value for a sample to be classified a *positive*. An example for ROC is given the Figure 2-11. Also, some researchers report the classification results using the area under the curve (AUC), under the ROC curve. The AUC of 1 is for a perfect model (100% classification accuracy, meaning TPR =1 and FPR =0). The model *b* in Figure 2-11 has AUC of 0.5 which represents a theoretical random accuracy for two balanced classes, and the model *b* on the other hand has an AUC greater than 0.5.

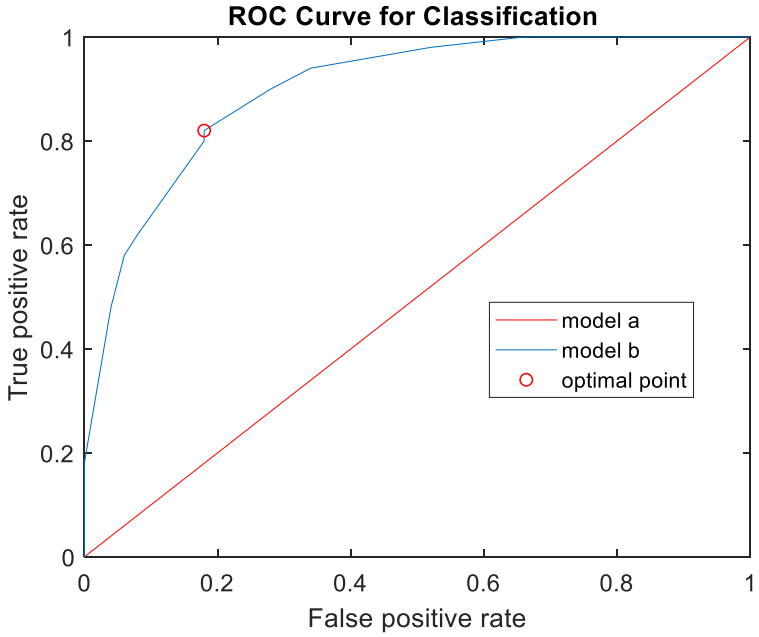

Figure 2-11. An example for a ROC curve results for two arbitrary classifier models: model 'a' and model 'b'.

2.2.4.2 Information transfer rate

Apart from the classification accuracy measure, the BCI performance is often evaluated in term of information transfer rate (ITR). The ITR conveys the accuracy and the speed at which the BCI system carries out the classifications (Wolpaw et al., 1998). The ITR is expressed in bits per minute (bits/min). Since most of the BCI systems require a minimum data length (e.g., a 2s window data) to carry out classification of different classes, the ITR conveys how much information such BCI systems can communicate in a given time window.

2.2.5 Brain-computer interfaces systems summary

There has been a significant progress in the development of BCI systems, and the focus has been on developing appropriate signal processing methods for BCIs and devising tasks and/or paradigms leading to modulation of brain activity of interest. There are BCI systems which rely on the user to voluntarily modulate his/her brain activity through engaging into a mental activity (e.g., motor imagery), BCI systems relying on the external stimuli to evoke some activity into the user's brain, and there have been some effort to develop hybrid BCI systems. The signal processing methods used in BCI systems, as it has been already mentioned in earlier sections, span the utilization of time domain, frequency domain, and time-frequency domain features.

Some researchers have reported that not all the users are capable of learning to modulate the brain activity in BCI systems such as motor imagery-based BCI (Bamdadian et al., 2014) (Vidaurre et al., 2011), and novel BCI strategies should be investigated for these users. There have been investigation of alternative imageries including mental arithmetic operations, mental rotation of objects, and mental navigation (Curran and Stokes, 2003) (Myrden and Chau, 2015). In the ongoing effort to investigate novel imagery strategies, emotion-inducing imagery has been investigated in this research work (this is reported in chapter 4 and 5 of this dissertation). Emotion-inducing imagery is motivated by the findings from brain-activity based emotion classification studies; mainly the evidence that different emotions are associated with different neural correlates. Brain activity-based emotion classification studies are discussed further in the next sections.

2.3 Brain Activity-Based Emotion Classification Studies

Now that we have established a background for BCI systems, the following section looks at emotion studies based on the same brain activity recordings as in the BCI systems covered in previous sections. Studies on emotions recognition have increased significantly in the last two decades, and these studies utilise various modalities including heart rate and skin conductance measures (Healey & Picard, 1998), facial expressions, and neuroimaging such as magnetic resonance imaging (MRI), near-infrared spectroscopy (NIRS), magnetoencephalography (MEG), and electroencephalography (EEG). Facial expressions and peripheral physiological measures have been popular methods in emotions detection but can be inappropriate in the case of voluntary emotion concealment or due to physical disabilities or to diseases. The focus of this thesis is on EEG/MEG-based studies. MEG/EEG-based emotion recognition studies and potential exploitation of emotion classification to augment the existing BCI approach are reviewed.

Emotion studies based on brain activity date back to nineteenth century. In 1868 Harlow established that prefrontal cortex (PFC) is involved in emotion processing after observing the dramatic changes in Phineas Gage's emotional behaviour following Gage's accident that damaged his PFC (Harlow, 1868). In 1872 Erwin Darwin published '*The Expression of Emotions in Man and Animals*'(Darwin, 1956). In this section, a review of the recent progress and methods used in emotion recognition studies based on brain activity data is presented. The growing literature of emotion studies using varied brain imaging modalities in the two last decades is depicted in Figure 2-12. The research articles reported here were a result from a search in Google Scholar database, and only peer-reviewed journal and conference articles and masters and doctoral dissertations are reported here. The search for the surveyed articles was constrained by the condition of finding all the keywords in the title of the article,

and the keywords were 'emotion EEG' for EEG articles, 'emotion MEG' for MEG articles, and 'emotion fMRI' for fMRI articles. The trend in the surveyed literature suggests that EEG and fMRI are the most used brain imaging modalities in emotion studies. Furthermore, the last decade has shown a faster growing literature, especially in journal publication for emotion studies with the EEG and fMRI as neuroimaging modalities.

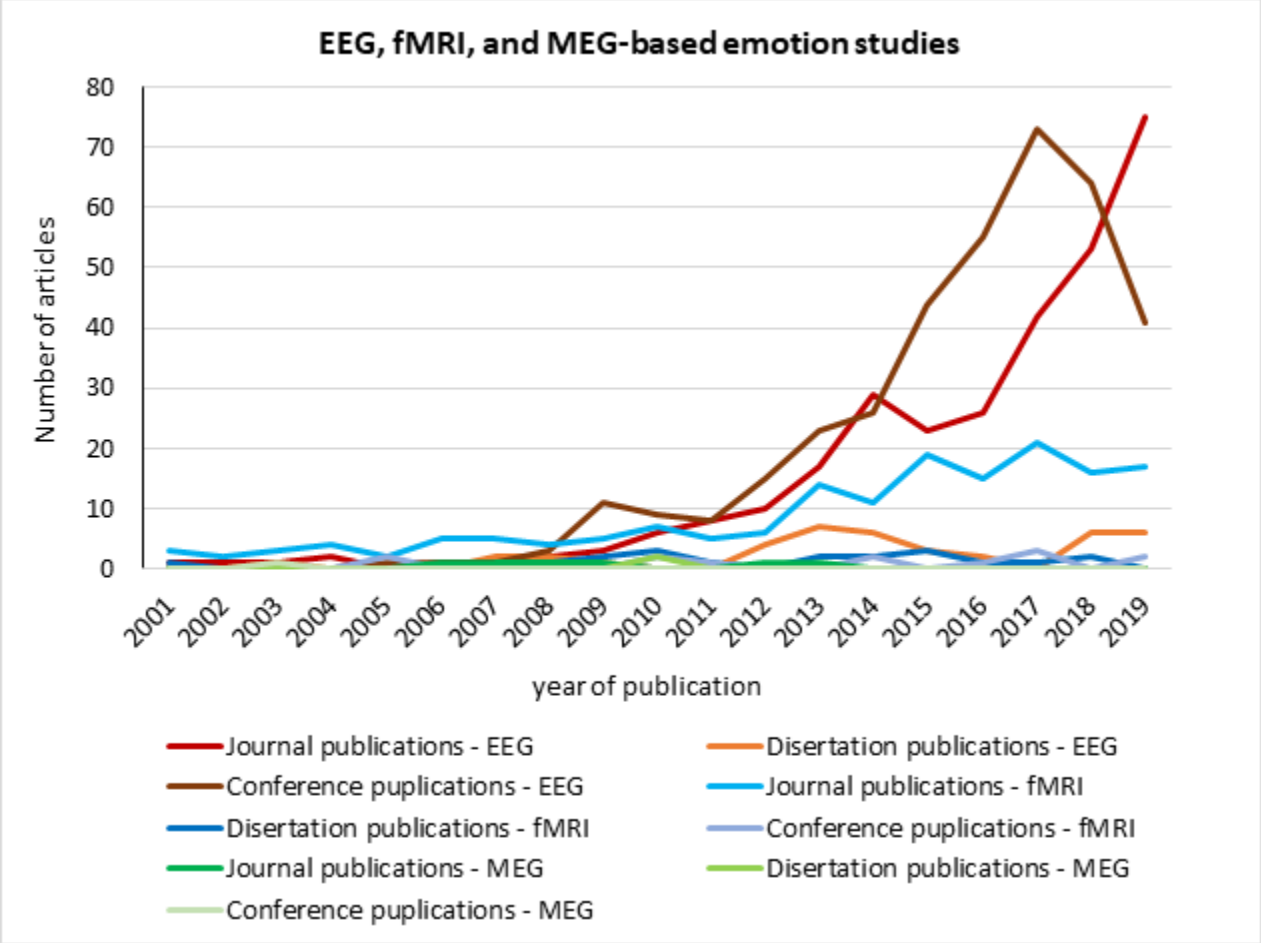

Figure 2-12. Chronological trends of literature (extracted from Google Scholars on 12th December 2015 and updated on 19th January 2020), the keywords used here were: "EEG emotion", "fMRI emotion", and "MEG emotion" with restriction of keywords being all in the title of the article.

The general format for brain-activity based emotion recognition studies in the literature include three main phases: (i) identify emotion of interest, (ii) stimulate or induce this emotion into the participant while recording the brain activity, and (iii) analysing the recorded brain-activity to deduct findings.

2.3.1 Emotion Definition – 'identifying the emotion of interest'

The main challenge in detecting emotions from brain activity is the lack of a reliable neural ground truth for the detection which is worsened by discrepancies in emotion definitions across the literature.

Emotional state can be defined as "*interrelated and synchronized changes"* in psychological and physiological states (Scherer, 2005); this definition implies that human emotion processing is rather complex. In many instances in the literature, the terms 'affect' and 'emotion' are utilised interchangeably even though the term 'emotion' covers a subset of affective states. The affective states can be defined as psychological states associated with some appraisal, and these states include emotions (e.g., happy, sad, and angry), moods (e.g., grumpy), and stress responses(Gross, 2015). Several models of emotion, based on experiments or social observations, have been proposed to allow emotion measurements or detection to some extent. The proposed models include multidimensional models (e.g. arousal-valence models) and basic emotion models.

2.3.1.1 Multidimensional Model

The popular multidimensional model is the valence-arousal model, also known as Russel model (Russell, 1980), emotional state is identified using arousal and valence coordinates as shown in Figure 2-13. The arousal coordinate varies between positive activation or excitement and negative activation (deactivation) or sleepy. The valence coordinate varies between pleasant (positive valence) and unpleasant (negative valence). In some studies, the ground truth for emotions experienced by participants is collected as subjective arousal-valence ratings using self-assessment manikin (SAM) which is a non-verbal pictorial assessment technique (Bradley and Lang, 1994) shown in Figure 2-14 or versions of SAM such as the affective slider by (Betella and Verschure, 2016) shown in Figure 2-15. After an emotional stimulus is presented to a participant, the SAM is used to map the emotion felt into the arousal-valence coordinates. Based on the pleasantness rating, some emotions are labelled negative emotions (those with negative valence) and other positive emotions (those with positive valence).

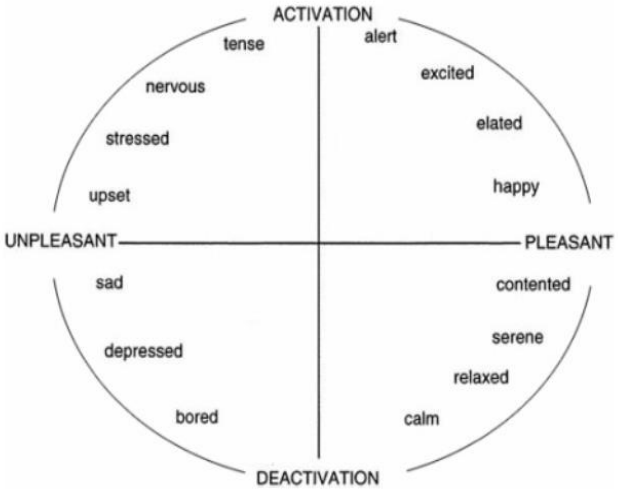

Figure 2-13. Emotions mapped using valence (pleasant/unpleasant) and arousal (activation/deactivation) coordinates (Posner et al., 2005)

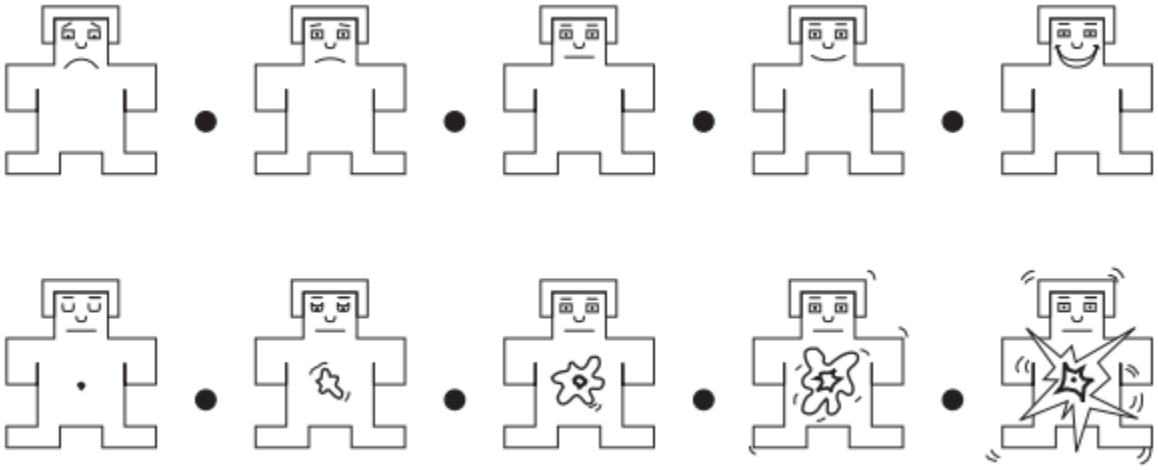

Figure 2-14. SAM valence (unpleasant -- pleasant, on top row) and arousal (sleepy -- widely awake, on bottom row), the black disks shows the middle point between successive graphics on each row. There are two standard scales: 1-5 discrete ratings (only graphics holds the ratings on each row) and 1-9 continuous ratings (ratings are obtained from clicking on graphics or anywhere between two successive graphics on each row).

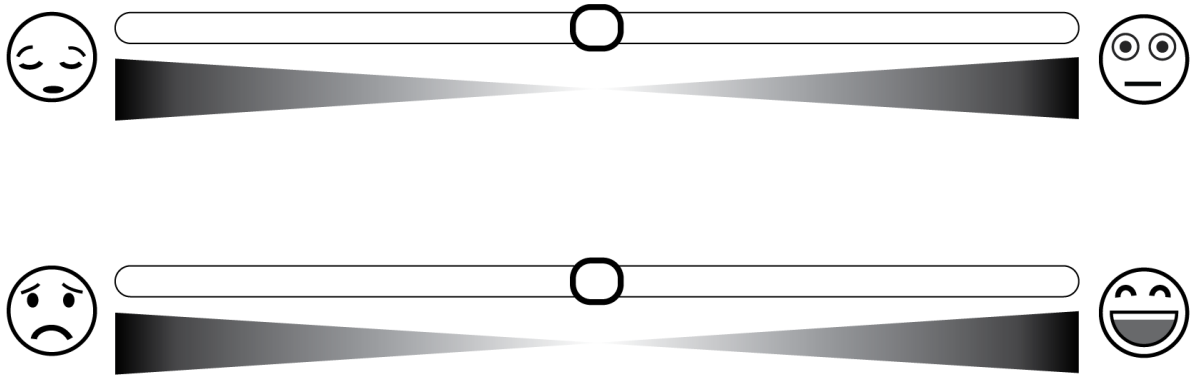

Figure 2-15. Affective slider bars: arousal (sleepy – widely awake bar, on top) and valence (unpleasant – pleasant bar, on bottom), the ratings are selected by clicking and sliding each button (shown in the middle of each bar) to an appropriate position corresponding to self-assessment of one's felling; with ratings reported from 0 to 1 with a 0.01 step.

2.3.1.2 Basic Emotions

On the other hand, basic emotions model lists emotional states argued to be universal with identifying names and suggests each of these states to have specific physiological characteristics (Ekman, 1999).

The most popular basic emotions are: angry, afraid, happy, sad, surprise, disgusted, and amused. However, with the current limited knowledge on emotion processing in the brain, there is a challenge in associating each emotion on the list of basic emotions with corresponding neural activities. Furthermore, it has been reported that there are individual differences in neural processes associated to emotional stimuli (Hamann and Canli, 2004). This makes it harder to argue for universality of the basic emotions.

2.3.2 Inducing Emotion of Interest

One of the crucial steps involved in emotion studies is inducing targeted emotions into the participants. In the literature, emotions are stimulated by internal stimulus such as mental activities, e.g., happy memory recall. Apart from internal stimulus, emotions are stimulated by external stimuli through the sensory system. The external stimuli include emotional images, sounds, and combination of sounds and visuals.

2.3.2.1 Emotion Stimulation by Videos, Audio or Pictures

During data acquisition for an emotion recognition study, emotions are often stimulated into the study's participants by presenting participants with emotional videos, sounds, or pictures stimuli. Some research groups have provided database of standardized stimuli for emotion studies. Lang and colleagues have provided the international affective picture system (IAPS) (Lang et al., 2008), a database of pictures for emotion elicitation. Bradley and colleagues also provided a database of sounds for emotion elicitation, the international affective digital sounds (IADS) (Bradley and Lang, 2007). Another database of pictures used in emotion studies is the Geneva affective picture database (GAPED) (Dan-Glauser and Scherer, 2011). The participants are usually asked to passively attend emotional stimuli. In some cases, participants are asked to attempt to feel the emotion represented by or loaded in the stimuli.

Few datasets of neurophysiological data, collected while the participants were being presented with videos stimuli, are available for emotion recognition methods assessment. These datasets include the database for emotion analysis using physiological signals (DEAP) (Koelstra et al., 2012), multimodal database for affect recognition and implicit tagging (MAHNOB HCI) (Soleymani et al., 2012), and Jiao Tong University emotion EEG dataset (SEED) (Zheng and Lu, 2015). The SEED dataset contains EEG data from 62 EEG electrodes from 15 participants, collected while they were presented with video clips targeting positive, negative, and neutral emotions. The DEAP dataset contains 32 EEG electrodes data and peripheral signals (galvanic skin response, respiration pattern, skin

temperature, electromyogram, and electrocardiogram) from 32 participants, and data were recorded while participants watched 40 one-minute long video clips. The MAHNOB HCI contains 32 EEG electrodes data and peripheral physiological data (respiration pattern, skin temperature, and electrocardiogram) from 30 participants while they were watching movies clips and pictures. The MAHNOB HCI also contain the synchronized monitoring data: from 6 video cameras, head-worn microphone, and from eye gaze tracker.

2.3.2.2 Self-Inducing Emotion

Emotions can be stimulated into participant by the participant engaging in mental activity (Damasio et al., 2000) (Smith et al., 2006). For example, Chanel and colleagues stimulated emotions by asking the participants recall past emotional episodes (Chanel et al., 2009). The fact that the participant actively participates in the emotion stimulation allows further application of such self-induced emotions. The self-inducing approach can be used to control some applications through BCI as shown by Makeig and colleagues in their musical emotional BCI (Makeig et al., 2011). The self-inducing approach is investigated further in the studies reported in chapters 4 and 5.

2.3.3 Brain structures involved in emotion processing

There certainly still is a lot to be uncovered about emotions processing in the brain, nevertheless researchers have identified some CNS behaviours associated with emotions. Several researchers described the neural circuits contributing to emotional processes; circuits that include hippocampus, insula, amygdala, anterior cingulate, and prefrontal cortex (PFC) (Davidson et al., 2003) (Dalgleish, 2004) (Barrett et al., 2007) (Kohn et al., 2014); Figure 2-17 shows some parts of this neural circuitry. The amygdala is more activated in the negative compared to positive emotions (Davidson, 2002), and amygdala has been associated with fear regulation (Numminen-Kontti, 2014). Right hemisphere activation has been associated with negative emotions (e.g., fear, anger, and disgust) and the left hemisphere with positive emotions (e.g., happy, joy). Davidson and colleagues, using EEG, observed less left anterior temporal and frontal alpha power (more activation) associated with "*approach"* and more activation of right anterior temporal and frontal cortex associated with "*withdraw"* (Davidson et al., 1990) (Davidson uses "*approach"* for emotions where ones tends to act (with a notion of reward), and he also uses *"withdraw"* for emotions where ones tries to withdraw (with a notion of punishment). Their EEG asymmetry was consistent with Ahern and Schwartz' s EEG spectral analysis study (Ahern and Schwartz, 1985). This asymmetry was also consistent with the findings of Robinson and colleagues in their studies on patients with brain injury. They found that patients with lesions in the left frontal brain area are more depressed than those who with lesions in other brain

areas (Robinson et al. , 1984). In this case of lesions in the left frontal areas, there is an inability to express positive emotion since the left side is damaged, an inference made by Davidson and colleagues (Davidson et al., 1990). The frontal asymmetry seems to be a useful marker for affective processing (Reznik and Allen, 2018).

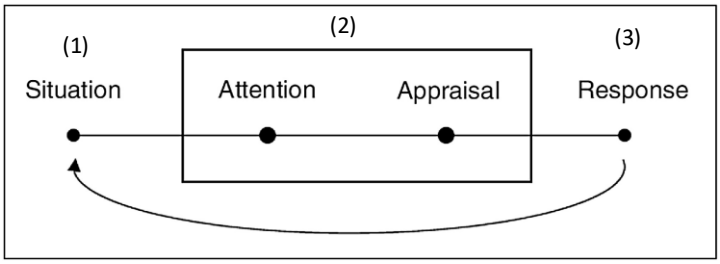

Figure 2-16. Modal model of emotion with three main steps: (1) attending the stimulus, (2) appraising the stimulus, and (3) producing emotion response

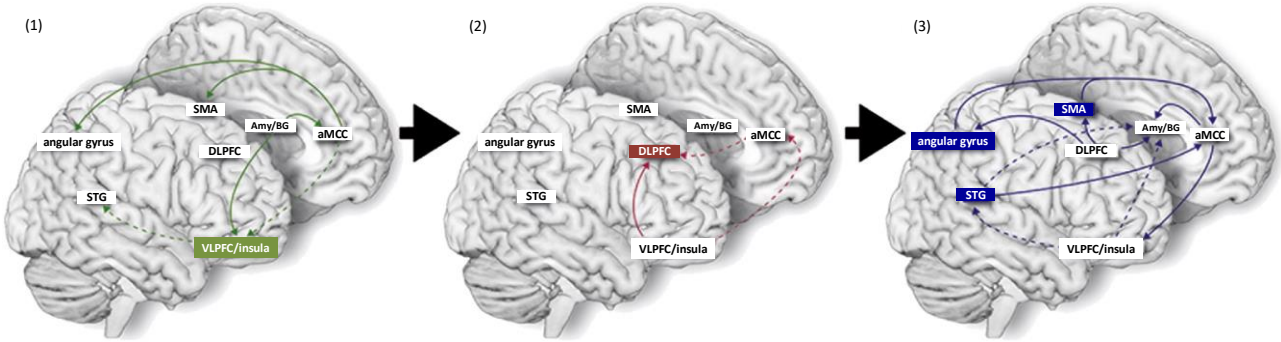

Figure 2-17. The activated network during emotion processing (prepared based on illustration from (Kohn et al., 2014)). The three steps presented in modal model of emotion processing are shown here. The activated neural circuitry includes: ventrolateral prefrontal cortex (VLPFC), dorsolateral prefrontal cortex (DLPFC), supplementary motor area (SMA), angular gyrus, amygdala (Amy), basal ganglia (BG), superior temporal gyrus (STG), and anterior middle cingulate gyrus (aMCC).

The current understanding on neural circuitry for emotion processing is mainly based on the modal model of emotion (Gross and Thompson, 2007) (Gross, 2015) (Palmer and Alfano, 2017). This model considers three main stages: (1) a subject is in the presence of an emotion-eliciting stimulus, (2) pays attention to and appraises that stimulus, (3) and then generates an emotional response as shown in Figure 2-16. The process repeats if the stimulus is still present. The meta-analysis of studies utilising this model (Kohn et al., 2014) found interaction between the ventrolateral prefrontal cortex (VLPFC), dorsolateral prefrontal cortex (DLPFC), supplementary motor area (SMA), angular gyrus, amygdala (Amy), and basal ganglia (BG). With respect to the modal model of emotion, the stimulus evaluation

is via Amyg and BG to the VLPFC and SMA, superior temporal gyrus (STG), angular gyrus, and anterior insula, see Figure 2-17(1), then the VLPFC informs the DLPFC that the affective regulation is needed, see Figure 2-17(2). DLPFC carries out the regulation process and sends feedforward signal to SMA, angular gyrus, STG, Amy, anterior middle cingulate gyrus (aMCC), and BG which participate in generating regulated affective state, see Figure 2-17(3).

2.3.4 Brain-activity based emotion classification studies

The studies of emotions based on brain-activity follow closely the standard BCI processing stages. After acquiring the brain-activity data, the data processing phase includes pre-processing, features extraction, features selection, classification, and the classification output is used as input to an application or to drive the feedback presented to the participant. This section looks at several popular data processing methods used in emotion recognition/classification studies.

The TABLE 2-3 shows sample studies on emotion classification based on EEG, and features extracted in the studies are shown as well. As shown in the sample studies, the popular features extraction methods found in EEG-based emotion recognition literature include frequency-domain features extracted through Fourier transform-based methods such as fast Fourier transform (FFT), periodogram, and Welch method (Palaniappan, 2010), time-domain features extracted as statistical measures of the signal or other temporal behaviours such as event-related potentials (ERPs), and features based on methods providing both temporal and frequency resolutions such as wavelet decomposition (Murugappan et al., 2009b), event-related (de)synchronization (ERD/S), (Pfurtscheller, 1992) and short-time Fourier transform (STFT) (Chanel et al., 2009).

TABLE 2-3. SAMPLE STUDIES OF EMOTION RECOGNITION/CLASSIFICATION UTILIZING TIME-DOMAIN, FREQUENCY DOMAIN OR TIME-FREQUENCY DOMAIN FEATURES

Source	Classes	subj	# EEG sensors	Bands	Features	Extraction methods	Trials / class	Classifier	CA (%)
(Murugappan et al., 2009a)	disgust, happy, surprise, sad and anger	5	64 (IS)	alpha	energy, power	DWT	5	MLP-BP	63.3
(Chanel et al., 2009)	calm, positive, negative	11	64 (IS)	4-22Hz	spectrograms	STFT (2Hz bands)	100	SVM	63
(Murugappan et al, 2010)	disgust, happy, surprise,	25	62 (IS)	Alpha, beta, and gamma	ALREE	DWT	5	KNN	83.26

	neutral and fear								
(Frantzidis et al., 2010)	HV/HA, HV/LA, LV/HA, and LV/LA	28	3 (Fz, Cz, Pz)	Delta, theta, and alpha	Latency and Ampl. for P100, N100, P200, N200, and P300 Ampl. of EROs	DWT	40	SVM	81.3
(Petrantonakis and Hadjileontiadis, 2010)	happy, surprise, anger, fear, disgust, and sad	16	3 (Fp1, Fp2, and F3/F4)		high order crossing (HOC)		10	SVM	83.33
(Wang et al., 2011)	joy, relax, sad, and fear	5	62 (IS)		μ_S, σ_S, δ_{S_1}, norm_δ_{S_1}, δ_{S_2}, and norm_δ_{S_2}		3	SVM	43.39
(Anh et al., 2012)	angry, happy, sad, neutral, and relaxed	96	3 (FC6, AF3, F4)		Fractal dimension (FD)	Higuchi method	40	SVM	70.5
(Valenzi et al., 2014)	sad, amused, neutral, and disgust	9	32 (IS)	Delta, alpha, beta, and gamma	average magnitude of band spectral power	STFT	4	SVM	97.2
(Bajaj and Pachori, 2014)	happy, neutral, sad, and fear	8	Fp1, Fp2, F3, F4		ratio of the norms, Shannon entropy and normalized Renyi entropy measures	Multiwavelet decomposition	5	SVM	84.79
(Mert and Akan, 2018)	2 classes (LV vs HV)	32	32 (IS)			MEMD	20	ANN	75
(Li et al., 2018)	positive, neutral, negative	15	62 (IS)			Entropy, and t-f features	15	SVM	83.33
(Nakisa et al., 2018)	4 classes (HVHA, HVLA, LVLA, LVHA)	32	32 (IS)			Statistical features and t-f features	10	PNN	67
(Alazrai et al., 2018)	4 classes (HVHA, HVLA,	32	32 (IS)			Statistical features and t-f features	10	SVM	60.50

	LVLA, LVHA)								
(Chao et al., 2019)	2 classes (LV vs HV)	32		Theta, alpha, beta, and gamma	band spectral power		20	capsule network	68.2
(Gupta et al., 2019)	HV/HA, HV/LA, LV/HA, and LV/LA	32		Theta, alpha, beta, and gamma		DWT	10	random forest with SVM	72.07

2.3.4.1 Time-domain features

The EEG time-domain features used for emotion recognition includes event-related potential (ERP), statistics of the recorded EEG, and measures such as Hjorth descriptors (Jenke et al., 2014).

2.3.4.1.1 ERP features

The stimulus presentation usually causes some voltage changes in the subject's EEG. These changes usually require the averaging of several trials for a particular stimulus in order to establish a relationship between that stimulus and corresponding changes. This requirement creates a downside for real-time systems, but ERPs can still be used in offline analysis. Considering emotion studies, some researches have correlated ERPs with emotional states. In their review, Olofsson and colleagues highlighted that the amplitude of P3b, one of the subcomponents of P300, is larger for high valence pictures (Olofsson et al, 2008).

2.3.4.1.2 Statistical features

The commonly used statistical measures, as in (Takahashi, 2004; Wang et al., 2011), are often the EEG power (p_S), mean (μ_S), standard deviation (σ_S), 1st difference (δ_{S_1}), normalized 1st difference ($norm\_\delta_{S\_1}$), 2nd difference (δ_{S_2}), and normalized 2nd difference ($norm\_\delta_{S\_2}$). These values are computed as in expressions (2-15) to (2-21):

$$p_S = \frac{1}{k}\sum_{t=1}^{k}|s(t)|^2 \qquad (2\text{-}15)$$

$$\mu_S = \frac{1}{k}\sum_{t=1}^{k}s(t) \qquad (2\text{-}16)$$

$$\sigma_s = \left(\frac{1}{k-1} \sum_{t=1}^{k} \left(s(t) - \mu_s \right)^2 \right)^{1/2} \quad (2\text{-}17)$$

$$\delta_{s\_1} = \frac{1}{k-1} \sum_{t=1}^{k-1} \left| s(t+1) - s(t) \right| \quad (2\text{-}18)$$

$$\delta_{s\_2} = \frac{1}{k-2} \sum_{t=1}^{k-2} \left| s(t+2) - s(t) \right| \quad (2\text{-}19)$$

$$norm\_\delta_{s\_1} = \frac{\delta_{s\_1}}{\sigma_s} \quad (2\text{-}20)$$

$$norm\_\delta_{s\_2} = \frac{\delta_{s\_2}}{\sigma_s} \quad (2\text{-}21)$$

where, $S(t)$ is the EEG signal sample at time t, with $t = 1,2,3, \ldots K$

Other related statistic measures are the Hjorth features which are composed of the activity, mobility (M_S) and complexity (C_S) measures. The activity is the variance of the signal while the mobility is computed as: $M_S = \frac{\sigma_{S'}}{\sigma_S}$ where S' is the signal's 1st derivative, and the complexity is given as: $C_S = \frac{M_{S'}}{M_S}$ (Palaniappan, 2010).

2.3.4.1.3 Fractal dimension

Additional to the statistical measures, other relevant time-domain features found in recent emotions detection studies include fractal dimension (FD) (Anh et al., 2012) and high order crossing (HOC) (Petrantonakis and Hadjileontiadis, 2010). Fractal dimension estimates the irregularities in the signal. The Higuchi method is the most common FD feature extraction method in emotion classification literature; this method is described in the following section: assuming a time series, $s(1), s(2), \ldots, s(k)$, let's build another n time series S_m^n as in

$$s_m^n = \left\{ s(m), s(m+n), s(m+2n), \ldots, s\left(m + \left\lfloor \frac{K-m}{n} \right\rfloor n \right) \right\} \quad (2\text{-}22)$$

where $m = 1,2, \ldots, n$; m denotes the time point and $n = 1,2, \ldots, n_{max}$ which is the delay between the time points

The averaged length for each time series, $l_m(n)$ is computed as in (2-23), and the total average length for all the time series $L(n)$ for a particular delay n is computed in (2-24) and is proportional to n^{-D},

with *D* being the Higuchi fractal dimension of the signal. *D* is the slope estimated from the plot of $ln\,L(n)$ against $ln\frac{1}{n}$

$$l_m(n) = \frac{K-1}{n^2\left\lfloor \frac{K-m}{n} \right\rfloor} \sum_{i=1}^{\left\lfloor \frac{K-m}{n} \right\rfloor} \left| s(m+in) - s(m-n+in) \right| \qquad (2\text{-}23)$$

$$L(n) = \sum_{m=1}^{n} l_m(n) \qquad (2\text{-}24)$$

2.3.4.2 Frequency-domain features

Power spectral density (PSD) analysis in different frequency bands of EEG is widely used in brain activity-based emotion classification studies. The analysis usually considers the brain power in theta band (0.5-4Hz), delta band (4-8Hz), alpha band (8-13Hz), beta band (14-30Hz), and gamma band (>30Hz) at different scalp locations. The goal is to extract different frequency content (PSD features) in EEG signal for different brain states associated to processing given emotional stimuli or events. The frequency features are often extracted as the band power, or power derived features such as spectral asymmetry measures.

2.3.4.2.1 Band power

The power spectrum in EEG rhythm bands is usually extracted using the fast Fourier transform (FFT) algorithm. Depending on the desired resolution or computational efficiency several PSD estimation methods are used including short-time Fourier transform (STFT), periodogram and Welch method (Palaniappan, 2010). Beside taking the entire EEG bands, the band power is often extracted from small frequency bins (e.g., 2Hz) as in (Chanel et al., 2009).

2.3.4.2.2 Emotions asymmetry based features

The emotion lateralization in the brain is exploited in hemispheric asymmetry feature extraction. The extracted features are often the difference or ratios of band powers at two locations one on the left and the other on right side (Lin et al., 2010a) (Huang et al., 2012) (Soleymani et al., 2012). Ratios, are usually used to determine the levels of stimuli response; for example the *beta/alpha* ratio can be used to detect the arousal of the subject (Zhou et al., 2014) (Huang et al., 2012).

2.3.4.3 Time-frequency domain features

In some of the brain activity-based emotions studies have utilised time-frequency methods such event-related de/synchronisation (ERD/S) and wavelet transform. The ERD/S is used as previously described in the previous section on BCI systems. Regarding the wavelet transform analysis, the discrete wavelet transform (DWT) is often used in EEG signal decomposition while keeping a high time-frequency resolution. EEG is decomposed into *detail coefficients* relating to high frequency EEG and *approximation coefficients* relating to time-domain estimation of the original EEG by correlating a wavelet function with EEG signal:

$$c_{s(t)}(a,b) = \int_{-\infty}^{\infty} s(t) w_{a,\mathrm{b}}(t) dt \qquad (2\text{-}25)$$

where *s(t)* is the brain activity signal (e.g., EEG), and *a* and *b* are respectively the scaling and translation factors for the wavelet function $w_{a,b}(t)$. Interesting results have been achieved using DWT to isolate EEG frequency bands of interest, which are then used to compute various features such as variance, standard deviation, power, and entropy (Murugappan et al., 2009b), amplitudes of event-related oscillations in delta, theta and alpha rhythms (Frantzidis et al., 2010). The resulting coefficient from DWT decomposition can be directly extracted as features and these feature types can achieve relatively high classification accuracy compared to entropy or energy features (Yohanes et al., 2012). Other interesting results have been achieved, about 84% classification accuracy for 4 different emotion classes, utilizing multiwavelet decomposition for entropy features extraction (Bajaj and Pachori, 2014). Further measures can be derived from the computed energy and/or entropy, and these measures are usually extracted as features for emotion classification. Measures such as *recursive energy efficiency* (REE) with its derived measures: logarithm of REE (LREE) or absolute logarithm REEE (ALREE) has also led to good classification accuracy in (Murugappan et al., 2010) where the band's REE was computed as a ratio of energy of one band over the total energy in the considered bands:

$$REE = \frac{E_{band}}{E_{alpha} + E_{beta} + E_{gamma}} \qquad (2\text{-}26)$$

2.3.5 Emotion classification studies to emotion-inducing imagery studies

The literature of emotion classification studies based on brain activity shows that various emotional states can be distinguished based on the associated neural activity. This distinction of neural correlates of emotions is achieved by using time-domain, frequency-domain and/or time-frequency dynamics

of the brain activity signals. The majority of the studies utilise the features extracted from the theta, alpha, beta, and gamma bands, and the time-frequency features seems give highest classification accuracies (Alarcao and Fonseca, 2017) (Shu et al., 2018). From EEG perspective, commonly used electrodes in emotion classification studies are (in their order of frequency): F4, F3, T7, FP1, FP2, T8, F7, F8, O1, P7, P8, O2, FC5, FC6, C4, C3, AF3, AF4, P3, P4, and Pz (Alarcao and Fonseca, 2017). The montage of these commonly used electrodes is shown in Figure 2-18. Electrodes setup depends on the kind of emotions being considered. In general the electrodes covering frontal and temporal areas are used as they are likely to pick up brain activity associated with emotion processing and presented stimuli. Electrodes over the visual processing area are used to detect activity associated with present visual stimuli. A subset of electrodes that gives the highest classification accuracy is usually obtained through features selection algorithm.

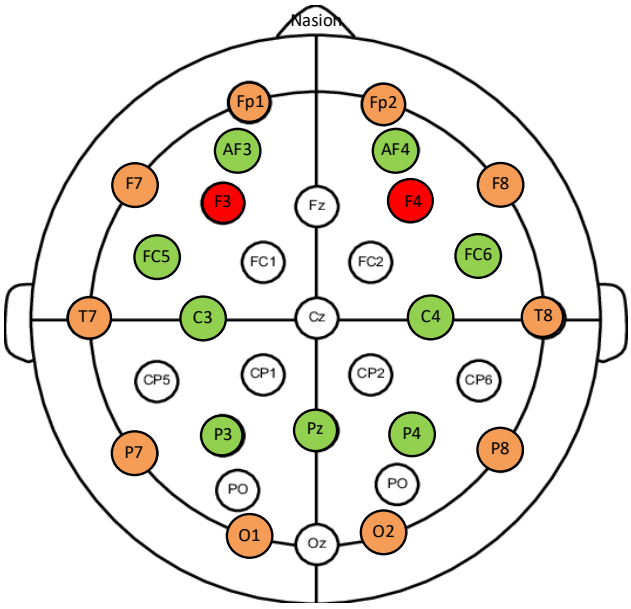

Figure 2-18. Most frequent EEG electrodes considered in emotion classification studies. Colour red indicates very high frequent, orange for high frequent, and green for moderate frequent.

The literature review identified some limitations and challenges found in emotion classification studies. These include the lack of a consistent definition for emotion classes across the literature, especially where discrete emotions are used. This variation in definition for classes of emotion makes it hard to compare the results from different brain activity-based emotion classification studies. Another challenge is the fact that there are only few datasets available for brain activity-based emotions studies, thus neural activity data acquisition is a crucial component in most emotion studies which then leads to variations in data and experimental setup. Furthermore, most of the state-of-the-art BCI signal processing methods have not been explored in emotion classification studies, and the

literature review shows that there are only few previous attempts of emotion-inducing imagery. Most of these previous emotion-inducing imagery are shown in Table 2-4, only peer-reviewed journal publications or book/book chapters were considered here. The main gap in most of the previous studies is the lack of feedback presentation to the participants, so EII was not really used in the context of BCI. In some of the studies a discrete feedback was provided to the participants, and wide window (> 8 s) was considered to provide this feedback (Makeig et al., 2011) or even participants were self-paced in carrying out the EIIs (Chanel et al., 2009). The other gap is the fact that these previous studies were based on small sample of participants, and the studies were based on signals recorded in one session. In this thesis, state-of-the-art motor-imagery BCI methods (i.e., FBCSP and NTSPP) are explored as emotion-inducing imagery signal processing frameworks.

TABLE 2-4. RELEVANT STUDIES EXPLOITING EMOTION-INDUCING IMAGERY

Source	Classes	subj	setup	Bands (Hz)	Features	Extraction methods	Trials/ class	Classifier	CA (%)	Online feedback
(Chanel et al., 2009)	Negative, positive imagery, and relax	11	64(IS)	4-45	t-f features	STFT	100	SVM	70.0	No online
(Makeig et al., 2011)	5 classes	1	128 (IS)	30-200	Log of variance	CSP	2	LDA	64.5	Discrete (audio)
(Sitaram et al., 2011)	3 classes (happy, disgust, and sad)	12	n/a (fMRI)	n/a	Effect maps	Intensity thresholding	12	SVM	60	Discrete (visual)
(Iacoviello et al., 2015)	Relax and disgust	10	8 (IS)			DWT	100	SVM	90.7	No online

2.4 Conclusion

The background for BCI systems was covered in this chapter, and the recent literature show that there have been significant progress in BCI development. This development include state-of-the-art neuroimaging signal processing and relevant features extraction methods. Despite the progress in BCI

systems, some users have been reported unable to one or all of the existing BCI systems, and investigation into alternative BCI approaches for the users is ongoing.

Also in this chapter, brain activity-based emotion classification studies were reviewed, and this review show that emotions can be reliably distinguished based on associated neural correlates. These studies follow the similar framework as the BCI framework, a framework that includes neural activity data acquisition, pre-processing, features extraction and selection, classification, and in some cases the feedback. The fact that emotions can be recognized from brain activity data creates an opportunity to augment the BCI by emotion recognition. The author exploits this opportunity in chapter 4 and 5 by investigating the emotion-inducing imagery as an alternative control approach for BCI.

CHAPTER 3

3 AUTOMATED ARTEFACTS REMOVAL FOR EEG-BASED EMOTION CLASSIFICATION

In this chapter, research completed on assessing various methods for removing artefacts from EEG signals is outlined. The methods assessed in this chapter include the band-pass filter, manual independent component analysis (ICA), artefact detection approach based on joint spatial and temporal characteristics (ADJUST), and the hybrid ICA-wavelet transform method (ICA-W). EEG signals from the DEAP dataset are used to assess these artefacts removal methods, and the resulting classification accuracies are reported for various setups. The contribution made in this chapter has been published in .(Bigirimana et al., 2016)

3.1 Introduction

One of the current trends in electroencephalographic (EEG)-based emotion recognition application is reducing human intervention in processing the EEG, automatizing emotion recognition systems as much as possible. This automatization should include noise and artefact removal techniques. The common artefacts in EEG include power line noise and physiological artefact mainly originating from heart activity – electrocardiography (ECG), eye movements or blinking – electrooculography (EOG), head and neck muscle activity – electromyography (EMG), and potentials from the brain (cephalic noise) not associated with the task (Nicolas-Alonso and Gomez-Gil, 2012). Emotion related brain activity involves several processes, including processing the emotional stimulus, production of an affective state in response to the stimulus, and the regulation of the affective state (Phillips et al., 2003) (Gross, 2015). With all these processes in the brain, additional artefacts can be detrimental to the discriminability of emotions from EEG.

Digital filters are widely used to reduce artefacts by extracting the relevant brain rhythms of interest, namely delta (0.1-4Hz), theta (4-8Hz), alpha (8-13Hz), beta (13-30Hz), and gamma (>30Hz), from the recorded data. Using appropriate bandpass filters, artefacts can be reduced assuming the artefacts' frequencies do not overlap with the targeted band. EMG artefacts cover a wide frequency range (from 0 to >200Hz) and are predominantly present in EEG frequencies higher than 20Hz [2, 3], especially in the temporal electrodes. In some studies, EOG artefacts are removed through adaptive filtering (Jafarifarmand and Badamchizadeh, 2013) however, this method requires recording the EOG reference

signal and may alter the non-artefactual EEG due to some EEG leaked in the artefact reference sensor. Other studies [6, 8] use independent component analysis (ICA), a blind source separation approach, to remove the EOG, EMG and ECG artefacts from EEG. ICA decomposes the signal into statistically independent components, and the artefactual components can be identified by visual inspection and removed. The cleaned signal is then obtained by recombining the remaining non-artefactual components.

Visually inspecting the independent components for artefacts requires some level of expertise, to identify artefacts in the EEG signal. This can be time consuming when dealing with large datasets or data recorded from multiple subjects. To automate this process, various methods including correlating the independent components with recorded reference artefacts (Hsu et al., 2012) and thresholding based on high order statistics of the independent components (Delorme et al., 2007) have been proposed. Castellanos et al (Castellanos and Makarov, 2006) have proposed a wavelet transform based approach to filter out artefacts from ICA generated independent components, an approach that can be automated. Other approaches for automation of artefact removal using ICA include an artefact detection approach based on joint spatial and temporal characteristics to identify artefactual components, a method also known as ADJUST (Mognon et al., 2011). The work in this chapter compares, for the first time, the performance of artefact removal of standard ICA and the ICA-wavelet (ICA-W) transform hybrid on emotion-related EEG signals classification. With the achieved classification accuracies we show that ICA-W can outperform the standard ICA-based method, and that the significant increase in accuracy is achieved in classifying statistical and wavelet features of the signal.

3.1.1 ICA-Based Artefacts Removal

The ICA algorithm assumes that the recorded EEG is a linear combination of temporal, independent and spatially fixed signals, and the algorithm estimates these independent components. The artefactual components are removed, and the remaining components are recombined into cleaned EEG data. This approach has been effective in removing noise and artefacts from EEG data (Jung et al., 2000). ICA-based artefact removal can be summarized in the following steps (where is it is assumed that EEG data were recorded using N electrodes): first, decompose the EEG data, X, into S containing n statistically independent components. Each signal (signal from each EEG channel) in X has M samples (with $n \leq N$). This decomposition is done with the assumption of linear mixing of the components and through estimation of an un-mixing matrix A:

$$S = AX \qquad (3\text{-}1)$$

The computed independent components are then inspected for artefacts, and artefactual components are set to zero. And finally, the remaining components are remix with an inverse of the un-mixing matrix *A* to get cleaned data:

$$X = A^{-1}S \qquad (3\text{-}2)$$

The ICA algorithms usually assume that the number of sources contributing to EEG data are less than or equal to the number of data channels (sensors), so ICA can only generate a number of independent components less than or equal to the number of channels. If there are only a limited number of channels, some cortical activity may be lost into artefactual components leading to alteration of neural content of the EEG. One of the solutions to this problem is to separate the leaked cortical signal from the noise in the generated components. This separation can be achieved by applying discrete wavelet transform (DWT) on the components, decomposing them into artefactual segments and residual segments (Castellanos and Makarov, 2006), then thresholding the resulting wavelet coefficients; note that the wavelet thresholding is applied after ICA (which leads to the notation 'ICA-W'). The wavelet thresholding process assumes that each of the components, especially artefactual components, is a sum of neural signal and Gaussian noise. Components are reconstructed by applying inverse DWT, and resulting components are remixed into cleaned EEG signal as in (3-2). The computation complexity in ICA-W can be reduced by using spatial constrained ICA followed by wavelet thresholding of the resulting independent components (Akhtar et al., 2012). The first step in this constrained ICA-W is to define the spatial constraints, usually done based on the signal sensor topographies.

The ICA-W was previously compared with regular ICA in (Castellanos and Makarov, 2006). Using simulated data ICA showed possible alterations in spectral content whereas ICA-W did not. In our evaluation, we compare the ICA-wavelet hybrid and regular ICA on their effect on classification of emotional states from real EEG data.

3.2 Methods

3.2.1 Data Acquisition

The data used in this study are taken from the database for emotion analysis using physiological signals, DEAP (Koelstra et al., 2012), acquired from Queen Mary University of London. In this dataset, 32 EEG electrodes, placed according to 10-20 system, were recorded at a sampling rate of 512 Hz. The data were recorded from 32 healthy subjects while they watched selected videos that stimulate different emotions. The videos were selected according to ratings attributed to them in terms of the

level of arousal and valence by volunteering subjects before the recordings. Forty videos were selected, 10 videos for each of the quadrants in the arousal-valence model (Russell, 1980), see Figure 3-1, and each video was 60 seconds long. In the current study, each of the quadrants is considered as one class of emotion, i.e., high/low arousal-valence (HAHV, LAHV, LALV, and HALV). Besides, volunteers' ratings, after each trial, the participant ranked the video's valence and arousal on a continuous scale of 1 to 9. In order to reinforce the trials labelling, only 14 participants who achieved correlation of 0.5 between their ratings and the volunteers' rating were considered in the current study.

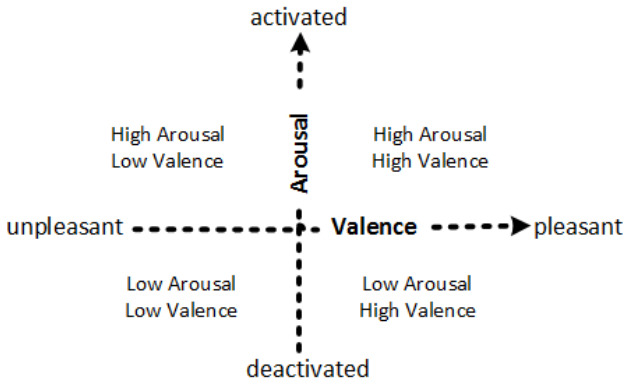

Figure 3-1.Valence-Arousal model used to map the participants' video ratings

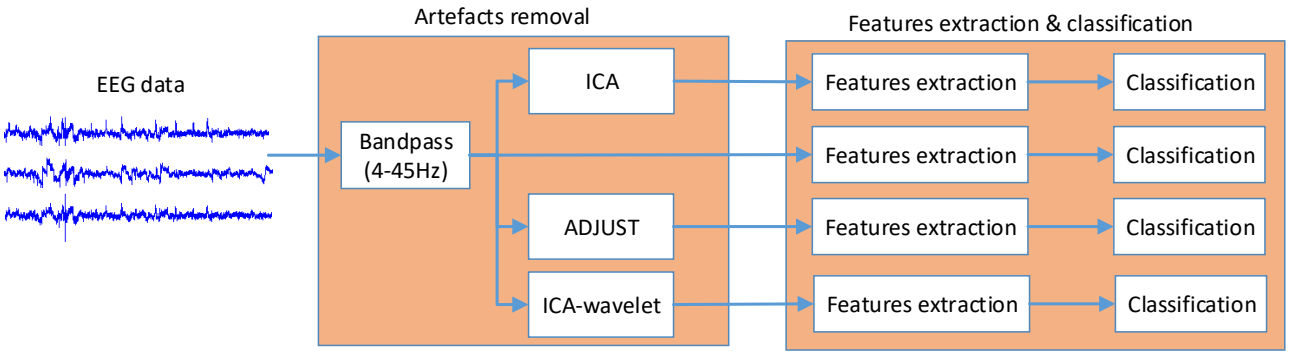

Figure 3-2. The four signal processing frameworks compared

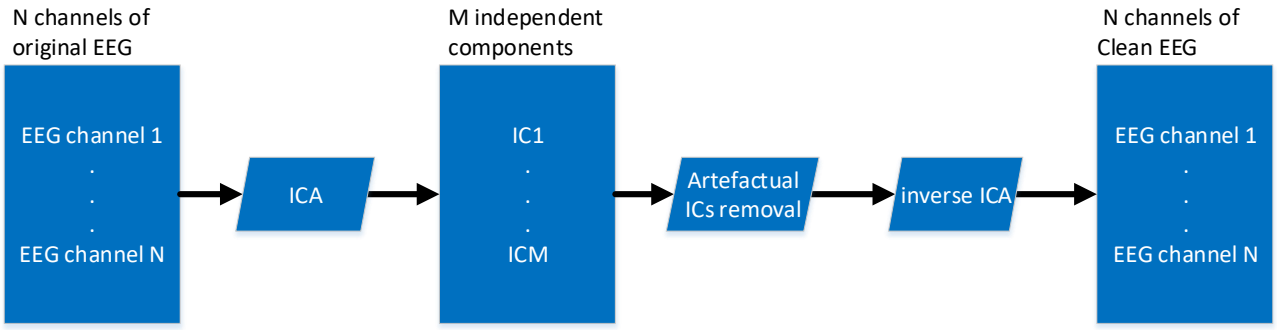

Figure 3-3. Regular ICA based artefact removal

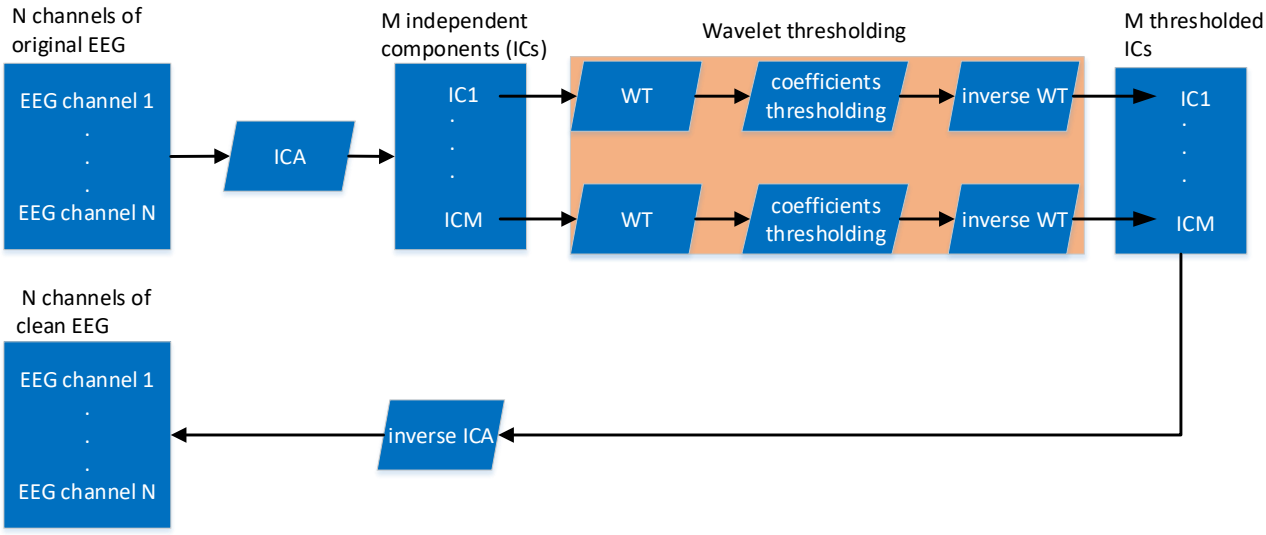

Figure 3-4. The ICA-W based artefact removal framework

3.2.2 Pre-processing Units

The raw EEG data were pre-processed using EEGLAB toolbox (Delorme and Makeig, 2004) and the DSP Toolbox under MATLAB®. The signals were re-referenced to a common average reference, and then down-sampled to 128 Hz. The resulting signals were then filtered with a pass-band filter of 4 and 45 Hz cut-off frequencies. The band-passed data are used as reference data. Then ICA and ICA-W were applied on the band-passed signals. The Runica function, an ICA algorithm included in the EEGLAB toolbox, was used in both regular ICA and ICA-W methods to find independent components. In the regular ICA case, the independent components generated by Runica were visually inspected for artefacts, and identified artefactual components were removed. Independently of the visual inspection, ADJUST was also utilized to automate artefactual components selection in a non-manual regular ICA as in (Mognon et al., 2011). For ICA-W, a multiresolution analysis of each of the components was carried out. This analysis utilized the wavelet and scaling functions given by recursive functions in (3-3) and (3-4) respectively:

$$\psi_{j,k}(t) = 2^{-j/2}\psi(2^{-j}t - k) \qquad (3\text{-}3)$$

$$\varphi_{j_0,k}(t) = 2^{-j_0}\varphi(2^{-j_0}t - k) \qquad (3\text{-}4)$$

where j and k are scaling and shifting parameters respectively, with j_0 being the arbitrary starting scale. Both j and k are nonnegative integers, with $j_0 \le j \le L$; here L is the maximum decomposition level.

Each component is decomposed into approximation coefficients (*cA*) and details coefficients (*cD*), computed as in (3-5) and (3-6), respectively:

$$cA_{j_0,k} = \sum_t S_i(t)\varphi_{j_0,k}(t) \qquad (3\text{-}5)$$

$$cD_{j,k} = \sum_t S_i(t)\psi_{j,k}(t) \qquad (3\text{-}6)$$

where S_i is i^{th} independent component, with $i = 1, 2, ..., n$.

Details coefficients from of each decomposition level were thresholded before reconstructing the components through an inverse wavelet transform. We adopted a level-dependent adaptive threshold, proposed in (Donoho, 1993); this threshold is computed based on the estimated standard deviation, σ, of the noise in detail coefficients. The threshold τ, and standard deviation, σ, estimations in (3-7) and (3-8), respectively, were used in this work.

$$\tau = \sigma(2\log K)^{1/2} \qquad (3\text{-}7)$$

$$\sigma = \left(\frac{median\left|cD_{jk}\right|}{0.6745} \right)^{1/2} \qquad (3\text{-}8)$$

K is the length of the detail coefficients, $cD_{j,k}$.

The thresholded details of level 1 to *L* and the approximation coefficients at the level *l* were used to reconstruct the component. Debauchies wavelet, 'bd4', function was used in the wavelet analysis, and since the data were down-sampled to 128 Hz, 4 levels of decomposition are suitable to cover the main brain rhythms as shown in TABLE 3-1.

TABLE 3-1. DECOMPOSITION OF EEG SIGNAL INTO VARIOUS FREQUENCY BANDS AND CORRESPONDING WAVELET DECOMPOSITION LEVELS ON DATA SAMPLED AT 128 HZ.

Frequency band (Hz)	Wavelet level/coefficients
0 - 4 (≈Delta)	0 (cA)
4 - 8 (≈ Theta)	1 (cD)
8 - 16 (≈ Alpha)	2 (cD)
16 - 32 (≈ Beta)	3 (cD)
32 - 64 (≈ Gamma)	4 (cD)

3.2.3 Features Extraction and Classification

From the 60 second trial data features were extracted from sliding windows with widths between 2 to 24s, every 2 seconds, with no overlap. In the first instance, an analysis with a window of 2 s was used, and the process was repeated for a window of 4 s and son on until a window of 24 s. A window starting from 2s was used as a training (the training segment always started at 2 s, meaning that the segment 0 to 2s (2s excluded) was never used) and the segments later in the trial were used to test the trained classifier as shown in Figure 3-5. For each training segment, all possible segments of the same size as the training segment were considered as testing segments. Also, the distance between two successive testing segments varied from 2 to 8 seconds with 1 second increment; this allowed testing several portions of the trial beyond the training segment. Statistical measures of the pre-processed signals and spectral power in brain rhythms were then extracted from both training and testing segments, then a comparison between these features was conducted.

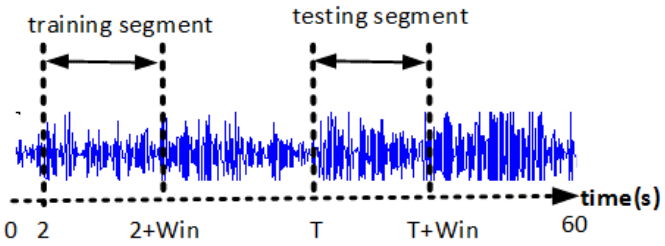

Figure 3-5. Training and testing segments. Win here represents the segment size in seconds and T specifies where the testing segment begins in the trial

3.2.3.1 Statistical features

The common statistical measures used in emotion recognition include the EEG signal power, mean, standard deviation, first difference, normalized first difference, second difference, and normalized second difference (Jenke et al., 2014). The extracted statistical measures in this study were: the power (p_x), mean (μ_x), standard deviation (σ_x), and first difference (δ_x), which are computed according from expressions in (3-9) to (3-12) respectively:

$$p_X = \frac{1}{m}\sum_{t=1}^{m} |\, x(t)\,|^2 \qquad (3\text{-}9)$$

$$\mu_X = \frac{1}{m}\sum_{t=1}^{m} x(t) \qquad (3\text{-}10)$$

$$\sigma_X = \left(\frac{1}{m-1} \sum_{t=1}^{m} \left(x(t) - \mu_X \right)^2 \right)^{1/2} \quad (3\text{-}11)$$

$$\delta_X = \frac{1}{m-1} \sum_{t=1}^{m-1} \left| x(t+1) - x(t) \right| \quad (3\text{-}12)$$

Here, $x(t)$ is the signal sample at the time t, with $t = 1, 2, 3\ldots m$; m being the number of samples in the window. The statistical measures were extracted from training and testing segments of each trial in the format below:

$$F_{Statistics} : \left\{ \left[p_X, \mu_X, \sigma_X, \delta_X \right] \times 32channels \right\}$$

3.2.3.2 Spectral features

Spectral band power in the theta (4-8 Hz), alpha (8-16 Hz), beta (16-32 Hz), and gamma (32-45 Hz) bands was extracted from the pre-processed data. Another version of spectral band power was extracted by first applying the wavelet transform to subdivide the pre-processed data into frequency bands relatively close to the brain rhythms, as shown in TABLE 3-1, then extracting the band power from bands corresponding to Theta, Alpha, Beta, and Gamma. The spectral band power extracted from the wavelet-generated frequency bands is referred to as wavelet features. The bandpower and wavelet features were extracted from each trial in the formats shown below:

$$F_{Bandpower} : \left\{ \left[theta, alpha, beta, gamma \right] \times 32channels \right\}$$

$$F_{Wavelet} : \left\{ \left[theta, alpha, beta, gamma \right] \times 32channels \right\}$$

3.2.3.3 Classification

Regularized support vector classification was used for classification (LIBSVM toolbox (Chang and Lin, 2011)). LIBSVM uses a *one-against-one* approach (Knerr et al., 1990) for multiclass discrimination. With this approach, assuming that c is the number of the classes, LIBSVM construct $c(c-1)/2$ binary classifiers, and each classifier is dedicated to one of the two-class pairs. The features extracted on the training segment were mapped into high dimensional space using the polynomial kernel defined in (3-13). The coefficient r, was set to 0 (its default value in LIBSVM). Other parameters including the degree of the polynomial, z, and kernel parameter γ were set through 10-fold cross-validation on the training data. The parameter γ controls the width of the kernel, very large γ

leads to overfitting (Huang and Wang, 2006). The trained model, for each segment size, was tested over the corresponding testing segments.

$$f(x_i, x_j) = (\gamma x_i^T x_j + r)^z \qquad (3\text{-}13)$$

The classification accuracies (CA) from each instance of a given segment size (size = 2 to 24 s) are averaged to represent the accuracy for of that particular segment size for each type of features in all the considered de-noising methods. The process was done for every subject, and the mean accuracies were averaged across all the 14 subjects to determine the segments' general accuracies. From the averaged accuracies, a best segment size was selected for each method, and highest accuracies for all the features were computed and averaged across subjects.

3.3 Results and Discussion

Figure 3-6 shows a sample visual comparison of artefact-corrected data for each of the two ICA based methods. Both the ICA and ICA-W eliminated the substantial artefacts found in the band-pass filtered data. The ICA-W seems to preserve the original signal trend while data cleaned with regular ICA tends to be flat at the artefactual segment.

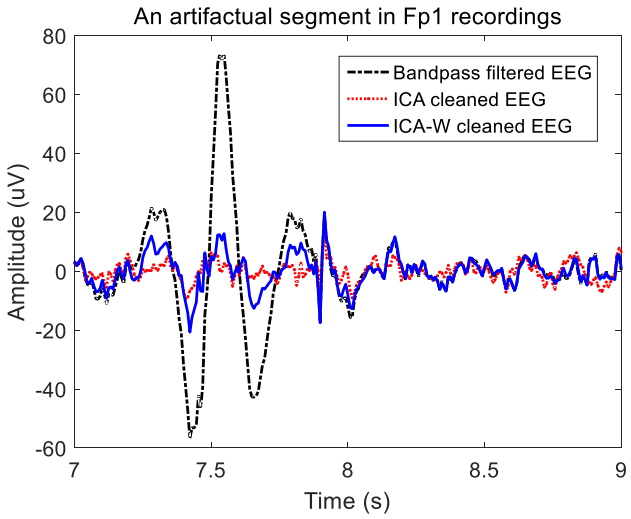

Figure 3-6. A sample visual comparison of the two ICA methods on an artefactual segment recorded at the channel Fp1 during one of the trials of subject 3

The classification accuracy of the three feature-types, i.e. statistics measures, band power and wavelet features corresponding to band-pass filtering, ICA, ADJUST and ICA-W for artefact removal methods are reported in Figure 3-7. The reported CA are averaged across all the subjects for each segment size.

The CA in the case of regular ICA (with components visual inspection) were slightly higher than automated regular ICA (ADJUST). CA increased as feature window size increased for wavelet and statistical features in the ICA-W cleaned data whereas the CA first slightly increases then slowly decreases in the other methods. The band power features performed poorly (the average CA < 60%) and remained nearly the same across all the segments in all the three methods. Slight improvement in band power performance was observed in both the ICA and ICA-W compared to band-pass filtering. Considering only the segment sizes with highest CA, the achieved high accuracies, averaged across all the 14 subjects, are 56.60% (statistical features), 60.18% (wavelet features), 56.61% (band power features) and 74.11% (statistical features) for pass-band filter, ICA, ADJUST, and ICA-W respectively, as shown in Figure 3-9. Repeated measures analysis of variance (RANOVA) with Bonferroni correction showed that there was no significant difference between CAs achieved with the data cleaned by all the considered methods in the case of band power features. However, there was significant differences in artefacts removal methods when considering the CA achieved with wavelet features; ICA-W led to significant) increases in classification accuracies over the regular ICA ($p = 0.027$), ADJUST ($p = 0.002$) and band filtering ($p = 0.003$). Also there was significant difference in statistical features where ICA-W led to higher CA compared to ICA ($p = 0.003$), ADJUST ($p < 0.0001$) and band-pass filtering ($p < 0.0001$). In statistical features the ICA with components visual inspection had significant classification accuracy over ADJUST ($p = 0.040$).

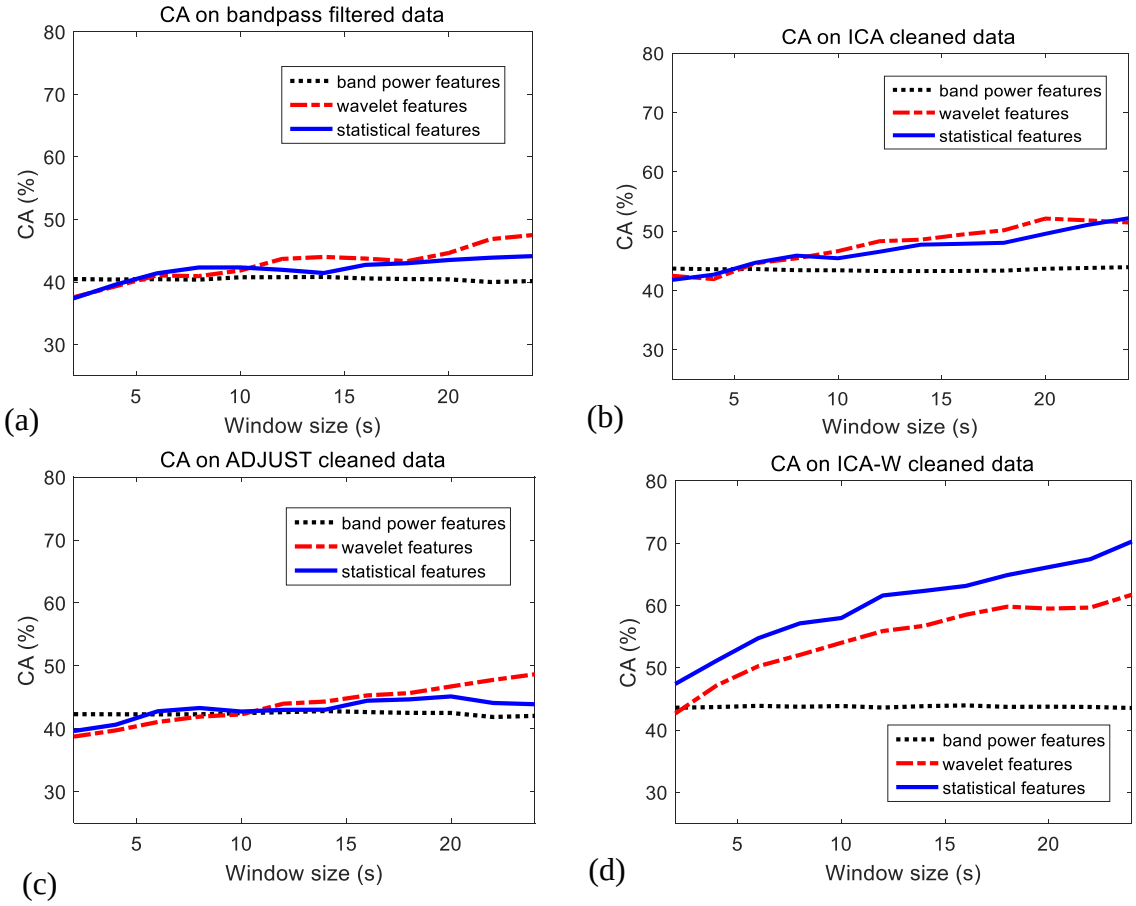

Figure 3-7. Classification accuracies (CA) over various segment sizes in the considered noise removal methods: (a) case of band-passed data, (b) case of ICA cleaned data, (c) case of ADJUST, and (d) case of ICA-W cleaned

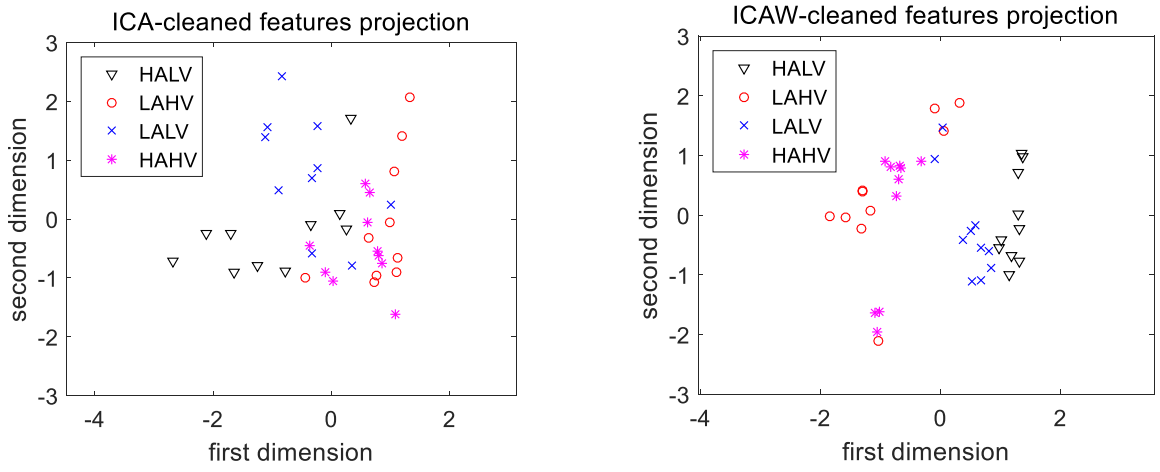

Figure 3-8. Statistical features extracted from a 6 s segment (test segment located 4s away from training segment) are reduced to two dimensions, and the classes are projected into those dimensions for the case of ICA cleaned data, and ICA-W cleaned data.

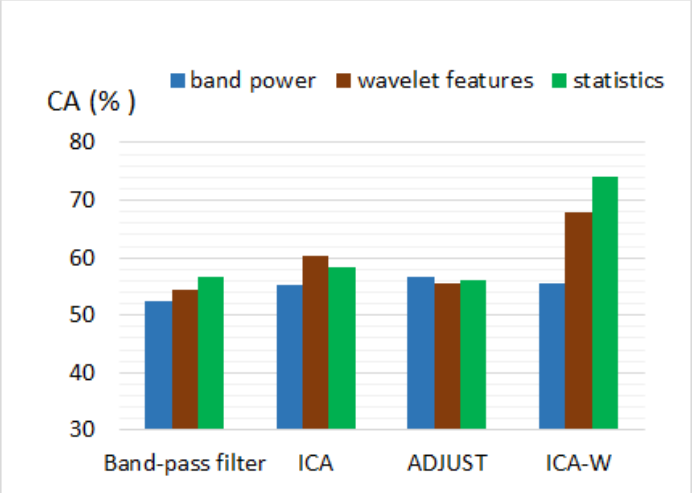

Figure 3-9. Classification accuracies of the three features averaged across the subjects using the best segment sizes for each of method: bandpass, ICA, Adjust, and ICA-W (sizes considered are 22, 20, 20 and 18 s respectively)

The observed higher CAs in the case of ICA-W method compared to traditional ICA suggests that ICA-W is more efficient for artefact removal than traditional ICA. Furthermore, the statistical features, extracted from data cleaned separately by different methods, were projected in two dimensions after principle components analysis-based dimension reduction projection. The distribution of classes' features in the case of ICA and ICA-W filtered data are shown in Figure 3-8 for one of the subjects; the shown distribution are associated with cross-validation accuracy of 52.00% and 67.00% respectively. With closer inspection of the features distributions, there is no strong separability of features, especially between features of LALV and HALV on one side, and on the other side LAHV and HAHV's features are not separable. Figure 3-8 seems to convey that features are more separable based on the valence level of the emotion. Comparing the de-noising methods used, the overall best separability of features is provided by the ICA-W approach. Table 3-2 shows related emotion recognition studies in which DEAP dataset was used, but since different classification frameworks were applied there is no direct comparison with the results from the work present in this chapter.

TABLE 3-2. RECENT RELATED STUDIES UTILISING THE DEAP DATASET

Sources	Classes	Classifier	CA (%)
(Chao et al., 2019)	2 classes (LV vs HV)	capsule network	68.2
(Gupta et al., 2019)	4 classes (HVHA, HVLA, LVLA, LVHA)	random forest with SVM	72.07
(Mert and Akan, 2018)	2 classes (LV vs HV)	ANN	75

(Li et al., 2018)	2 classes (LV vs HV)	SVM	59.06
(Nakisa et al., 2018)	4 classes (HVHA, HVLA, LVLA, LVHA)	PNN	67
(Alazrai et al., 2018)	4 classes (HVHA, HVLA, LVLA, LVHA)	SVM	60.50
Current work	4 classes (HVHA, HVLA, LVLA, LVHA)	SVM	74.11

3.4 Conclusion

The study in this chapter presented a comparison of ICA and the automated version of ICA (ICA-W) as an artefact removal methods using emotion-related EEG datasets. Due to being automated, ICA-W was easier to apply on the data compared to regular ICA since the dataset was relatively large. Classification accuracy for four emotional states was the performance measure in this study. The results suggest that EEG-based emotion recognition is improved when ICA-W is used to pre-process the EEG data compared to the regular ICA. Significant increases were found when using statistical features for both methods with ICA-W significantly outperforming all other methods. An analysis of the feature distributions shows improvement in features separability by ICA-W. Future related studies should investigate how ICA-W affect the EEG features selection and comparing the performance of ICA-W to other spatial filters. Given the good performance of ICA-W, it was also used to pre-process spontaneous EEG data recorded during pre-BCI use period reported in chapter 5. In the dataset used in this chapter, emotional states were induced by watching video clips, and this categorises the classification of emotions done in this chapter as passive emotion monitoring. Active emotion monitoring, where a participant intentionally self-induces emotion, is explored in the next chapter.

CHAPTER 4

4 EMOTION-INDUCING IMAGERY BASED BCI

In this chapter 4, emotion is exploited as a potential active control for brain-computer interfaces (BCIs) in two studies: study 1 and study 2. In the study 1, the investigation of emotion-inducing imagery is carried out with a set of healthy participants where the magnetoencephalogram (MEG) and electroencephalogram (EEG) were simultaneously used as neuroimaging modalities to allow high spatial resolution (many sensors covering most of the scalp). In the study 2, with another set of healthy participants the author made a preliminary comparison of emotion-inducing imagery versus motor-imagery as control strategies for an EEG-based BCI.

4.1 Introduction

Emotions recognition research involving neuroimaging data has increased considerably in the last two decades. In the majority of studies, emotions are stimulated through visual or audio stimuli presentation, and in only a few studies, participants were requested to self-induce emotions by engaging in emotional recall or imagining emotional scenarios (Makeig et al., 2011) (Kothe et al., 2013) (Chanel et al., 2009) (Iacoviello et al., 2015) (Sitaram et al., 2011). The strategy used in these studies, referred to in this thesis as emotion-inducing imagery (EII), could be used as an approach for independent brain-computer interfaces (BCIs). In such BCIs, the user intentionally self-induces a targeted emotion by engaging in a mental task, e.g., imagining or recalling emotional events or situations. Given that the EII tasks do not require learned skills, but rather acquired experience in life, the user should be able to carry out EII tasks.

BCIs are constructed around detecting the person's mental state or intent from direct measurement of brain activity (Wolpaw and Winter Wolpaw, 2012). Such BCIs enable the person to communicate or control various computer based applications without using the traditional neuromuscular pathway. As previously mentioned in the introduction chapter, the applications for BCIs span a wide range of fields include neurogaming (Ahn et al., 2014) (Coyle et al., 2016) (Beveridge et al., 2019), neuromuscular rehabilitation (Bundy et al., 2017) (Biasiucci et al., 2018) (Rathee et al., 2019), assistive technologies (Stawicki et al., 2016), (Abiyev et al., 2016) (Tang et al., 2018) (Vidaurre et al., 2016) (Tariq et al., 2018), and consciousness assessment (Wang et al., 2017) (Dayan et al., 2019). This chapter is looking into BCIs based on the user voluntarily modulating his/her brain signals by engaging into mental tasks,

often referred to as independent BCIs (Wolpaw et al., 2002). The most popular independent BCIs are based on imagining limbs movements, also known as motor imagery (MI) based BCIs.

Motor imagery based BCI exploit the fact that similar neural circuitry is recruited during motor imagery and actual limbs movements. There is a general census on the mapping of most limbs' movements to their associated neural activity. There are specific lateralized differences observed in left versus right side limbs' movements in the brain, and these sensorimotor rhythm modulations can also be achieved via motor imagery (Pfurtscheller and Neuper, 1997)(Gerloff et al., 1998) rendering motor imagery an ideal candidate for a BCI. For example, during left hand motor imagery we often observed contralateral activity in the motor cortex on right side, whereas the right-hand motor imagery is associated with contralateral activity in the left side. The dynamics of neural activity (increase in activity or inhibition) during motor imagery tasks can be studied through event related desynchronization or synchronization (ERD/S) analysis (Pfurtscheller and Lopes Da Silva, 1999). Despite the differences often observed in movement imageries of limbs, studies have shown that a non-negligible portion of users are unable to learn to control a MI BCI (Blankertz et al., 2010) (Ahn et al., 2013b) within a limited duration of training, hence we are investigating EII as a potential alternative imagery strategies for such users.

Happy and sad based imageries are used in this present study, and this is motivated by the neural activity differences reported between positive and negative emotions in the literature. Positive emotions (e.g., happy, joy) are associated with less relative alpha power in left frontal cortical regions than the right, whereas for negative emotions (e.g., sad, disgust) less relative alpha (8-13Hz) power is observed in the right frontal cortical area (Davidson et al., 1990) (Allen et al., 2001), and similar hemispheric asymmetry activation was reported in functional imaging (Canli, 1999). However, EII tasks are cognitive tasks which are likely to be associated with more complex neural activity than the simple case of emotion stimuli presentation. The EII tasks involve emotional memory retrieval which might recruit different brain circuitry depending on the content and complexity of the memory. Smith and colleagues (Smith et al., 2006) reported bidirectional increase in amygdala-hippocampal connectivity with modulatory input from orbitofrontal cortex during emotional retrieval. Damasio and colleagues (Damasio et al., 2000) reported that insular cortex, secondary somatosensory cortex, cingulate cortex, and nuclei in brainstem tegmentum and hypothalamus are recruited during the feeling of self-generated emotions.

In the work presented here was carried out in two studies: EII-study 1 and EII study 2. In the EII-study 1, the performance of EII is evaluated by means of classification accuracy of associated MEG/EEG

signals using state-of-the-art methods normally used in MI-based BCI. Since there is no general consensus found in the literature about brain circuitry recruited during EII task, this study also looks at brain topography and oscillations during emotional recall and associated frequency bands. The results of EII-study 1 show significant differences between frequency content associated with happy and sad imagery tasks in the frontal and parietal EEG electrodes. In the EII study 2, the emotion-inducing imagery is compared to motor imagery as imagery strategies for controlling a BCI, and the results show that the performance with EII is comparable to the performance with MI.

4.2 EII Study 1: Emotion-Inducing Imagery for a BCI– A MEG/EEG Study

4.2.1 Materials and Methods

4.2.1.1 Participants

Ten participants (9 males and 1 female; mean age 26 years, range 20-40 years) participated in this study. All participants had normal or corrected to normal vision and were not suffering from any condition that would impede their participation in experiment. The participants reported no neurological disease or mental illnesses, no brain injury or brain surgery, and they had no metal implant or metal fragments in their body. The study was approved by Ulster University's Faculty of Computing, Engineering and Built Environment research ethics committee, and written informed consent was provided by each participant before participating in the study. The study was conducted at the Northern Ireland Functional Brain Mapping Facility located at Ulster University's Intelligent Systems Research Centre.

4.2.1.2 Experimental Setup

4.2.1.2.1 Participant preparation

The study was conducted with an Elekta Neuromag® TRIUX system, a MEG/EEG device shown in Figure 4-1. Before entering the recording room, participants were asked to remove and store personal objects (cell phones, wrist watches, rings, earrings, piercings, and hairclips) which may act as magnetic sources. 72 equidistant EEG electrodes mounted on a MEG compatible Easy-Cap in a 10%-system, as show in Figure 4-2, were prepared for simultaneous MEG-EEG recording. Using gel, the impedance of each EEG electrode was kept below 5KΩ. The reference electrode for EEG was mounted on the left ear and the ground was mounted on the participant's right cheek. In addition to EEG electrodes, two electrodes (bi-polar setup) were mounted below and above the left eye to record electrooculogram (EOG) and two electrodes were mounted on left and right side of the participant's neck base to record

electrocardiogram (ECG). After mounting the electrodes, five head position indicator (HPI) coils were attached to the participant's head. Using a digitizer module and Polhemus stylus the locations of left pre-auricular (LPA), nasion, right pre-auricular points (RPA) were recorded, respectively, followed by the locations of the five HPI coils and EEG electrodes on the head. Before each experiment block, the head location in the MEG scanner was measured by detecting the initial HPI coils position for that block, an option offered in the Elekta Neuromag® data acquisition system. The participant was instructed to avoid head movement and to minimize body movement as much as possible once in the scanner.

Figure 4-1. An example of a participant taking part in data recording with Elekta Neuromag® TRIUX system; projection screen (not shown in the image) and armrest is also available. MEG sensors are housed into the scanner's helmet, and they measure the magnetic fields produced by activation of several neurons in the brain.

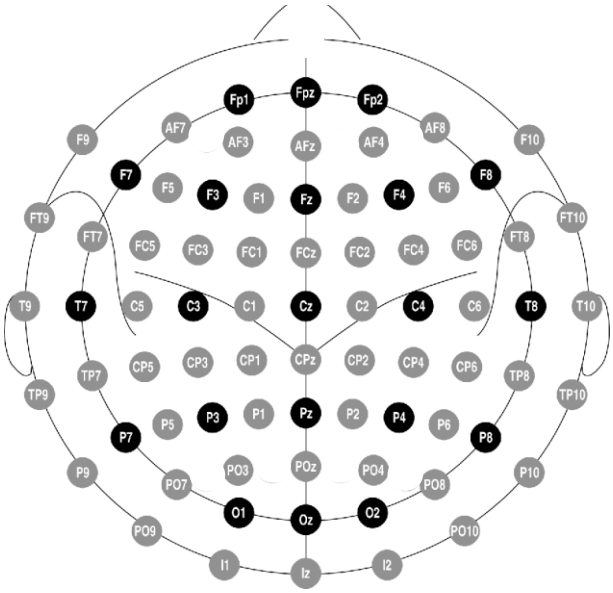

Figure 4-2. EEG electrode montage setup

4.2.1.2.2 Emotion-inducing-imagery (EII) tasks

Before starting the recording, the participant was instructed to identify a mnemonic emotional event that makes him/her feel sad and another event that makes him/her feel happy. Participants were informed that they can choose to use a real event from thier life experience or fiction events. Once the two events were identified, the participant was instructed to recall one of the events according to a cue projected on the screen in the MEG scanner room. A fixation cross was displayed for 3s for a ready period, then the cue as shown in Figure 4-3. The cue for imagery was an arrow pointing on left (happy event) or right (sad event) in the centre of the screen. The arrow stayed on the screen for 5s and disappeared to mark the end of the imagery task. The participant was instructed to avoid blinking once the fixation cross appeared and before the arrow disappeared. The cueing arrow was followed by a blank screen (dark grey) which lasted 1.5 to 2.5s, during which the participant was instructed to relax and blink if needed. The background colour was kept the same, dark grey. The participant was first given a brief practice run mode of 4 trials for each class to familiarize with the tasks before starting the actual recording. The actual recording was made of two blocks with a 1 to 5 minutes of rest. Each block contained 20 trials of each class presented in a random order (the total trials for each class was 40).

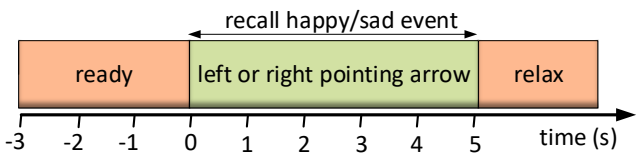

Figure 4-3. The imagery task trial structure

4.2.1.3 Brain activity data and analysis

4.2.1.3.1 Data acquisition

The MEG sensors include 204 planar gradiometers (GRAD) and 102 magnetometers (MAG) (totalling to 306 MEG sensors). Simultaneous MEG, EEG, ECG and EOG data were recorded at 1000Hz sampling rate, and at acquisition the data were bandpass filtered between 0.3 and 330Hz.

4.2.1.3.2 Data pre-processing

EEG electrodes and MEG sensors with consistent noise, identified by visually inspecting the data during acquisition and, after recording, data browsing/visual inspection, were removed from further analysis. Elekta Neuromag® MaxFilter software was used to run temporal extension of signal-space separation (tSSS) on MEG data to reduce noise originating inside and outside of the MEG sensory array. After the tSSS process, the data were down sampled to 125Hz to speed up further analysis. A 50Hz notch filter was applied on the data to remove the 50Hz noise line. The eye blinks and heart beats artefacts were removed from the MAG, GRAD and EEG data separately. Principle components analysis (PCA) was applied on the data segments with tagged eye blinks and/or heartbeats to identify and remove components representing these artefacts.

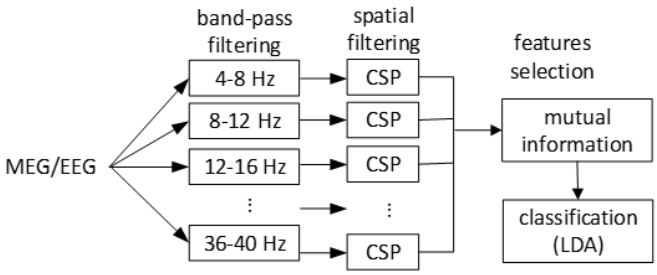

Figure 4-4. The FBCSP-based framework with 9 frequency bands from 4Hz to 40Hz with 4Hz increments.

4.2.1.3.3 Time-Course cross-validation classification accuracy

The author also carried out an offline analysis, through a filter bank common spatial patterns (FBCSP) (Ang et al., 2012) framework. This FBCSP framework includes spectral filtering (SF) the EEG data in different frequency bands and applying common spatial patterns (CSP) to the data from each frequency band as shown in Figure 4-4. CSP is used to maximize the ratio of class-conditional variances of MEG or EEG sources. CSP is applied by pooled estimates of the covariance matrices, Σ_1 and Σ_2, for two classes, as previously discussed in section 2.2.3.2.3:

$$\sum_c = \frac{1}{I_c} \sum_{i=1}^{I_c} X_i X_i^t \quad (c \in \{1, 2\}), \qquad (4\text{-}1)$$

where I_c is the number of trials for class c and X_i is the $M \times N$ matrices containing the i^{th} windowed segment of trial i; N is the window length and M is the number of electrodes/sensors. The two covariance matrices, Σ_1 and Σ_2, are simultaneously diagonalized such that the Eigenvalues sum to 1. This is achieved by calculating the generalized eigenvectors W:

$$\sum_1 W = (\sum_1 + \sum_2) WD, \qquad (4\text{-}2)$$

where the diagonal matrix D contains the Eigenvalue of Σ_1 and the column vectors of W are the filters for the CSP projections. With this projection matrix the decomposition mapping, E, of the windowed trials X is given as:

$$E = WX. \qquad (4\text{-}3)$$

Features, $\bar{\omega}$, are derived from the log-variance of pre-processed/surrogate signals, E, within a 2 second sliding window:

$$\bar{\omega} = \log(\mathrm{var}(E)). \qquad (4\text{-}4)$$

The dimensionality of $\bar{\omega}$ depends on the number of surrogate signals used from E. The common practice is to use several (between 2 and 6) eigenvectors from both ends of the eigenvector spectrum i.e., the columns of W. The parameters considered in this setup are the number of features, number of CSP filter pairs, and the best time during the trial for train the classifier.

The features are extracted on a 2s sliding window, and the number of filter pairs and number of features are optimized in a 6-fold-cross-validation setup with an inner 5-folds-cross-validation. The number of selected features varies from 4 to 16. These features are selected based on *mutual information best individual feature* (MIBIF) algorithm (Kai Keng Ang et al., 2006). The MIBIF computes mutual information for each individual features, and a subset of features with highest mutual information is selected. The accuracy for each outer-fold is given by applying an LDA classifier, trained on the inner-folds with optimized parameters, on the outer-fold's test set. The time-course cross-validation classification accuracy (CA) is given by averaging the outer-folds' accuracies at each time sample.

4.2.1.3.4 Cross- validation accuracy versus random accuracy

A permutation test was used to evaluate if the CA during the task execution is significantly higher than random accuracy with a 95% confidence interval. The random accuracy is computed by repeating the 6-fold cross-validation 100 times, but each time the trials' labels are randomized. This leads to 100 time-courses of random CA corresponding to 100 permutations. At each time-point of non-random

CA, the probability that the accuracy is achieved by chance is computed using expression (4-5) as in (Ojala and Garriga, 2010):

$$p = \frac{|\{D' \in \hat{D} : ac(D') \geq ac(D)\}| + 1}{n + 1} \qquad (4\text{-}5)$$

where, $\hat{D}$ is a set of n-randomized versions *D'* of the original data *D*, and *ac(D)* is the accuracy achieved with the non-randomized data *D*. The computed *p* is the probability that given the permuted data, we can achieve accuracy level that is higher or equal to the accuracy achieved with non-permuted data. The Null hypothesis that classification accuracy was achieved by chance is rejected for $p < 0.05$. The *p*-value at each time point is computed allowing to assess the time-course of CA significance.

4.2.1.3.5 Relevant Electrodes and Frequency Bands

In order to identify the most relevant frequency bands and topography of activation during execution of happy and sad event recall/ imagination across participants, the CSP weights and mutual information weights are combined. After optimizing the parameters (number of CSP filters pairs, number of features, and time-point for the peak cross-validation accuracy) through cross-validation in the FBCSP framework, a final CSP projection matrix *W* (as in (4-2)) is computed for each frequency band. Each projection matrix *W*, gives us the weights for each electrode's contribution to the surrogate data resulting from CSP filtering in each frequency band. Log-variance features are then extracted with a 2s sliding window. The global weights for electrodes at a time-sample *t*, are given by the weights matrix *K(t)*, computed in (4-6), from projection matrices across ten frequency bands and mutual information associated to extracted features using the projection matrices at a given time-sample. To average topographic *K(t)* (CSP-MIBIF) weights, across different sessions at a given time-sample, topographic CSP-MIBIF weights are first normalized to the electrode with highest weight for each individual run.

$$K(t) = \sum_{n=1}^{9} W_n(t) \cdot Y_n(t) \qquad (4\text{-}6)$$

where W_n is the projection matrix in the frequency band *n*, and $Y_n(t)$ is the mutual information (weights) given to the features extracted with W_n at the time-sample *t* in frequency band *n*.

Apart from the CSP-MIBIF weights of electrodes, the CSP-MIBIF weight of each frequency band is computed by adding the mutual information of features extracted from the same frequency band. At each time-sample (from 2s in the trial as a 2s window was used in the analysis), the features are extracted with optimized parameters and then the next step is to compute the mutual information for

each features using MIBIF. This allows to establish a time-course of weights for the ten frequency bands for each participant and to compute an average time-course of weights across participants.

4.2.1.3.6 Time- frequency differences between sad and happy imageries

Differences have been reported between positive and negative emotions in frontal alpha (8-13Hz) (Davidson et al., 1990) (Allen et al., 2001). Due to the complexity of the neural circuitry involved in emotion processing in the brain (Dalgleish, 2004) and the usage of mental imagery tasks, differences could be manifested in different areas of the scalp. The author compared time-frequency representations (TFRs) for happy (positive) EII and sad (negative) EII to identify their differences. A permutation test is then used to test the null hypothesis that the probability distribution of TFRs averages for happy IEE and sad EII is identical.

The time-frequency analysis was done using Morlet wavelets. Time-frequency data were normalized relative to the baseline (-3 to 0s). The time of interest included relax period (-3 to 0s) and task period (0 to 5s), and the frequencies of interest included 0.5 to 45Hz range. The permutation test with Monte Carlo sampling (Fay and Follmann, 2002) (n = 1000 permutations) was used in a repeated (10 participants) measures design with two conditions (happy and sad imageries). The cluster-based method was used for multiple comparisons correction (Maris and Oostenveld, 2007).

4.2.2 Results

4.2.2.1 Cross-validation classification accuracy

The peak of time-course cross-validation classification accuracy (CA) for each participant is reported in Figure 4-5(a). Five of the 10 participants achieved CA higher than 70%, with two participants (*te* and *bn*) achieving CA higher than 90% for EEG data. Except the participant *ba*, all the participant achieved CA significantly higher than random CA with EEG data. For the MEG-magnetometers data, eight participants achieved CA significantly higher than the random CA, with three (*pa*, *te*, and *bn*) achieving CA higher than 70% whilst one participant (*bn*) achieved CA higher than 90%. For the MEG-gradiometers data, eight participants achieved CA significantly higher than the random CA, and two (*te*, and *bn*) achieving CA higher than 70% with no participant achieving CA higher than 90%. The mean accuracy across the participants for each of the considered sensor types is show in Figure 4-5(b). Pair-wise comparison using t-test showed no significant difference between CA performance with EEG data and CA with MEG data. There was a tendency towards CA with EEG data being significant higher than CA with magnetometers' data ($p = 0.057$) and than CA with gradiometers' data ($p = 0.061$).

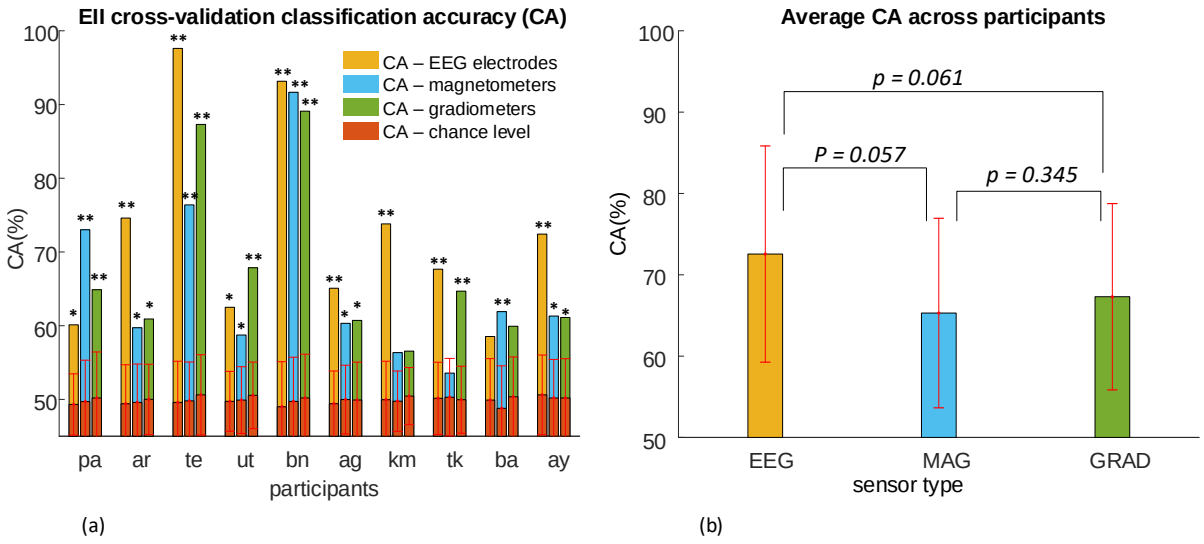

Figure 4-5. Cross-validation accuracy for each sensor type is shown in (a); the '' and '**' indicate that the CA is significantly higher than the random CA with p-value < 0.05, and p-value < 0.01 respectively. In (b), the averaged accuracies across participants for each sensor type are shown with associated p-values for their t-test pairwise comparison*

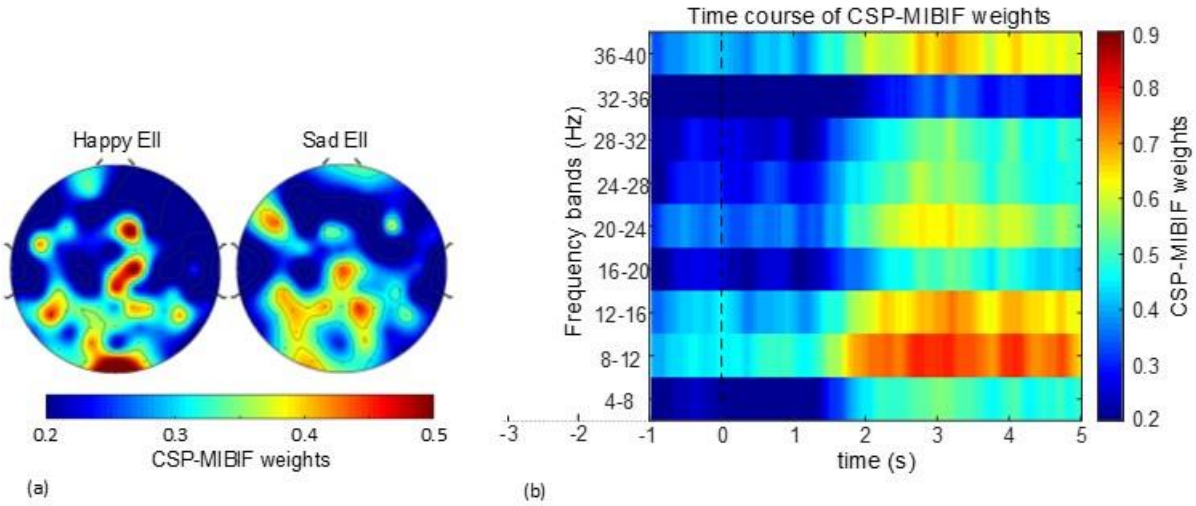

Figure 4-6. In (a) EEG electrodes contribution weights for happy (left) and sad (right) emotion-inducing imageries across participants are shown. And in (b) Frequency bands contribution weights across participants throughout the trial time for EEG data are shown.

4.2.2.2 Weights for electrodes and frequency bands

Only EEG sensors were considered in assessing the electrodes and frequency bands of relevancy across participants. The EEG electrodes CSP-MIBIF weights for happy and sad imageries averaged across participants are shown in the topographic maps in the Figure 4-6(a). The most weights for happy imagery are found on the middle-line frontal and central electrodes, left parietal and occipital

electrodes. For the sad imagery, the most weights are found in the left frontal, middle-line central, left and right parietal electrodes.

The weighted contributions of different frequency bands averaged across participants is shown as time-course of CSP-MIBIF weights in Figure 4-6(b). With respect to the baseline (period pre-cue, before 0s), the CSP-MIBIF weights get higher after about 1.7s in the imagery task. Different frequency bands exhibited patterns of increases and decrease in their CSP-MIBIF weights. The bands 4-8Hz and 32-35Hz have lower weights throughout the entire time-course than the other frequency bands. The bands 8-12Hz and 12-16Hz have sustained high weights from 1.8s and 2.2s respectively. Most of the weights seem to be concentrated between 2.5s and 3.5s across all the frequency bands.

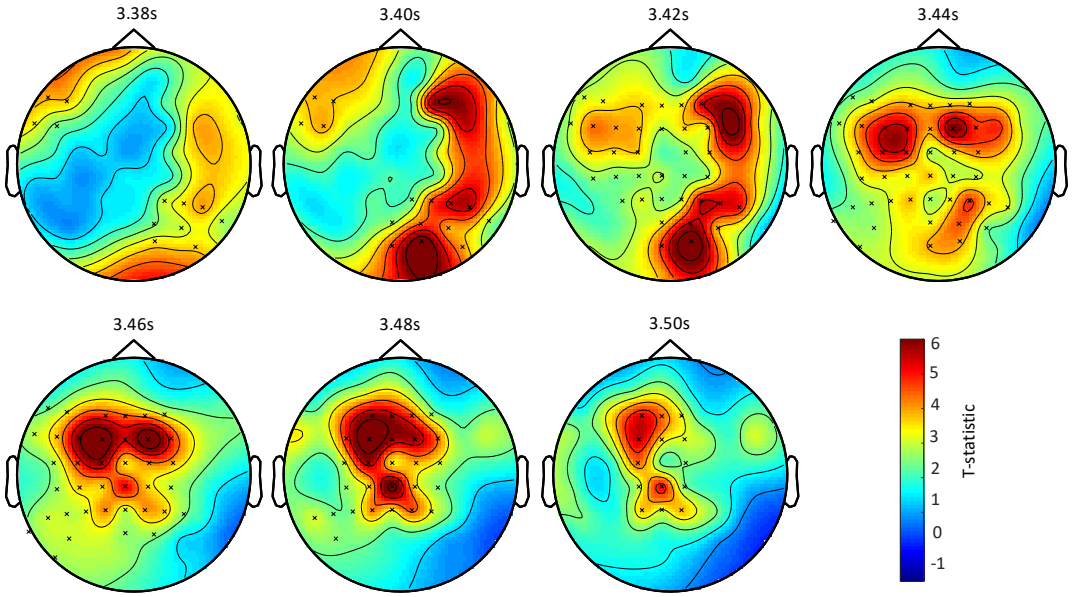

Figure 4-7. T-statistic of the difference between the time-frequency representations of power in EEG during happy EII and sad EII) and largest channel-time clusters. The mark 'x' in the plots indicates the cluster with $p < 0.05$ (corrected for multiple comparison), the significant cluster shown here were observed at 14Hz.

4.2.2.3 Time- frequency representations difference Between Sad versus Happy Imageries

The results for the comparison between TFRs for happy and sad imageries across participants are reported in Figure 4-7. One positive cluster-level with *p-value <0.05* (corrected for multiple comparison) was found from 3.38s to 3.50s, at the frequencies 14Hz. At the beginning (3.38s), the significant clusters include electrodes on the left frontal, middle line occipital and right parietal. As time progresses, the significant clusters cover most of the left frontal, left central, middle line parietal, and middle line occipital. At 3.46s, there is no significant cluster in the occipital area; significant

clusters are only found in the frontal, central and parietal areas. At the end (3.50s), significant clusters are located only in the frontal, central and parietal areas close to the middle line.

4.2.3 Results Discussion

The aim of this study was to evaluate emotion inducing-imagery as an active BCI strategy by assessing the classification performance of EII and difference in neural data associated with the EII tasks. The results show that some of the participants (5 out of 10) can achieve acceptable BCI performance. CA of 70% and above is considered as acceptable performance for a 2-class BCI setup (Vidaurre and Blankertz, 2010). Higher classification accuracies were achieved with EEG electrodes data than with MEG sensors (magnetometers and gradiometers)' data, but this difference was not statistically significant ($p > 0.05$). The slight lower classification accuracy of MEG sensors' data compared to EEG electrodes' data may be mainly due to the head shift and movements in the MEG scanner during the recording. Since a spatial filters based method was used to extract the features in this study's setup, the head movements introduce shift in the MEG sensors' positions with respect to the participant's head leading to substandard spatial filter for the MEG sensors data. Due to the potential problem of position-shifting in MEG sensors, the relevancy of different scalp areas and frequency bands was estimated using EEG data since the sensors were attached to the participant's head.

The CSP-MIBIF weights of electrodes suggest that the relevant EEG electrodes for happy and sad imageries are in the frontal, middle line central, parietal and occipital areas. The emotion inducing imageries are likely to recruit a complex neural circuitry that covers memory, emotion, and vision processing. Looking closer at the results for CSP-MIBIF weights of electrodes, the relevant electrodes were mounted on the parietal and occipital areas, but these electrodes varied across participants.

The CSP-MIBIF weights for frequency bands suggest that it takes some time (about 1.8s) for participants to exhibit change in a given relevant frequency band with respect to the period before the cue of EII task. This hints that the difference between the happy and sad imageries is stronger after about 1.8s in the task execution. The weights for frequency bands also indicate that the frequency bands 8-12Hz and 12-16Hz have sustained relevancy after 1.8s. This sustained high weights for 8-12Hz and 12-16Hz suggest that happy and sad imageries are most distinct in these two frequency bands.

Apart from the assessment based on our FBCSP framework, namely the classification accuracy and CSP-MIBIF weights, the results present the difference in TFRs of the EII tasks used. The significant difference in the TFRs was achieved at the frequency 14Hz which lies in the 12-16Hz band, one of the

frequency bands with sustained relevancy. The difference between positive and negative emotions has been reported in alpha band (8-13Hz) (Davidson et al., 1990) (Allen et al., 2001). The deviation from alpha band, in this study, might be associated to other processes involved in EII tasks on top of the emotion's processes. Analysis of the significant electrodes' clusters at 14Hz shows that the significant clusters are mainly in the frontal and parietal areas as time progresses. Considering both CSP-MIBIF weights for frequency bands and TFRs difference, we can round up the time window of significant difference between happy and sad EII to 2.5 to 4s post cue across participants. This time window, and frequency bands covering 8-16Hz, and scalp areas of interest (frontal and parietal) provide a step closer toward optimizing EII tasks for BCI. However, due the variation in selected events to recall or imagine across participants, it is challenging to assess how much the imagery vividness affected the CA performance and difference between imageries. Future related studies should minimize the variation in imageries by instructing participants to recall attributes or objects, as in (Korik et al., 2018), which can be associated with some emotional events or with emotional states, e.g. odours, as in (Iacoviello et al., 2015).

4.2.4 Summary

The performance assessment of emotion-inducing imagery as an approach for BCI using FBCSP, the state-of-the-art framework for motor-imagery based BCI, shows good performance in some participants. We established a time window in EII task execution, frequency and spatial information associated with significant difference between happy and sad imageries which should be exploited by future EII studies.

EII may offer a viable alternative in some cases for subjects who cannot control a motor imagery BCI, but further investigation is necessary to identify effective EII tasks that might be easy to execute in a BCI paradigm and potentially be combined with other imagery tasks to create a multi-class or hybrid BCI. The following section presents a pilot study to address the question around whether EEI maybe a viable alternative to MI to realise a BCI.

4.3 EII study 2: Comparison of Emotion-Inducing Imagery versus Motor Imagery

The results of the EII study 1 show that some BCI users may be able to achieve good performance with EII as a control strategy for BCI. To build on these results, the following section present the investigation of how performance with EII compares to performance with MI in a standard MI-based

BCI setup. Performance results of imageries induced by sad versus happy events are compared to left versus right hand motor imagery results during the one-dimensional control of a video game character.

4.3.1 Materials and Methods

4.3.1.1 Participants

Seven healthy participants (1 female and 6 men, mean age 29, SD = 6) were recruited at Ulster University. Each subject, individually participated in one EEG recording session, and after the session the subject was asked, in an informal interview, what he/she thought about his/her performance in task execution during the session. Six subjects had previously participated in at least one motor imagery BCI study, and one of these six participants was known to have a good performance in MI. The remaining subject was participating in active BCI paradigm for the first time; all seven subjects had not previously participated in EII BCI training prior to the study.

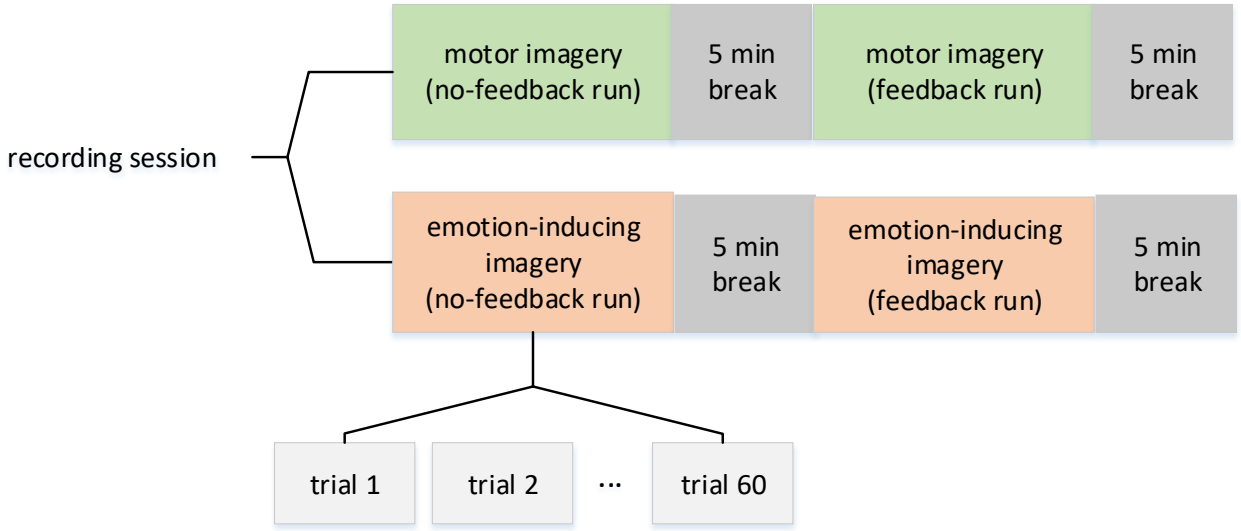

Figure 4-8. The structure of recording session. Each recording session has 4 runs of imagery tasks, each run with 60 trials (see details in text).

4.3.1.2 Experimental Setup

Each EEG recording session includes four runs: two EII runs and two motor imagery runs. Each type of imagery, consisted of one training run and one online feedback run as shown in Figure 4-8. The order of runs was randomized between subjects i.e., either EII or MI was performed in the first two runs. The recording session utilized a computer game paradigm called NeuroSensi, in which a light, representing a neuronal spike, traversed the left or right graphical axon (see Figure 4-9) on the computer screen (lasting 5 s falling on the screen), cued the participant to perform one of two imageries i.e., left versus right movement, or sad versus happy emotion-inducing imagery. After the

spike disappeared, the participant was give 3 to 3.5 s to relax before the next spike). The In feedback runs, the game objective was to collect the spike by moving the game character (a graphical representation of neuron's cell body and dendrites as shown in Figure 4-9).

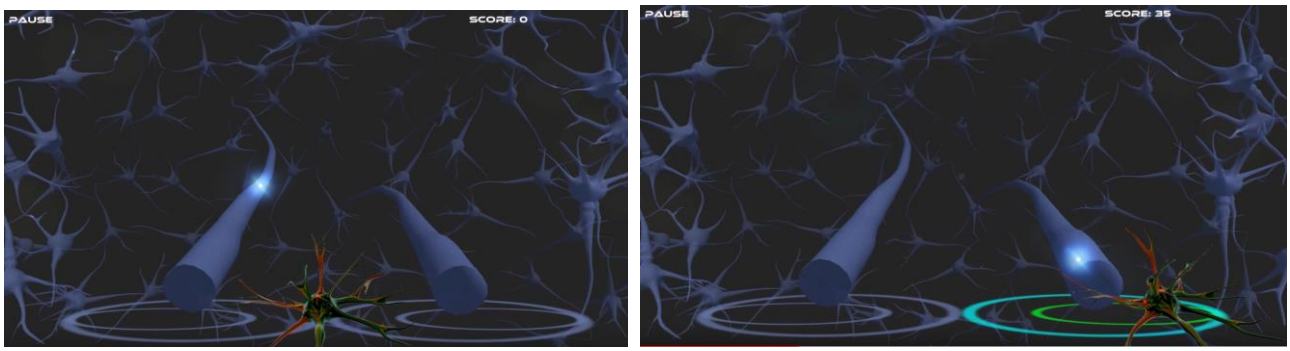

Figure 4-9. The screenshots of the BCI game used in cueing and feedback presentation. The neuron character is fixed in the middle of the two axons during no-feedback run (screenshot on the left), and it moves horizontally to collect the spike during the feedback run (screenshot on the right).

Points were awarded for moving the game character in the right direction and positioning the character as close as possible to the axon when the spike reached the end of the axon. Additional points are awarded for collecting more than three spikes consecutively without failure; these bonus points are accompanied with background neurons firing and propagating several spikes for about 1s (after task execution). The continuous feedback, i.e., movement of the game character, was controlled by the BCI; the BCI produced classification at each sample point. Each run included 60 trials randomly ordered for two class tasks, 30 trials for each class. In EII training runs, subjects were asked to imagine or recall a scenario that they thought would make them sad when the spike was cued on the left axon, and to imagine an event that would make them happy when the cue appeared on the right hand side axon. In the case of motor imagery tasks, the subject was asked to imagine right hand movement when the cue is on right, and left hand movement when the cue appeared on the left side.

EEG data were sampled at 125 Hz from 16 channels (Fp1, Fp2, F3, Fz, F4, T7, C3, Cz, C4, T8, P3, Pz, P4, PO7, PO8, Oz) setup in 10-20 system. EEG was then processed through a multistage signal processing framework which includes neural-time-series-prediction-pre-processing (NTSPP), spectral filtering (SF) in subject specific frequency bands and common spatial patterns (CSP) as previously used in (Coyle, 2009; Coyle et al., 2011). This signal processing framework is illustrated in Figure 4-10.

4.3.1.3 Neural-Time-Series-Prediction-Pre-Processing (NTSPP) framework

In the NTSPP framework different prediction networks are trained to specialize in predicting future samples of different EEG signals. Due to network specialization, features extracted from the predicted signals are more separable and thus easier to classify. The number of time-series available and the number of classes governs the number of specialized predictor networks and the resultant number of predicted time-series from which to extract features

$$P = M \times C \qquad (4\text{-}7)$$

where P is the number of networks (= number of predicted time-series), M is the number of EEG channels and C is the number of classes. For prediction,

$$\hat{x}_{ci}(t+\pi) = f_{ci}\left\langle x_i(t),...,x_i(t-(\Delta-1)\tau\right\rangle \qquad (4\text{-}8)$$

where t is the current time instant, Δ is the embedding dimension and τ is the time delay, π is the prediction horizon, f_{ci} is the prediction model trained on the i^{th} EEG channel, x_i, i=1,..,M, for class c, c =1,..C, and $\hat{x}_{ci}$ is the predicted time series produced for channel i by the predictor for class c. NTSPP adapts to each subject autonomously using self-organizing fuzzy neural networks (SOFNN) (Coyle et al., 2009).

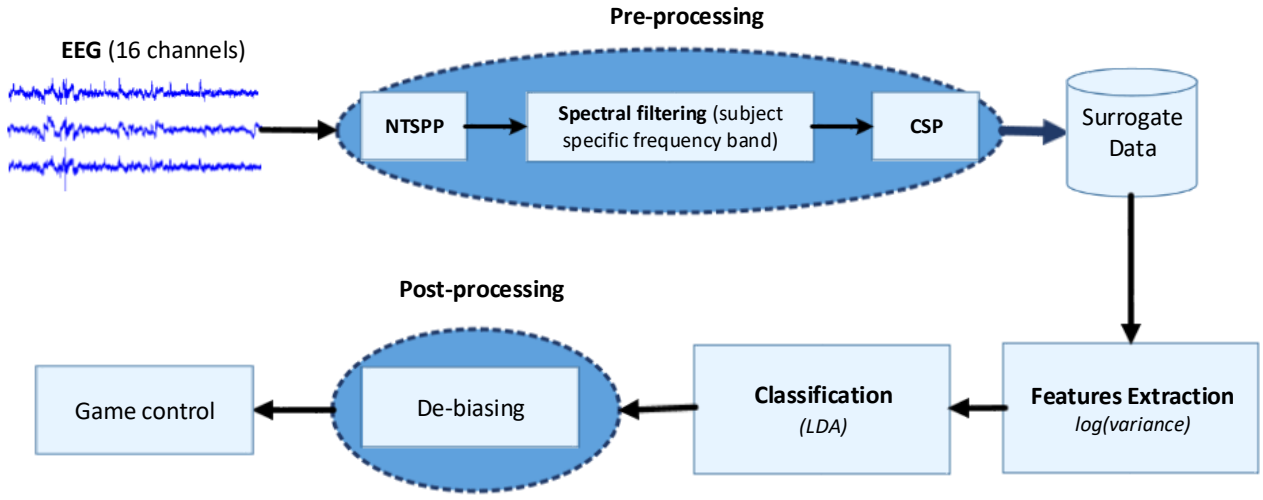

Figure 4-10. BCI setup used to pre-process EEG, extract and classify EEG features correlating to imageries; in the feedback session, the classifier's output is de-biased to adapt the feedback

4.3.1.4 Common Spatial Patterns (CSP)

As already mentioned in the section covering FBCSP in the EII study 1, CSP is used to maximize the ratio of class-conditional variances of EEG sources. CSP is applied by pooled estimates of the covariance matrices, Σ_1 and Σ_2, for two classes using the expression in (4-1), and the number of EEG channels, $M=P$.

4.3.1.5 Spectral Filtering

Prior to the calculation of the spatial filters, X can be pre-processed with NTSPP and/or spectrally filtered in specific frequency bands. The bands are selected autonomously in the offline data processing stage using a heuristic search and are subsequently used to band pass filter the data before CSP is applied. The search space is every possible band size in the 8 - 28Hz range. These bands encompass the alpha, beta bands which are altered during sensorimotor processing (Coyle et al., 2009; Johnston et al., 2010; Pfurtscheller et al., 1998) and for emotional state detection these bands or sub-bands within these bands are often used (Kim et al., 2013; Mauss and Robinson, 2009).

4.3.1.6 Feature Extraction and Classification

Features, $\overline{\omega}$, are derived from the log-variance of pre-processed/surrogate signals within a 2 second sliding window. Linear discriminant analysis (LDA) is used to classify the features at the rate of the sampling interval. But first, an inner-outer cross-validation (CV), with 5 outer folds, is performed to find the optimal subject-specific frequency. In the outer fold NTSPP is trained on up 10 trials randomly selected from each class (2 seconds of event related data from each trial). The trained networks then predict all the data from the training folds to produce a surrogate set of trials containing only EEG predictions. The 4 training folds from the outer splits are then split into 5 folds on which an inner 5-fold cross validation is performed for best subject specific frequency selection. After the subject specific frequency band selection, NTSPP-SF-CSP is then applied on the outer fold training set, where a feature set is extracted and LDA classifier is trained at every time point across the trials and tested for that point on the outer test folds. The average across the five-folds is used to identify the optimal number of CSPs (between 1-3 from each side of W) and the final time point of maximum separation which are then used to setup the final classifier using all the training data, to be deployed online.

In the online processing, the classifier's output translation to the game character movement was de-biased to account for class bias behaviour and improve feedback stability. This de-biasing was carried out by continuous removal of the mean from the continuous classifier output, where the mean was calculated with a 35s window on the most recent classifier output.

Additionally, EEG dynamics throughout tasks execution were also explored through event-related (de)synchronization (ERD/S) analysis. The ERD/S was computed as power change respective to the baseline power as in (Pfurtscheller, 1992) within the subject's selected frequency band after artefacts removal based on independent components analysis (Mognon et al., 2011).

4.3.2 Results

Offline cross-validation classification accuracy (CA) for each run, along with online single-trial CA results for feedback runs, online results, and sample results from event-related (de)synchronization analysis are reported in Figure 4-11, Figure 4-12, Figure 4-13, and Figure 4-14 respectively. Wilcoxon signed rank tests showed no significant differences between EII and MI ($p > 0.05$), although the EII training accuracies exceed the MI accuracies for most of the participants. ERD/S analysis showed EII tasks separability in the temporal and frontal channels; this can be seen in sample topographic maps for subjects 2 in Figure 4-14. The online classification results in Figure 4-12 show decrease in accuracies for most of the participants compared to what was achieved in offline analysis for the no-feedback run. However, there was one participant who achieved good online performance in each of the considered BCI strategies: one experienced subject achieved 81% in MI and another achieved 90% in EII online performance. The achieved online performance in the remaining participants is 64.18 ± 4.75% and 62.09 ± 2.03% for EII and MI, respectively.

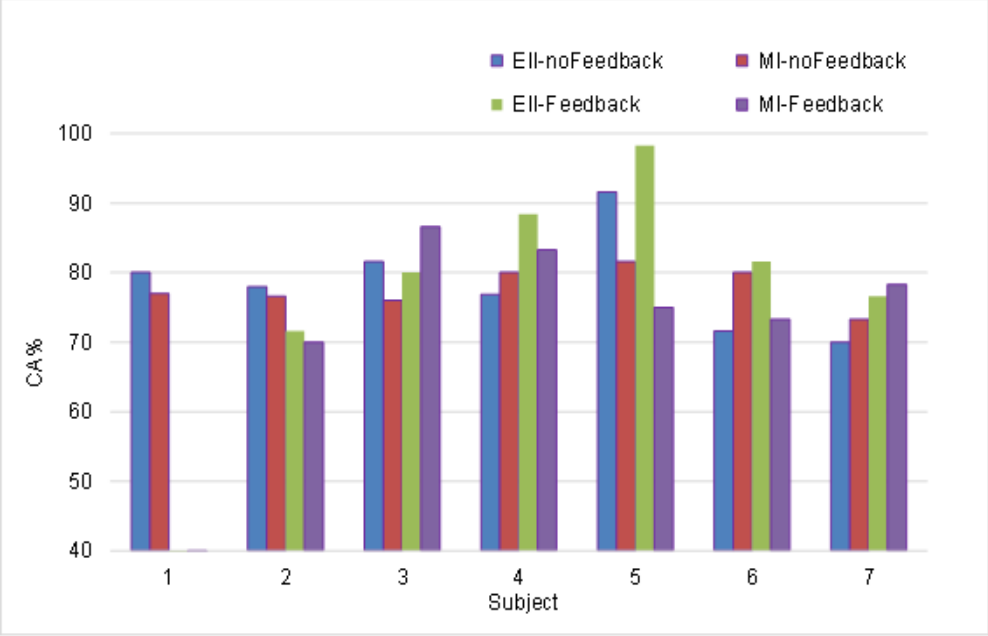

Figure 4-11. The LOOCV classification accuracy for feedback and no-feedback runs. There were no feedback runs for subject 1.

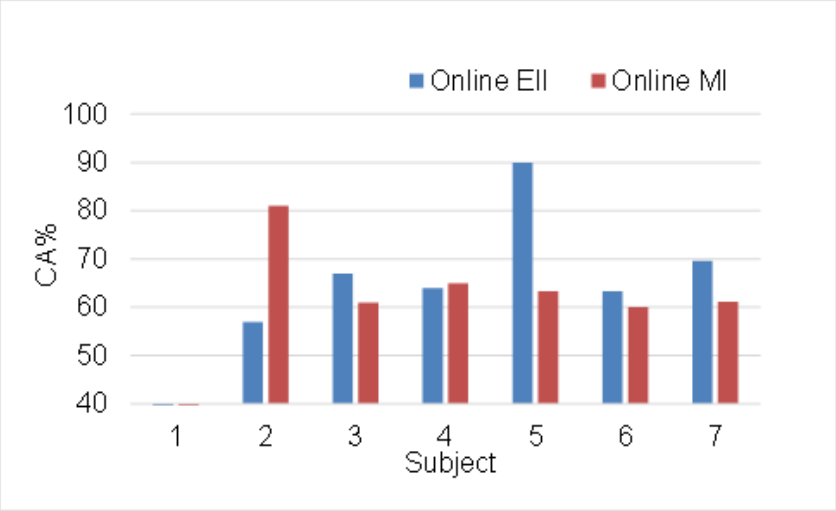

Figure 4-12. Online task classification accuracies for emotion inducing imagery and motor imagery during feedback runs. Note that there were no feedback runs for subject 1.

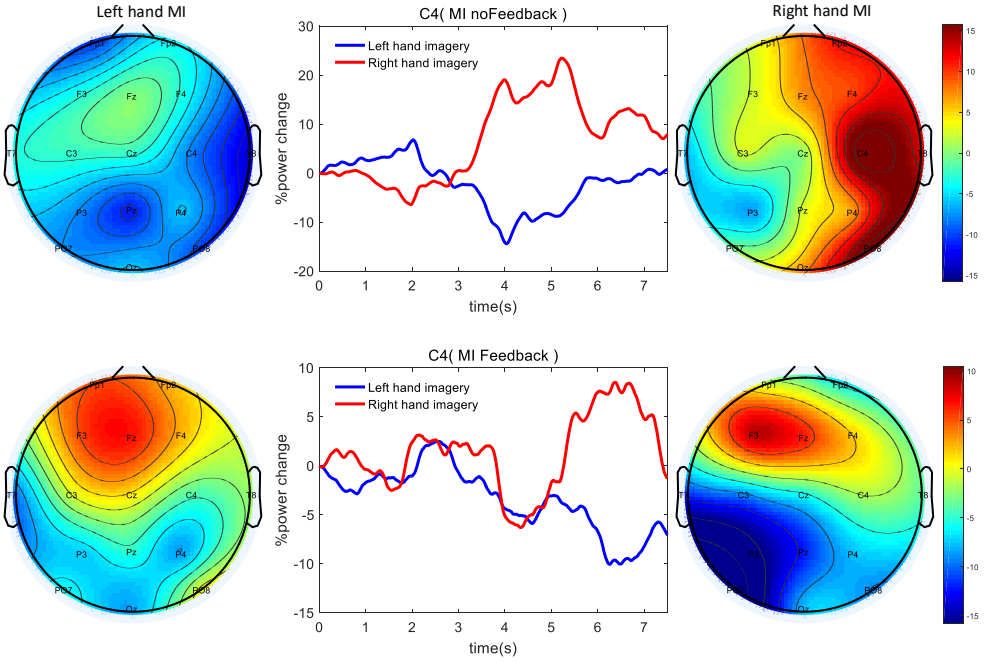

Figure 4-13. Topographic maps of band power changes (ERD/S) in [8 – 13] Hz band during motor imagery task execution for subject 2, and time-course ERD/S observed at channel C4.

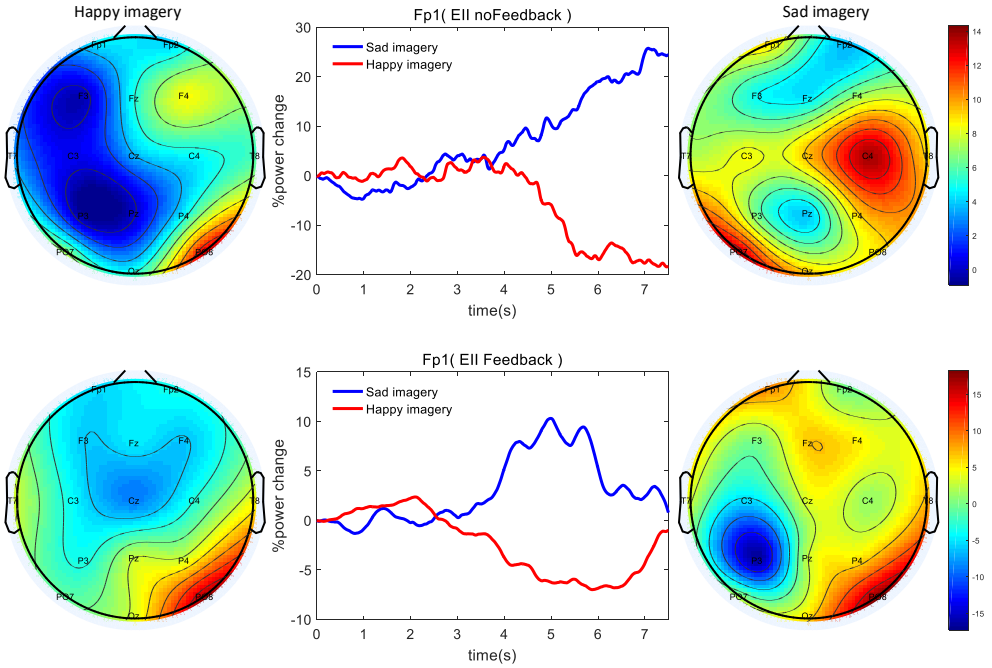

Figure 4-14. Topographic maps of band power changes in [8 – 20] Hz band during emotion inducing tasks execution for subject 2, and time-course ERD/S from channel Fp1.

4.3.3 Discussion

The objective of the EII study 2 was to investigate the discriminability of EEG during emotion inducing imagery, to investigate if emotion inducing imageries could be used to control a video game using a BCI and to compare performances of EII with the extensively studied motor imagery based control strategies. The results suggest that emotions, which normally influence the way we live (Giorgetta et al., 2013), may be intentionally modulated and actively translated in a BCI control paradigm. Consequently, the study shows some of the first evidences to support the use of emotion-inducing imagery as a potential alternative to motor imagery. This study was based on one off-line training session and online training session for both MI and EII. Although participants were limited by the amount of training, their classification accuracies exceed chance level which was 62.39% for our binary classification setup with 95% of confidence interval (Müller-putz et al., 2008). It usually requires several training sessions to achieve good accuracy in motor imagery performance, so further validation with multiple sessions training and on a larger sample of subjects is required to determine if emotion-inducing imagery could be used by BCI users who do not perform well with motor imagery. Furthermore, the sudden drop in accuracies observed in the online classification accuracies for both MI and EII suggests that the models deployed online might have been over-trained. This is likely to

be the case as there is was small number of trials for model optimisation. Future studies should attempt to acquire many trials to reduce the likelihood of over-training.

Subject 2 achieved high online performance in MI, was familiar with motor imagery based BCI and had achieved good accuracies in the past. The participant with highest accuracy in online EII (subject 5) reported in the post-session interview that meditation practice was the key technique used in executing tasks for EII; meditation has been shown to improve BCI performance (Eskandari and Erfanian, 2008; Tan et al., 2014b). Subject 2 also reported regular meditation practice. Two participants showed acceptable online performance, whereas for the other participants' online performance is diminished compared to the calibration run (the run without feedback)'s offline results. Even though a reduction in accuracy was observed in the online runs, the baseline accuracy (1s before cue) were significantly lower than the peak accuracy during the task execution ($p < 0.05$) for all the participants indicating that above chance performance was achieved. In addition, as this is single session and participants experienced feedback for the first time (except subject 2) along with distractors in the games (game score updates and bonus firing spikes), this likely had an impact on subject concentration, cognitive load (de Jong, 2010) and maintaining focus and consistency between the runs. With additional sessions the BCI and subject performance may be more robust for both of the two imagery strategies (EII and MI).

4.4 Conclusion

This chapter has presented an investigation on using emotion-inducing imagery as an imagery strategy for intentionally controlling a BCI. The study 1 found that the frequency content of EEG associated with imagery for sad and happy events is significantly different in the frontal and parietal EEG electrodes. The results of two the studies presented in this chapter show that some BCI users may be able to use EII as an imagery strategy for BCI, and that the performance of EII is comparable to the performance of motor imagery, the established imagery strategy for independent BCIs. The findings from the studies presented in this chapter suggest that existing BCI can potentially be augmented by the EII. However, the results in each of the two studies are based on one session, thus further investigation are necessary to validate the results reported in this chapter. A related study comparing EII versus MI based on multiple sessions is presented in chapter 5.

The methods used in the two studies presented in this chapter, the NTSPP and FBCSP, introduced in section 2.2.3.2.3 of chapter 2, are popularly used in MI-based BCI. This might have biased the comparison of EII and MI performance, done in EII study 2, toward the MI task. Further investigation using known methods to extract features related to emotions should be carried out to further validate

the finding of the studies in this chapter. In a related study presented in chapter 5, the EII performance is compared to MI performance across different signal processing framework including a framework based on asymmetry features introduced in the section 2.3.4.2.2 of chapter 2.

CHAPTER 5

5 EMOTION-INDUCING IMAGERY VERSUS MOTOR IMAGERY FOR A BCI

In chapter 4, emotion-inducing imagery (EII) was investigated and compared to motor imagery (MI) as a BCI control strategies in a single session pilot study. In this chapter 5, imagining fictional or recalling mnemonic sad and happy events, emotion-inducing imagery, is compared to motor imagery (MI) in a study involving multiple sessions using a two-class electroencephalogram (EEG)-based BCI paradigm with 12 participants. The BCI setup in this study allowed online continuous visual feedback presentation in a game involving one-dimensional control of a game character. MI and EII are compared across different signal-processing frameworks which are based on neural-time-series-prediction-pre-processing (NTSPP), filter bank common spatial patterns (FBCSP) and hemispheric asymmetry (ASYM). Online single-trial classification accuracies (CA) results indicate that MI performance across all participants is 77.54% compared to EII performance of 68.78% ($p<0.05$), NTSPP was the framework used in the actual online setup.. The results show that combining the NTSPP, FBCSP and ASYM frameworks creates a best framework for EII with average CA of 71.64% across all participants.

5.1 Introduction

As previously highlighted, one of the challenges in BCI is that there are limited control strategy options available to users: some strategies, e.g., motor imagery, are challenging for some users (Blankertz et al., 2010) (Ahn et al., 2013b) and require training, and other strategies (evoked potentials) often require gaze control and are dependent on external stimuli. As a non-negligible portion of users are unable to learn to control a motor imagery (MI)-based BCI (Blankertz et al., 2010) (Ahn et al., 2013b) within a limited duration of training, there is a necessity to investigate alternative imagery strategies for such users. As discussed in section 1.2, there is an ongoing effort to investigated alternative imagery for BCI. In this chapter, the viability of EII as a potential BCI control alternative strategy is investigated. We are interested in assessing EII strategy because the associated tasks can be constructed from the user's natural experience.

The EII strategy exploits the differences observed in brain responses to different emotional stimuli or recall of emotional events, and this may even enable a multi-class BCI (Makeig et al., 2011). Positive

emotions (e.g., happy, joy) are associated with less relative alpha power in left frontal cortical regions than the right, whereas for negative emotions (e.g., sad, disgust) less relative alpha power is observed in the right frontal cortical area (Davidson et al., 1990) (Allen et al., 2001), and similar hemispheric asymmetry activation was reported in functional imaging (Canli, 1999). In addition to the differences in brain activity associated with different emotions, for emotion to be useful in active, independent BCIs, where the user issues a command as opposed to waiting on a stimulus to evoke a brain response, the BCI user is required to imagine or recall emotional situations. Chanel et al. (Kothe et al., 2013) reported an accuracy of 71.3% across participants in a two-class classification of valence ratings, where the participants were self-paced in recalling positive and negative valence emotions. In a similar study, but with discrete classification with a wide window segment, Chanel et al (Chanel et al., 2009) achieved an accuracy of 63% in a three-class (negative emotion, positive emotion, and neutral) and 80% for two-class classification, where each emotion-inducing imagery task lasted at least 8s. Furthermore, Iacoviello and colleagues in an offline discrete classification setup (Iacoviello et al., 2015) achieved a classification accuracy of 90.2% for imagery induced by remembering an unpleasing odour versus a relaxed state. Sitaram and colleagues (Sitaram et al., 2011), in an fMRI-based study, presented performance-based discrete feedback to participants who were recalling sad, happy, and disgust emotions (three-classes), and achieved an accuracy of 60% classification with feedback presentation.

Only a limited number of previous studies have applied emotion-inducing imagery with real- or pseudo-real-time feedback presentation. In a typical BCI system, the user should be provided with feedback interaction as the feedback implicitly acts as a motivating reward to the user during brain modulation tasks (Fetz, 2007) and helps users learn and develop their imagery strategy. As shown in EII study 2 in chapter 4, participants controlled a video game character by recalling sad and happy events, and their performance was not significantly different from performance achieved using classical right versus left hand motor imagery. However, further investigation across multiple sessions is necessary to establish the viability of EII compared to motor imagery.

In the current study, we present a comprehensive analysis of the viability of EII, comparing multiple online feedback sessions and single-trial classification accuracy for EII tasks versus MI with 12 participants. Since the participants participated in multiple sessions, we also investigated the potential correlation between their online performance and the relative band power in various frequency bands of EEG recorded prior to each run i.e., before the subjects engage in MI and EII tasks. We also investigated the most relevant frequency bands and scalp areas for MI and EII. The participants' online

performance across multiple sessions with EII and MI during one-dimensional control of a video game character are reported. The comparison between performance of MI and EII across a range of signal processing frameworks (NTSPP, ASYM, and FBCSP) is reported as well. In addition to EEG based analysis, the participants' subjective responses to a questionnaire are reported. This questionnaire assessed participants' favourite imagery strategy as a BCI control approach and which imagery they perceived to offer most accurate feedback.

5.2 Methods: Stimuli, Study design, and Data Analysis

5.2.1 Participants

The Study involved 12 healthy volunteering participants (2 females and 10 males, mean age = 29 years, SD = 8), recruited at Ulster University. All these participants had normal or corrected to normal vision and were not suffering from any condition that would impede their participation in BCI experiments. The participants reported no neurological disease or mental illnesses. The study was approved by Ulster University's Faculty of Computing, Engineering and Built Environment research ethics committee, and written informed consent was provided by each participant prior participating in the study. Two participants had previously participated in BCI studies and had good performance in MI. Ten participants had no previous BCI participation experience prior this study. Participants were given some practice and demonstration to get them comfortable with the experiment before participating in the first session

5.2.2 Experiment setup

This study was organized in multiple sessions scheduled on different days. Each session includes four runs: two EII runs and two MI runs. Each type of imagery consisted of at least one run with feedback as shown in Figure 5-1. In each session, the participant begins with either EII or MI in the first run (selected randomly), and for the remaining runs of that session, he/she alternates between EII and MI i.e., there were no successive EII runs or MI runs in one session. There were rest breaks of 2 to 5 minutes between runs. Each run started with participant relaxing while minimizing eye-blinks for a period of 60 s followed by 60 trials, randomly ordered, 30 trials per class. The session format and trial timing are shown in Figure 5-1.

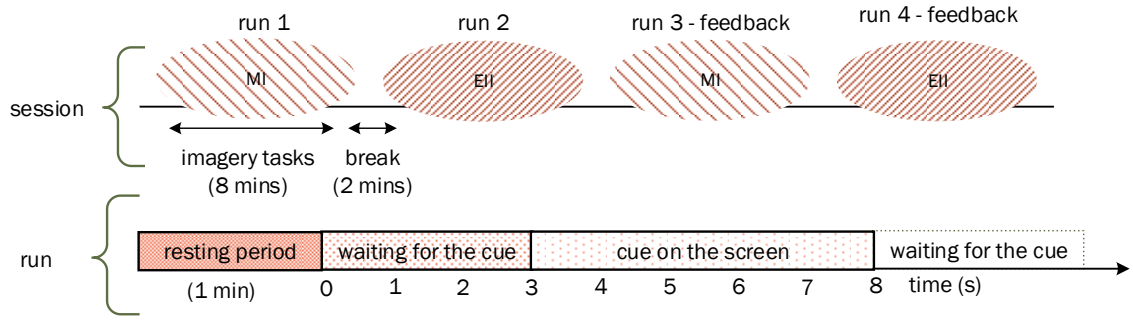

Figure 5-1. Session structure: four runs alternating between EII and MI. A run starts with resting period of 1 minute. The first two runs are used to train classifiers which are then applied in the corresponding feedback runs.

5.2.2.1 Imagery tasks, cue and feedback presentation

Before starting the sessions, the participant was instructed to identify two real or fictitious emotional events: one event that the participant considers as a sad event and another event that he/she considers as a happy event. To avoid possible emotional stress in the participants, they were instructed to refrain from using extremely sad events. Participants were instructed to keep the event very brief and preferably to focus on the most emotional episode of the event. The tasks during EII run are to recall the happy event when the presented cue appears on the right-hand side on the computer screen and to recall the sad event if the cue appears on the left side. The tasks for MI run are to imagine moving the right hand when the cue is on the right and to imagine moving the left hand if the cue appears on the left side (without actually moving the hands). Participants were instructed to be consistent in their imagery strategy during the session.

In each run, we utilized a computer game paradigm called NeuroSensi, as in the EII study 2 presented in chapter 4, to cue the tasks. In this game, a light, representing a neuronal spike, travels through one of the two graphical axons (left-side or right-side axon) on the computer screen, see Figure 5-2 (which is the same as the Figure 4-9 in chapter 4). The appearance of the spike (light) cues the imagery task. Once the spike reaches the end of the axon and disappears, the participant stops the imagery task, relaxes and waits for the next spike. The time on and off the screen of the cueing spike follows the trial structure (0 to 8s of the shown segment of a run) in Figure 5-1, where the cue appears at 3s and disappears at 8s.

In the feedback run, a continuous feedback is given as a horizontally moving game character (a graphical representation of neuron's cell body and dendrites), and the game challenge is to move this character to collect the light (spike), shown on the right in Figure 5-2. Points are awarded for moving

the game character in the right direction and positioning the character as close as possible to the axon when the spike reaches the end of the axon. Additional points are awarded for collecting more than three spikes consecutively without failure. These bonus points are accompanied with background neurons firing and propagating several spikes, extending the waiting period (after the cueing spike disappears) by 2s. This continuous feedback, i.e., movement of the game character, is controlled by the BCI. Participants were instructed to focus on executing the cued task during the task execution as much as possible. This instruction was given to reduce potential frustration resulting from poor classification of the task.

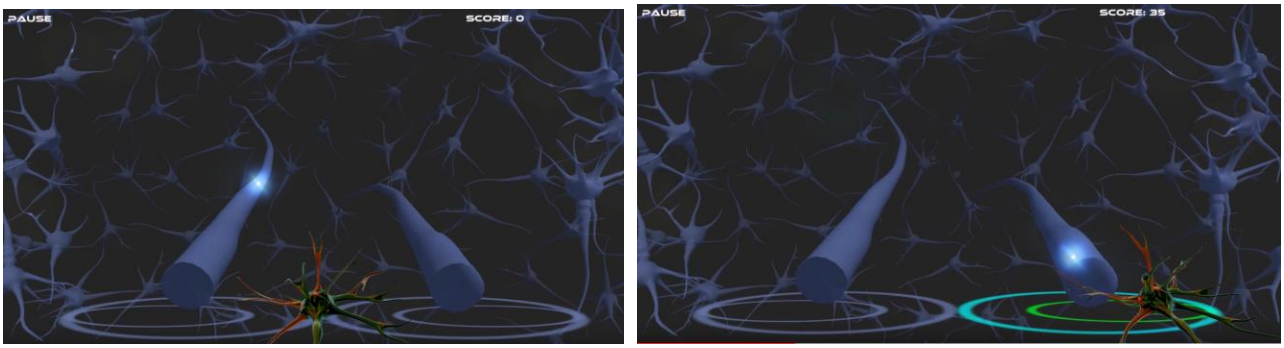

Figure 5-2. The screenshots of the BCI game used in cueing and feedback presentation. The neuron character is fixed in the middle of the two axons during no-feedback run (screenshot on the left), and it moves horizontally to collect the spike during the feedback run (screenshot on the right).

5.2.2.2 Participant's subjective responses

After each experiment session, each participant reported his/her favourite control approach and the imagery strategy perceived to provide best control over the game character. This was done through a short questionnaire where the participant answered by selecting "*MI", "EII"*, or "*equally the same"* on the questionnaire.

5.2.3 Data processing

5.2.3.1 EEG data

The EEG data were acquired using g.tec (Guger Technologies, http://www.gtec.at/Products) biosignal amplifiers (g.BSAmp) setup with 30 active EEG electrodes (g.GAMMAsys, g.Ladybird) positioned in a 10-20 system see Figure 5-3, plus two electrooculagram electrodes (F3, F4, FC5, FC1, FC2, FC6, C3, CZ, C4, CP5, CP1, CP2, CP6, P3, PZ, P4, AF3, AF4, F7, FZ, F8, T7, T8, P7, P8, PO3, PO4, O1, OZ, O2, HEOG, and VEOG). The data were recorded with sampling rate of 250Hz then down-sampled to 125Hz. The author visually inspected the data recorded in non-feedback runs for significant artefacts

(e.g., eye-blinks), and then carried out an offline analysis to find optimal parameters to be applied in feedback runs.

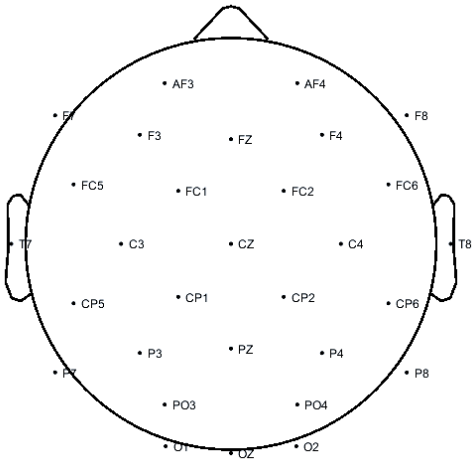

Figure 5-3. 30-EEG electrodes montage

5.2.3.2 Signal Processing Frameworks

The study compared the performance of EII and MI across different signal processing frameworks: neural-time-series-prediction-pre-processing (NTSPP) framework, a hemispheric asymmetry (ASYM) framework, a filter-bank common spatial pattern (FBCSP) framework, framework combining NTSPP and FBCSP (NTSPP-FBCSP), and framework combining NTSPP, FBCSP and ASYM (referred to as COMB in this chapter). NTSPP is a framework that has been used for years at our BCI lab with MI based BCI. FBCSP is one of the state-of-the-art framework for MI based BCI (Ang et al., 2012). ASYM framework is inspired by the hemispheric asymmetry of emotions; different asymmetry features are usually used for emotion recognition (Alarcao and Fonseca, 2017). In each of these frameworks, the data for the no-feedback run are used to generate optimized settings which are deployed to drive the feedback in the online run or to simulate online run.

5.2.3.2.1 NTSPP Framework

The NTSPP framework, as previously described in methods of EII study 2 in chapter 4 (see section 4.3.1.3), includes NTSPP to produce a surrogate data space, spectral filtering (SF) in 8 – 30Hz frequency band, and common spatial patterns (CSP) to maximize the separability between classes. The NTSPP framework is illustrated in Figure 5-4.

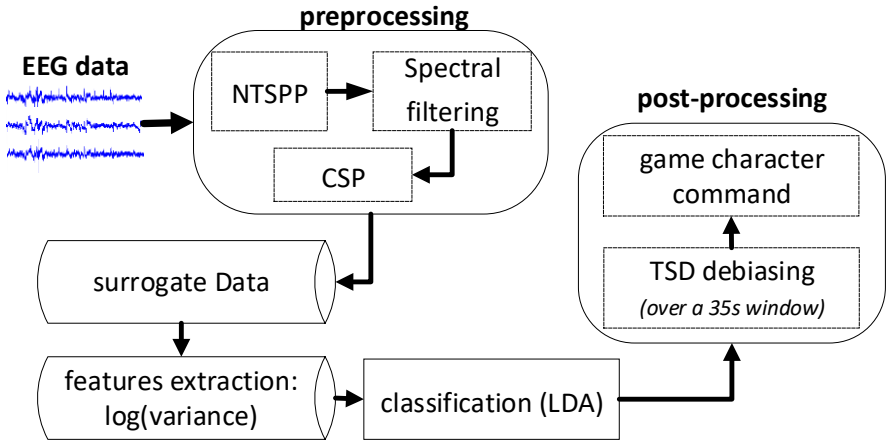

Figure 5-4. The NTSPP framework

Prior to the calculation of the spatial filters, the output X of NTSPP, is spectrally filtered in a specific frequency band, 8 – 30Hz. This band encompasses the alpha, beta bands which are relevant during sensorimotor processing (Coyle et al., 2009) (Pfurtscheller et al., 1998), and these bands or sub-bands within these bands are often used for emotional states detection (Kim et al., 2013). The features,$\bar{\omega}$, are derived from the log-variance of pre-processed/surrogate signals, E, within a 2s sliding window. The number of CSP filters and time points with maximum separability are assessed using leave-2 trials (one trial from each class)-out cross-validation on a 2s sliding window features with linear discriminant analysis (LDA).

The optimized parameters, number of CSP filters and identified time point of maximum separation, are used to setup the final classifier using all the training data. This classifier is then deployed online, in a MATLAB© Simulink model. In the online processing, the classifier's output translation to the game character movement is de-biased to account for class bias behaviour and to improve feedback stability by continuously removing the mean of recent classifier's outputs. This mean is computed from a 35s window on the most recent classifier outputs. At each sample point, the classifier's output is a distance computed from the classifier's learned weights vector; this distance is often referred to as time-varying signed distance (TSD) (Pfurtscheller et al., 2000) (Schlögl et al., 2002). The TSD value at a given time point t during nth trial is given by expression in (5-1). The distance's sign indicates the classifier's output label and its magnitude measures the classification confidence. The magnitude of the TSD indicates how far the game character moves, and the sign indicates the direction of the character's movement (moving to the right or to the left). The value of current TSD is de-biased by subtracting from it the mean of TSD values for the previous 35s (based on previous MI –BCI study (Coyle et al., 2011)). After the feedback run, the continuous classification performance is assessed by

computing the percentage of trials having TSD (de-biased) values with the same sign as the targeted class, at each time point *t*.

$$TSD_t^{(n)} = w^T \bar{\omega}_t^{(n)} - a_0 \qquad (5\text{-}1)$$

where w^T and a_0 are slope and bias of the discriminant hyperplane, respectively, of the trained LDA trained, $\bar{\omega}_t^{(n)}$ is the features vector at the time point t of the nth trial.

5.2.3.2.2 Hemispheric Asymmetry (ASYM) Framework

Electrodes located on the left and right hemispheres, at equivalent positions, are paired into thirteen pairs for asymmetry feature extraction in different frequency bands: theta (4-7Hz), alpha (8-12Hz), beta (13-30Hz), and low gamma (31-45Hz). Differential, *D*, and ratio, *R*, asymmetry features are extracted from a 2 s sliding window.

$$D_{asym} = r_i - l_j \qquad (5\text{-}2)$$

$$R_{asym} = r_i / l_j \qquad (5\text{-}3)$$

where the r_i is band power in the frequency band *i* at the right-side electrode and l_j the band power in the frequency band *j* at the left-side electrode of the pair.

The parameters to be optimized in this framework are the number of the features and the best time in the trial for classifier training. The parameters are optimized through a leave-2 trials (one trial from each class)-out cross-validation setup. The final number of features varies from 4 to 16. These features are selected based on *mutual information best individual feature* (MIBIF) algorithm (Kai Keng Ang et al., 2006). The MIBIF computes mutual information for each individual features, and a subset of features with highest mutual information is selected. An LDA classifier is trained with optimized parameters and then deployed in a MATLAB© Simulink model that simulates an online run with data from the feedback run.

5.2.3.2.3 Filter Bank Common Spatial Patterns (FBCSP) Framework

In the FBCSP, the EEG data from calibration run (run without feedback) are filtered in nine different frequency bands (4-8Hz, 8-12Hz, 12-16Hz, 16-20Hz, 20-24Hz, 24-28Hz, 28-32Hz, 32-36Hz, and 36-40Hz), and then CSP-based features, as in (6), are extracted from each band-filtered signals as shown in the Figure 5-5. The parameters considered in this setup are the number of features, number of CSP filter pairs, and the best time during the trial to train the classifier.

The CSP features (log-variance) are extracted on a 2s sliding window, and the number of CSP filter pairs together with number of features (4 to 16 features) are optimized in a 6-fold-cross-validation

setup with an inner 5-fold-cross-validation. The best features are selected based on MIBIF algorithm. The peak for the average time-course given by six time-courses of accuracy from the six folds is used as the best time (during the task execution) period for training the classifier. After optimizing the parameters, an LDA classifier is trained and then deployed in a MATLAB© Simulink model that simulates online run with data from feedback run.

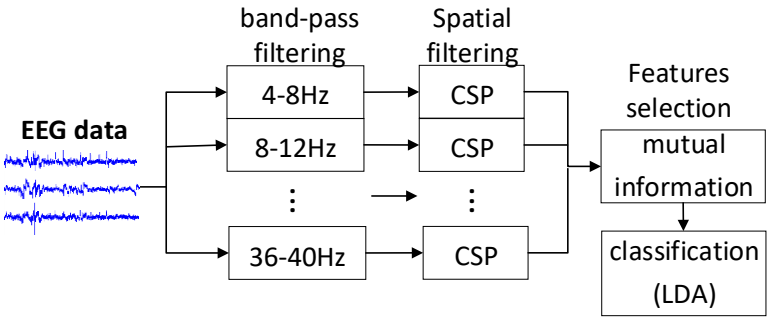

Figure 5-5. FBCSP framework setup

5.2.3.2.4 NTSPP-FBCSP and COMB Frameworks

The study also evaluated the CA performance with signal processing frameworks that combine different setups. The author combined the outputs from individual frameworks into one output during online re-simulation. Before combining the frameworks' outputs, each framework's output is individually de-biased as in (5-1), and the combined output is de-biased in the same way. NTSPP-based setup was combined with FBCSP, and this was motivated by the fact they are both CSP-based. Additional motivation was to augment the NTSPP-based setup that uses one wide frequency band, by the FBCSP-setup which utilizes nine small frequency bands. The output TSD of NTSPP-FBCSP combination was given by the individual framework's TSD with highest magnitude among the two as shown in (5-4).

Apart from NTSPP-FBCSP, the initial three frameworks (NTSPP, ASYM, and FBCSP) were combined into one framework, COMB. For the COMB framework, the output TSD is given by the mean of the individual TSDs which have matching signs, i.e. if two or three of the three TSDs match their signs, the overall TSD for the combination is the average of those individual TSDs.

$$TSD_{NTSPP-FBCSP} = s \times max(|TSD_{NTSPP}|, |TSD_{FBCSP}|) \qquad (5\text{-}4)$$

where s is the sign of the TSD with the highest absolute value.

5.2.3.3 Contribution of Different Electrodes and Frequency Bands

In the same way as introduced in the section 4.2.1.3.5 of chapter 4, in the order to identify the most relevant frequency bands and scalp areas for MI and EII during the task execution, the feedback runs'

data were run, as training data, through FBCSP framework in an offline analysis. Then the global weights for electrodes at a time-sample *t*, are given by the weights matrix *K(t)*, computed in (5-5) (the expression introduced as (4-6) in chapter 4), from projection matrices across nine frequency bands and mutual information associated to extracted features using the projection matrices at a given time-sample.

$$K(t) = \sum_{n=1}^{9} W_n(t) \cdot Y_n(t) \qquad (5\text{-}5)$$

where W_n is the projection matrix in the frequency band *n*, and $Y_n(t)$ is the mutual information (weights) given to the features extracted with W_n at the time-sample *t* in frequency band *n*.

Apart from the CSP-MIBIF weights of electrodes, the CSP-MIBIF weight of each frequency band is computed by adding the mutual information of features extracted from the same frequency band. At each time-sample (from 2s in the trial as a 2s window was used in the analysis), features were extracted with optimized parameters and mutual information was computed for the features using MIBIF. This allows to establish a time-course of weights for the nine frequency bands for each feedback run and to compute an average time-course of weights from several feedback runs.

5.2.3.4 Pre-run EEG Analysis

Resting state EEG recorded at the beginning of each run was investigated retrospectively to determine if the spectral power ratios for specific frequency bands, with respect to total frequency content, may be used as a predictor for performance during BCI. Previously, high ratio for theta and low ratio for alpha were reported to be associated with poor performance in motor imagery (Ahn et al., 2013b). In the study presented in this chapter, the author computed the spectral power ratios for theta, alpha, beta, and gamma bands at five topographical areas covered by EEG electrodes: frontal, temporal, central, parietal and occipital area.

Before computing power ratios for various frequency bands, the channels with noise were removed from the data by applying kurtosis and spectrum threshold, utilities of the EEGLAB toolbox (Delorme and Makeig, 2004). The data were then filtered with a high-pass filter (0.5Hz) followed by further automated artefact removal using a method introduced in the chapter 3, the hybrid independent component analysis (ICA) – wavelet transform (WT) (Bigirimana et al., 2016). In this ICA-W analysis, the *runICA* algorithm from the EEGLAB toolbox was applied on the data, and the resulting independent components were individually decomposed in wavelet coefficients by wavelet transform. The wavelet coefficients were thresholded then followed by reconstructing independent components

by an inverse wavelet transform. The reconstructed independent components were re-mixed to produce clean EEG data.

The cleaned data were filtered by a low-pass filter (45Hz), and the ratio, *R*, for each band was calculated as the spectral power of the signal filtered in a given frequency band divided by the total spectral power in the signal. The spectral power was computed as in (5-6):

$$p = (1/m)\sum_{t=1}^{m} x(t)^2, \qquad (5\text{-}6)$$

where *x* is the band-pass filtered signal, and *x(t)* is the signal sample at the time *t*, with *t = 1, 2, 3… m*; *m* being the number of samples in the signal *x*.

$$R_b = p_b/p_{total}, \qquad (5\text{-}7)$$

where *b* is one of the frequency bands, and *total* is the entire 0.5 – 45Hz band.

The author computed Pearson correlation between each frequency band's ratios and online classification accuracies across participants.

5.2.4 Statistical analysis

In this study, the author compared single-trial classification accuracy (CA) performance for two imagery approaches (MI and EII) across different signal processing frameworks (FBCSP, ASYM, NTSPP-FBCSP, and COMB). Wilcoxon signed rank test, with significance level of 0.05, was used to evaluate the difference between online CA of MI and online CA of EII across the participants during the feedback runs. Furthermore, repeated analysis of variance (ANOVA), with a significance level of 0.05, is used to compare the two imagery approaches' performance across five frameworks considered in this study, i.e. NTSPP (used in the actual online setup) and the frameworks used in the re-simulation of feedback runs.

5.3 Results

5.3.1 Classification Accuracy (CA)

The online single-trial CA for feedback runs averaged across sessions for each participant are reported in Figure 5-6. All the participants performed above chance level in all their MI sessions, for EII on the other hand, 9 participants performed above chance level in all their sessions. The participant *'ak'*, *'pr'*, and '*rm*' each performed below chance level in one of their EII sessions (the chance level upper limit is 62.39% for a 2-class problem, 30 trials per class, with 95% of confidence interval (Müller-putz et

al., 2008)), but the average performance across their sessions is above the chance level for each of these three participants. Wilcoxon signed rank test showed that averaged online MI CA are higher than EII CA ($p < 0.05$).

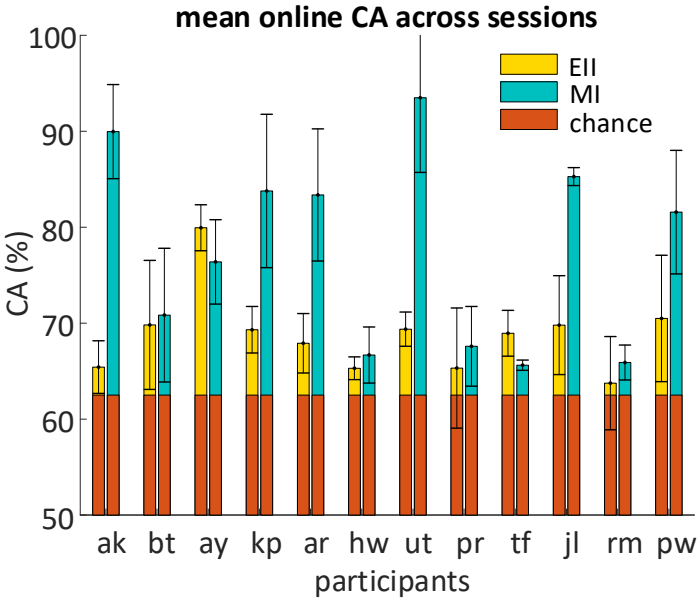

Figure 5-6. Online single trial classification accuracies averaged across sessions for each participant with theoretical chancel level (random-CA)

The re-simulated online single trial classification accuracy results are reported in Figure 5-7 (the NTSPP results are from actual online runs with participants). The framework with highest averaged CA across participants, for EII, is the COMB framework with averaged CA of 71.64% across participants. The frameworks with lowest performance in EII case are observed in FBCSP and ASYM frameworks with average CAs across participants of 66.82% and 66.92%, respectively. For MI, the best performing framework is the NTSPP-based framework with average CA of 77.54% across participants, and ASYM-based framework least performing with average CA of 67.05%.

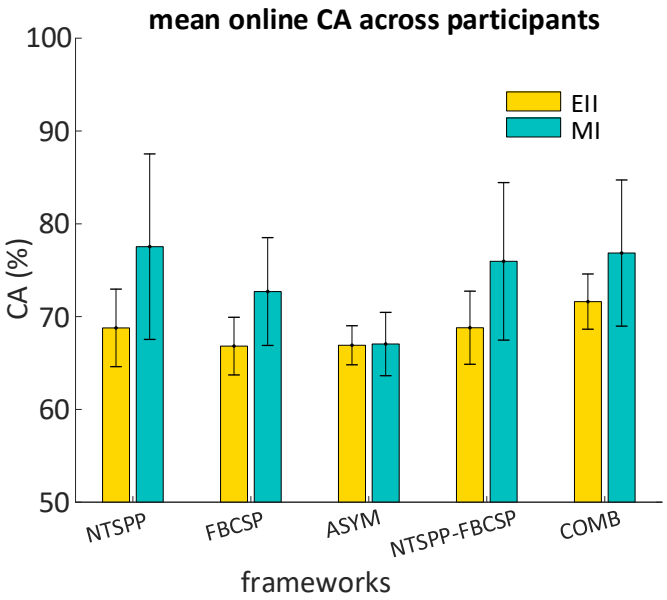

Figure 5-7. The online single-trial CA during recording (with NTSPP) and re-simulated single-trial CA (with FBCSP, ASYM, NTSPP-FBCSP, and COMB frameworks) averaged across all participants for EII and MI approaches.

The repeated analysis of variance (ANOVA) results show that the performance of the two imagery types are significantly different, $F(1, 11) = 8.45$, $p < 0.05$, $\eta^2 = 0.44$; the performance with MI is significantly higher than performance with EII ($p < 0.05$, Bonferroni corrected). The ANOVA results also show that there is a significant difference of performance across the frameworks, $F(4, 44) = 13.79$, $p < 0.001$, $\eta^2 = 0.56$. Further pairwise comparisons (Bonferroni corrected) shows that the performance with ASYM framework is significantly lower than the performance with NTSPP framework ($p < 0.05$), significantly lower than the performance with NTSPP-FBCSP framework ($p < 0.05$), significantly lower than the performance with COMB ($p < 0.001$), but not significantly different from the performance with FBCSP-framework ($p = 0.21$). The performance achieved with COMB framework is significantly higher than the performance with FBCSP framework ($p < 0.05$), but not different from performance achieved with NTSPP framework ($p = 1$) and not significantly different from the performance with NTSPP-FBCSP framework ($p = 0.11$). The performance with NTSPP framework was not significantly higher than performance with FBCSP framework ($p = 0.25$).

5.3.2 The Weighted Contribution of Different Electrodes and Frequency Bands

The contribution of different scalp areas (electrodes) toward MI and EII performance across participants is shown in Figure 5-8*(a)*. The electrodes contribution is shown as topographic map of

CSP-MIBIF weights averaged across participants at the time of peak cross-validation accuracy. For MI, the right and left central electrodes (C3, C4, and CP2) showed high weights. On the other hand, the electrodes with high weights for EII are located in central-parietal area (CP1, CP2, Cp6), parietal (PZ), and occipital (OZ). Comparing the colormap of the most relevant electrodes, the weights in the case of MI are higher than those in EII which suggests higher consistency in electrodes from MI.

The weighted contribution of different frequency bands is shown Figure 5-8*(b)*. Frequency bands contribution is presented as time-course of CSP-MIBIF weights for each frequency bands averaged across participants. The frequency bands covering 4-16Hz and 20-40Hz hold most of weight for EII, with high weights most prominent in the last 0.5s of the task execution across participants. For the MI case, most of the weight is distributed from frequency bands covering 4 to 32Hz, with high weights most prominent in the last 1.5s of the task execution.

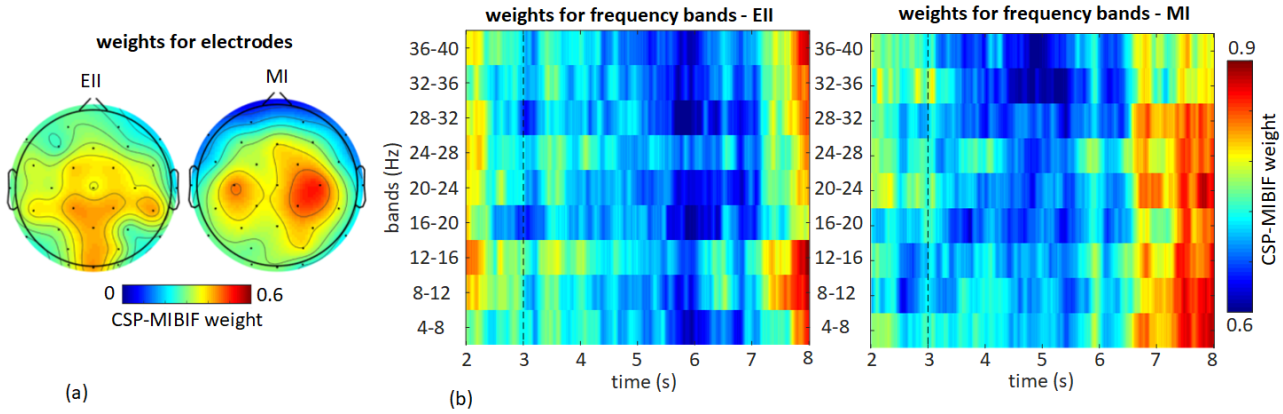

Figure 5-8. The CSP-mutual information best individual feature (MBIF) weights (a) for each electrodes at the time of peak cross-validation accuracy averaged across participants and (b) time-course weights for frequency bands for the two BCI approaches (EII and MI); the vertical dotted line in (b) indicate the task's cue, at 3s. The time-course in (b) starts at 2s because the analysis was based on a 2s sliding window.

5.3.3 Participants' Subjective Responses

In 88.24% of the sessions, the participants reported that MI was the favourite approach versus 11.76% for EII. Also participants reported that MI is the approach in which they perceived most control in 89.71% of the sessions versus 10.29% for EII.

5.3.4 Correlation between Pre-run EEG and Performance

The correlation between participants' performance and pre-run band power ratios is shown in the TABLE 5-1 for the EII and MI. Significant positive correlation between performance and frontal and parietal alpha ratio was observed for EII. For MI, significant positive correlation between performance and frontal and parietal beta ratio was observed, and frontal gamma ratio was significantly correlated with performance across participants.

TABLE 5-1. Pearson correlation results of frequency bands ratios during pre-run EEG and classification accuracy across participants. The significant correlations are represented by '' for p-value < 0.05, '**' for p-value < 0.01 and '*** for p-value <0.001.*

	Alpha ratio		***Beta ratio***		***Gamma ratio***	
Scalp areas	EII	MI	EII	MI	EII	MI
left frontal	***			***		*
right frontal	***			***		*
left central parietal	***			***		
right central parietal	***			**		
middle line parietal	**			*		

5.4 Discussion

5.4.1 Performance of EII versus MI

The main aim of this study was to compare performance of emotion-inducing imagery versus motor imagery BCI strategies across multiple recording sessions involving online visual feedback. A preliminary single-session based study previously reported comparable performance between EII and MI (Bigirimana et al., 2017), however the results presented here show that performance with MI is significantly higher than EII performance. Nine out of the twelve participants performed above chance level CA in all their EII runs, but only 4 participants (*bt*, *ay*, *jl* and *pw*) achieved mean online $CA \geq 70\%$, usually considered as acceptable performance for BCI setup used in this study (Vidaurre and Blankertz, 2010). Some of the participants (i.e. *ak*, *kp*, *ar*, and *ut*) showed acceptable MI performance but poor EII performance. Some of the participants (i.e. *ay* and *tf*) performed better with EII than with MI.

The results from re-simulating online runs using various frameworks show that MI outperforms EII. These results also show that among BCIs tested (NTSPP, FBCSP, ASYM, NTSPP-FBCSP, and COMB), the best performing BCI setup is NTSPP for MI which is also the setup used during the online runs. To our knowledge, this is the first time the NTSPP is compared to FBCSP in a multi-session MI. For EII, the combination of all the frameworks led to best performing framework but not significantly different from the NTSPP-based setup used in the actual EII feedback runs.

Four participants achieved acceptable performance (above 70% for CA) with EII, and one of them (i.e. *ay*) performed better than with MI, as shown in Figure 5-6. This result suggests that these four participants, especially '*ay*', may be able used EII as an alternative imagery approach for BCI. On the other hand, eight participants achieved acceptable accuracy with MI, and six of them performed better than with EII. These results suggest a hybrid MI-EII BCI may suit some BCI users. Since in our study the tasks used in EII were limited to imagining (or recalling) sad and happy events, future work should consider widening the range of imagery tasks selection to include emotional faces, scenes, objects, pictures, words, and sounds. With a wide range of imagery tasks, BCI users, especially those with poor MI performance, are likely to find suitable imagery tasks that may lead to improved performance in classification accuracy and comfort of use.

Apart from the superior CA performance of MI over EII, participants preferred MI to EII as a BCI control approach. This preference is likely influenced by difficulty experienced in accessing repeatedly similar events in memory in a short time-period. Furthermore, recalling emotional events may trigger a series of memories, which make it hard to focus on the targeted event. This issue could be alleviated by asking participants to recall attributes or objects (Korik et al., 2018) which can be associated with some emotional events or with emotional states, e.g. odours, as in (Iacoviello et al., 2015).

5.4.2 Signal processing frameworks performance comparison

In this study, the performance of MI was consistently higher than the performance of EII across NTSPP, FBCP, NTSPP-FBCSP and COMB frameworks. The NTSPP framework averaged the highest performance across participants for MI but not in the case of EII. The average performance of EII is higher with a signal processing framework that combines the NTSPP, FBCSP and ASYM frameworks (COMB). The observed high EII performance could be due to the COMB framework accessing several different features associated to complex processes of emotions in the brain. Emotions are claimed to be associated with complex neural circuitry (Dalgleish, 2004). Having different setups combined into the COMB framework and each setup individually discriminating the classes by using different

features, this allows extraction of features associated to neural processes of interest. The resulting decision for COMB is likely to consider relevant features associated to EII processes in the brain.

5.4.3 Pre BCI-use and BCI performance relationship

Through frequency content analysis of brain activity before feedback run, we identified different scalp areas and frequency bands correlating with performance in EII and MI across participants, but there were not enough samples to establish such associations per participant. Previously, Ahn and colleagues (Ahn et al., 2013a), from recordings runs scheduled on the same day, have reported significant correlation of gamma power ratio during resting state magnetoencephalogram (MEG) and motor imagery classification performance achieved with EEG (simultaneously recorded with MEG). In the study presented in this chapter, the correlation analysis involves several sessions scheduled at different days for each individual participant, and there was a significant correlation between frontal gamma ratio and MI performance was observed. To the best knowledge of to the author, there are no previous studies assessing the relationship between spectral content of EEG before using BCI (pre-run) and EII BCI performance. The knowledge of how pre-run power ratios are associated with a given participant's performance may enable monitoring and identification of the participant's optimal state for good performance and/or adaption and selection of BCI parameters. Future effort should focus on identifying activity or tasks that increase or decrease targeted spectral content in neural signals during the period before using BCI.

5.4.4 Frequency Bands and Electrodes Contribution to MI and EII Performance

The results for relevant electrodes during task execution show that the electrodes mounted on sensorimotor cortex are most important for MI across participants. This finding is in line with the claim that a MI task activate sensorimotor cortex (Pfurtscheller and Neuper, 1997). For EII, the electrodes with most weights are mounted on central-parietal, parietal and occipital areas. The weights for relevant electrodes across participants are lower in EII case than in MI. The low weights of electrodes after averaging across participants, in EII case, suggest that spatial patterns and frequencies engaged by EII tasks are different across participants. EII task may activate several areas of the brain including the frontal, temporal and visual areas (Addis et al., 2007) depending on the imagery vividness, and this might be the reason we observe non-negligible weights for frontal electrodes with EII in Figure 5-8*(a)*.

The time-course of weights for frequency bands relevancy across participant shows that after the cue (3s), the weights decrease (mostly visible from 4 to 6s, in Figure 5-8*(b)*), and then increase for both EII and MI. The high weights indicate most relevant frequency bands across participants at a given

time during the task execution. The high weights are mainly observed during the last 0.5s in the task execution for EII whereas for MI this is observed during the last 1.5s. The high weights observed at the end of the task execution for EII case suggests that the EII tasks classification performance may benefit from increasing the task execution period. The high weights being sustained for short period in EII case may be due to variation of imageries used in EII tasks across participants. Future studies on EII should consider minimizing variation in imageries, by using imagery of specific objects or attributes commonly associated with emotional states (e.g., baby's laugh, which could be associated with happy event) consistently across participants as stimuli.

5.5 Conclusion

The comparison between motor imagery and emotion-inducing imagery as BCI control strategies across several recording sessions with online feedback control showed that MI outperforms EII. The MI performed best with NTSPP among the considered signal processing frameworks which included FBCSP, the state-of-the-art framework for MI based BCI. We found that EII performance benefits from fusing varied EEG features, EII performs best in the framework that combines all the considered frameworks here, and this finding should be exploited by future EII studies.

EII may offer a viable alternative in some cases for subjects who cannot control a motor imagery BCI, but, given the small number of participants in the present study, further investigation is necessary to identify effective EII tasks that might be easy to execute in a BCI paradigm and potentially combined with MI tasks to create a multi-class and/or hybrid BCI. It would be also worth a while investigating the neural profile for users who achieve good performance with EII.

CHAPTER 6

6 CONCLUSION AND FUTURE WORK

6.1 Concluding Summary

This chapter summarises the work presented in the thesis and outlines the contributions of this work. The thesis focused on investigating emotions in the framework of enhancing BCI with emotion classification. In chapter 2, various types of BCIs were outlined, and different stages involved in BCI development were reviewed. One type of BCIs is active BCI which requires the user to intentionally modulate the brain signals by engaging in specific mental tasks. Another type of BCIs is passive BCI which relies on modulating brain activity by presenting some stimuli to the BCI's user. The BCI development is based on extracting and classifying features representing the changes in brain activity associated with neural processing of the mental task or presented stimulus. The state-of-the-art BCIs are built on established knowledge of brain areas activated during processing mental tasks or presented stimuli. Motor imagery-based BCI targets the features associated with activity on the motor cortex. Visual-evoked-based BCI targets the features from visual processing areas in the occipital and parietal lobes. Brain areas associated with different emotions are yet to be established, but some progress has been made. Some studies found increase of activation in left prefrontal area associated with positive emotions and increase of activation in right prefrontal area associated with negative emotions. Emotion classification studies utilize similar features extraction methods as in BCI, and in most of the cases, no specific area of the brain is targeted in feature extraction. The studies reviewed in chapter 2 show that good accuracy can be achieved in emotion classification using features extracted from brain activity data.

In chapter 3, building on the review of classification studies in chapter 2, the effect on classification accuracy of different methods for removing artefacts from EEG data were compared. This investigation made use of EEG dataset containing four classes of emotions defined in terms of arousal and valence levels (see section 2.3.1.1): high arousal-high valence (HAHV), high arousal-low valence (HALV), low arousal-high valence (LAHV), and low arousal-low valence (LALV). The results indicated that automated hybrid ICA-wavelet transform method (ICA-W) combined with statistical features enhanced emotion classification accuracy compared to the rest of the methods: band-pass filtering, manual independent component analysis (ICA), and artefact detection approach based on joint spatial and temporal characteristics (ADJUST). ICA-W was associated with higher classification

accuracy performance compared to the performance of other emotion recognition studies utilising the same emotion dataset, DEAP.

In chapter 4, emotion-inducing imagery (EII) was presented as a novel potential alternative BCI control strategy for motor imagery (MI). During EII, a participant intentionally modulates the brain signals by recalling happy and events or imagining happy and sad events. Two studies are reported in chapter 4, and in both of them, the data recording followed the standard motor imagery paradigm, and the features extraction method was based on common spatial patterns (CSP). One of the studies looked at the classification performance of EII using EEG and MEEG data, and it also looked at the difference in the brain activity for happy and sad imageries across 10 participants. The results showed that half of the participants achieved acceptable BCI performance with EII, CA of 70% and above which is considered as acceptable performance for a 2-class BCI setup (Vidaurre and Blankertz, 2010). Furthermore, imageries for sad events were significantly different from imageries for happy events in EEG electrodes mounted in the frontal, central and parietal areas close to the middle line. The second study carried out preliminary comparison between classification performance of EII and performance of MI. Seven participants participated in a calibration run and an online feedback run. A linear discriminant analysis (LDA) classifier was trained on CSP-based features from the calibration run and applied on the online run to drive the feedback. The results showed no significant difference between the performance of EII and performance of MI in this preliminary comparison study.

In chapter 5, building on the results from preliminary comparison study in chapter 4, a comprehensive comparison between the performance of EII and performance of MI as a BCI control strategy was reported. EII and MI were compared in a study with 12 participants across multiple EEG data recording sessions, and each session was made of a calibration run and feedback run for both EII and MI. EII and MI are compared across different signal-processing frameworks: neural-time-series-prediction-pre-processing (NTSPP), filter bank common spatial patterns (FBCSP), hemispheric asymmetry (ASYM), combination of NTSPP and FBCSP, and combination of all the three (NTSPP, FBCSP, and ASYM). The relationship between the brain state prior to engaging in the feedback run and the performance for the feedback run for EII and MI was established as well. The results showed significant correlation across participants in relationship between alpha power ratio in EEG before using a BCI and the EII performance achieved during the BCI use. For the MI, significant correlation between MI performance during BCI use and the beta and frontal gamma ratios in the EEG prior to using BCI was observed. Besides pre-BCI use and BCI use relationship, the results in chapter 5 showed that MI classification performance was significantly higher than EII classification performance across

participants, and that the majority of the participants preferred MI over the EII as their favourite imagery and imagery strategy with most control. The results also showed that some participants were able to consistently achieve good performance with EII which suggests that EII may be a viable alternative imagery for some BCI users.

6.2 Summary of contributions

In summary, there four main contributions associated with passive and active emotions monitoring presented in this thesis:

- ***The first contribution*** consists of introducing hybrid ICA-Wavelet transform (ICA-W) as a pre-processing method to enhance emotion classification. This contribution is associated with the objective 1 of this thesis. The ICA-W is automated, and the results presented in this thesis showed that ICA-W is associated with higher classification accuracy compared to other automated or manual ICA methods.
- ***The second contribution*** consists of introducing emotion-inducing imagery as a potential alternative imagery of motor imagery for BCI control. The second contribution is associated with objective 2 of this thesis. A single session based MEG/EEG pilot study and multiple sessions-based EEG study were carried out, and the results established that some BCI users can achieve good performance with EII. Furthermore, significant differences were observed between time-frequency analysis of happy and sad imageries in the frontal, central and parietal areas close to the middle line. The results from multiple sessions-based study showed that the EEG electrodes from these areas are the most relevant for classification of EEI tasks used (happy, sad imageries).
- ***The third contribution*** is the comparison of EII and MI as BCI control strategies. This contribution is associated with the objective 4 of the thesis. In a multisession study, some of the participants (i.e. *ay* and *tf*, see section 5.4.1) achieved better performance with EII than with MI. However, MI outperformed EII across participants overall, and MI was also the favourite imagery strategy and the imagery strategy with most control for the majority of the participants.
- ***The fourth contribution*** consists of establishing the correlation between prior BCI use period and performance during BCI usage. The results from a study consisting of multiple sessions, reported in chapter 5, showed significant correlation between the band power ratios computed from EEG data recorded during pre-BCI use and the EII-based BCI performance of some participants (see section 5.3.4). Identifying pre-BCI use brain activity features associated with increase in BCI performance may enable to target optimal mental state prior using BCI.

- ***The fifth contribution*** consists of establishing the road toward the best signal processing framework for EII. This contribution is associated with objective 3 of this thesis. The analysis of EII across several signal processing frameworks showed that a combination of NTSPP, FBCSP, and ASYM establishes the optimal signal processing framework for EII. A related secondary contribution consists of establishing that NTSPP is the best framework for MI.

6.3 Future work direction

Despite the promising findings reported in this thesis for ICA-W as pre-processing method and EII as a BCI control strategy, there are various limitations and challenges. These limitations are discussed in the following sections together with potential future work direction.

6.3.1 ICA-W future directions

The assessment that led to ICA-W as the best performing pre-processing method included only other ICA-based pre-processing and band pass filtering. The future work should look how ICA-W compares to spatial filters, such as Laplacian filtering (Gordon and Rzempoluck, 2004) (Murugappan et al., 2011). Future studies should also investigate how ICA-W affect the features selection, not just the classification accuracy.

6.3.2 EII future directions

The EII studies in this thesis utilized EII tasks: recalling or imagining happy versus sad events. The tasks were selected based on literature review which suggests fundamental differences in brain activation for positive (e.g., happy) and negative emotions (e.g., sad) (Davidson et al., 1990) (Canli, 1999) (Allen et al., 2001). Even though, each participant carried out the same types of EII tasks, the actual EII varied across participants as each participant selected his/her happy and sad events on his/her own. These led to some limitations in EII group analysis: originally recorded brain activity data vary significantly from participant to participant, and with the variation in tasks carried out across participants (especially variation in the task's content: valence and arousal content). Future work should consider minimizing variation in EII tasks by using imagery associated to specific objects, e.g., odour as in (Iacoviello et al., 2015). Further comprehensive investigation is recommended in order to establish effective tasks which should be easy to execute in a standard BCI setup. In addition to the EII tasks limitations, signal processing methods were limited only to standard emotion recognition frameworks and common high performing motor imagery based machine learning methods. Future studies should investigate any benefit from using deep learning methods (Bashivan et al., 2016) (Jodat

and Amirizadeh, 2017) (Craik et al., 2019) in segregating information from EEG or MEG data associated with EII tasks. Future work should also consider combining EII and MI into a multi-class BCI or hybrid BCI.

REFERENCES

7 REFERENCES

Abiyev, R. H., Akkaya, N., Aytac, E., Günsel, I., and Çağman, A. (2016). Brain-Computer Interface for Control of Wheelchair Using Fuzzy Neural Networks. *Biomed Res. Int.* 2016. doi:10.1155/2016/9359868.

Addis, D. R., Wong, A. T., and Schacter, D. L. (2007). Remembering the past and imagining the future: Common and distinct neural substrates during event construction and elaboration. *Neuropsychologia* 45, 1363–1377. doi:10.1016/j.neuropsychologia.2006.10.016.

Ahern, G. L., and Schwartz, G. E. (1985). Differential lateralization for positive and negative emotion in the human brain: EEG spectral analysis. *Neuropsychologia* 23, 745–755. doi:10.1016/0028-3932(85)90081-8.

Ahn, M., Ahn, S., Hong, J. H., Cho, H., Kim, K., Kim, B. S., et al. (2013a). Gamma band activity associated with BCI performance: simultaneous MEG/EEG study. *Front. Hum. Neurosci.* 7, 1–10. doi:10.3389/fnhum.2013.00848.

Ahn, M., Cho, H., Ahn, S., and Jun, S. C. (2013b). High Theta and Low Alpha Powers May Be Indicative of BCI-Illiteracy in Motor Imagery. *PLoS One* 8, e80886. doi:10.1371/journal.pone.0080886.

Ahn, M., Lee, M., Choi, J., and Jun, S. C. han (2014). A review of brain-computer interface games and an opinion survey from researchers, developers and users. *Sensors (Basel).* 14, 14601–14633. doi:10.3390/s140814601.

Akhtar, M. T., Mitsuhashi, W., and James, C. J. (2012). Employing spatially constrained ICA and wavelet denoising, for automatic removal of artifacts from multichannel EEG data. *Signal Processing* 92, 401–416. doi:10.1016/j.sigpro.2011.08.005.

Alarcao, S. M., and Fonseca, M. J. (2017). Emotions Recognition Using EEG Signals: A Survey. *IEEE Trans. Affect. Comput.* 3045, 1–20. doi:10.1109/TAFFC.2017.2714671.

Alazrai, R., Homoud, R., Alwanni, H., and Daoud, M. I. (2018). EEG-based emotion recognition using quadratic time-frequency distribution. *Sensors* 18, 1–32. doi:10.3390/s18082739.

Allen, J. J. B., Harmon-Jones, E., and Cavender, J. H. (2001). Manipulation of frontal EEG asymmetry

through biofeedback alters self-reported emotional responses and facial EMG. *Psychophysiology* 38, 685–693. doi:10.1111/1469-8986.3840685.

Ang, K. K., Chin, Z. Y., Wang, C., Guan, C., and Zhang, H. (2012). Filter Bank Common Spatial Pattern Algorithm on BCI Competition IV Datasets 2a and 2b. *Front. Neurosci.* 6, 1–9. doi:10.3389/fnins.2012.00039.

Anh, V. H., Van, M. N., Ha, B. B., and Quyet, T. H. (2012). A Real-Time Model Based Support Vector Machine for Emotion Recognition Through EEG. in *2012 International Conference on Control, Automation and Information Sciences (ICCAIS)* (Ho Chi Minh City: IEEE), 191–196. doi:10.1109/ICCAIS.2012.6466585.

Armstrong, R. W. (2007). Definition and classification of cerebral palsy. *Dev. Med. Child Neurol.* 49, 166. doi:10.1111/j.1469-8749.2007.00166.x.

Babiloni, F., Bianchi, L., Semeraro, F., del R. Millan, J., Mourino, J., Cattini, A., et al. (2001). Mahalanobis distance-based classifiers are able to recognize EEG patterns by using few EEG electrodes. in *2001 Conference Proceedings of the 23rd Annual International Conference of the IEEE Engineering in Medicine and Biology Society*, 651–654. doi:10.1109/IEMBS.2001.1019019.

Baillet, S., Mosher, J. C., and Leahy, R. M. (2001). Electromagnetic brain mapping. *IEEE Signal Process. Mag.* 18, 14–30. doi:10.1109/79.962275.

Bajaj, V., and Pachori, R. B. (2014). "Detection of Human Emotions Using Features Based on the Multiwavelet Transform of EEG Signals," in *Brain-Computer Interfaces: Current Trends and Applications*, 215–240. doi:10.1007/978-3-319-10978-7_8.

Balconi, M., and Pozzoli, U. (2009). Arousal effect on emotional face comprehension. Frequency band changes in different time intervals. *Physiol. Behav.* 97, 455–462. doi:10.1016/j.physbeh.2009.03.023.

Bamdadian, A., Guan, C., Ang, K. K., and Xu, J. (2014). The predictive role of pre-cue EEG rhythms on MI-based BCI classification performance. *J. Neurosci. Methods* 235, 138–144. doi:10.1016/j.jneumeth.2014.06.011.

Barrett, L. F., Mesquita, B., Ochsner, K. N., and Gross, J. J. (2007). The Experience of Emotion. *Emotion* 58, 373–403. doi:10.1146/annurev.psych.58.110405.085709.

Bashivan, P., Rish, I., Yeasin, M., and Codella, N. (2016). Learning Representations From Eeg With

Deep Recurrent-Convolutional Neural Networks. in *ICLR 2016*, 1–15.

Betella, A., and Verschure, P. F. M. J. (2016). The affective slider: A digital self-assessment scale for the measurement of human emotions. *PLoS One* 11, 1–11. doi:10.1371/journal.pone.0148037.

Beveridge, R., Marshall, D., Wilson, S., and Coyle, D. (2015). Classification effects on Motion-Onset Visual Evoked Potentials using commercially available video games. in *2015 Computer Games: AI, Animation, Mobile, Multimedia, Educational and Serious Games (CGAMES)* (IEEE), 28–37. doi:10.1109/CGames.2015.7272958.

Beveridge, R., Wilson, S., Callaghan, M., and Coyle, D. (2019). Neurogaming with Motion-Onset Visual Evoked Potentials (mVEPs): Adults Versus Teenagers. *IEEE Trans. Neural Syst. Rehabil. Eng.* 27, 572–581. doi:10.1109/TNSRE.2019.2904260.

Biasiucci, A., Leeb, R., Iturrate, I., Perdikis, S., Al-Khodairy, A., Corbet, T., et al. (2018). Brain-actuated functional electrical stimulation elicits lasting arm motor recovery after stroke. *Nat. Commun.* 9, 1–13. doi:10.1038/s41467-018-04673-z.

Bigirimana, A. D., Siddique, N., and Coyle, D. (2016). A hybrid ICA-wavelet transform for automated artefact removal in EEG-based emotion recognition. in *2016 IEEE International Conference on Systems, Man, and Cybernetics (SMC)* (Budapest, Hungary: IEEE), 004429–004434. doi:10.1109/SMC.2016.7844928.

Bigirimana, A. D., Siddique, N., and Coyle, D. (2017). Brain-Computer Interfacing with Emotion-Inducing Imagery: A Pilot Study. in *7th Graz Brain-Computer Interface Conference (GBCIC)* (Graz, Austria: Verlag der TU Graz Graz University of Technology), 26–31. doi:10.3217/978-3-85125-533-1-06.

Blankertz, B., Dornhege, G., Krauledat, M., Müller, K. R., and Curio, G. (2007). The non-invasive Berlin Brain-Computer Interface: Fast acquisition of effective performance in untrained subjects. *Neuroimage* 37, 539–550. doi:10.1016/j.neuroimage.2007.01.051.

Blankertz, B., Sannelli, C., Halder, S., Hammer, E. M., Kübler, A., Müller, K. R., et al. (2010). Neurophysiological predictor of SMR-based BCI performance. *Neuroimage* 51, 1303–1309. doi:10.1016/j.neuroimage.2010.03.022.

Bradberry, T. J., Gentili, R. J., and Contreras-Vidal, J. L. (2010). Reconstructing three-dimensional hand movements from noninvasive electroencephalographic signals. *J. Neurosci.* 30, 3432–3437. doi:10.1523/JNEUROSCI.6107-09.2010.

Bradley, M. M., and Lang, P. J. (1994). Measuring emotion: The self-assessment manikin and the semantic differential. *J. Behav. Ther. Exp. Psychiatry* 25, 49–59. doi:10.1016/0005-7916(94)90063-9.

Bradley, M. M., and Lang, P. J. (2007). The International Affective Digitized Sounds (2nd Edition; IADS-2): Affective ratings of sounds and instruction manual. *Tech. Rep. B-3, Univ. Florida*.

Bundy, D. T., Souders, L., Baranyai, K., Leonard, L., Schalk, G., Coker, R., et al. (2017). Contralesional Brain-Computer Interface Control of a Powered Exoskeleton for Motor Recovery in Chronic Stroke Survivors. *Stroke* 48, 1908–1915. doi:10.1161/STROKEAHA.116.016304.

Burges, C. (1998). A Tutorial on Support Vector Machines for Pattern Recognition. *Data Min. Knowl. Discov.* 2, 121–167. doi:10.1023/A:1009715923555.

Canli, T. (1999). Hemispheric Asymmetry in the Experience of Emotion: A Perspective from Functional Imaging. *Neurosci.* 5, 201–207. doi:10.1177/107385849900500409.

Cans, C. (2007). Surveillance of cerebral palsy in Europe: a collaboration of cerebral palsy surveys and registers. *Dev. Med. Child Neurol.* 42, 816–824. doi:10.1111/j.1469-8749.2000.tb00695.x.

Cao, L., Liu, T., Hou, L., Wang, Z., Fan, C., Li, J., et al. (2019). A Novel Real-Time Multi-Phase BCI Speller Based on Sliding Control Paradigm of SSVEP. *IEEE Access* 7, 133974–133981. doi:10.1109/ACCESS.2019.2941642.

Castellanos, N. P., and Makarov, V. a. (2006). Recovering EEG brain signals: Artifact suppression with wavelet enhanced independent component analysis. *J. Neurosci. Methods* 158, 300–312. doi:10.1016/j.jneumeth.2006.05.033.

Chanel, G., Kierkels, J. J. M., Soleymani, M., and Pun, T. (2009). Short-term emotion assessment in a recall paradigm. *Int. J. Hum. Comput. Stud.* 67, 607–627. doi:10.1016/j.ijhcs.2009.03.005.

Chang, C., and Lin, C. (2011). LIBSVM : A Library for Support Vector Machines. *ACM Trans. Intell. Syst. Technol.* 2, 1–27. doi:10.1145/1961189.1961199.

Chao, H., Dong, L., Liu, Y., and Lu, B. (2019). Emotion recognition from multiband eeg signals using capsnet. *Sensors* 19. doi:10.3390/s19092212.

Chumerin, N., Manyakov, N. V., Van Vliet, M., Robben, A., Combaz, A., and Van Hulle, M. M. (2013). Steady-state visual evoked potential-based computer gaming on a consumer-grade EEG device. *IEEE Trans. Comput. Intell. AI Games* 5, 100–110. doi:10.1109/TCIAIG.2012.2225623.

Coan, J. a., and Allen, J. J. B. (2004). Frontal EEG asymmetry as a moderator and mediator of emotion.

Biol. Psychol. 67, 7–49. doi:10.1016/j.biopsycho.2004.03.002.

Cole, H. W., and Ray, W. J. (1985). EEG correlates of emotional tasks related to attentional demands. *Int. J. Psychophysiol.* 3, 33–41. doi:10.1016/0167-8760(85)90017-0.

Coyle, D. (2005). Intelligent Feature Extraction and Classification Techniques for Realisation of Brain-Computer Interface Systems.

Coyle, D. (2009). Neural network based auto association and time-series prediction for biosignal processing in brain-computer interfaces. *IEEE Comput. Intell. Mag.* 4, 47–59. doi:10.1109/MCI.2009.934560.

Coyle, D., Garcia, J., Satti, A. R., and McGinnity, T. M. (2011). EEG-based continuous control of a game using a 3 channel motor imagery BCI: BCI game. in *2011 IEEE Symposium on Computational Intelligence, Cognitive Algorithms, Mind, and Brain (CCMB)* (IEEE), 1–7. doi:10.1109/CCMB.2011.5952128.

Coyle, D., Prasad, G., and McGinnity, T. M. (2005). A time-frequency approach to feature extraction for a brain-computer interface with a comparative analysis of performance measures. *EURASIP J. Appl. Signal Processing* 2005, 3141–3151. doi:10.1155/ASP.2005.3141.

Coyle, D., Prasad, G., and McGinnity, T. M. (2009). Faster self-organizing fuzzy neural network training and a hyperparameter analysis for a brain-computer interface. *IEEE Trans. Syst. Man, Cybern. Part B Cybern.* 39, 1458–1471. doi:10.1109/TSMCB.2009.2018469.

Coyle, D., Stow, J., McCreadie, A. K., Li, C., Garcia, J., McElligott, J., et al. (2016). "Action Games, Motor Imagery, and Control Strategies: Toward a Multi-button Controller," in *Handbook of Digital Games and Entertainment Technologies*, eds. M. Cavazza and R. M. Young, 1–16.

Craik, A., He, Y., and Contreras-Vidal, J. L. (2019). Deep learning for electroencephalogram (EEG) classification tasks: a review. *J. Neural Eng.* 16, 031001. doi:10.1088/1741-2552/ab0ab5.

Curran, E. A., and Stokes, M. J. (2003). Learning to control brain activity: A review of the production and control of EEG components for driving brain-computer interface (BCI) systems. *Brain Cogn.* 51, 326–336. doi:10.1016/S0278-2626(03)00036-8.

Curran, E., Sykacek, P., Stokes, M., Roberts, S. J., Penny, W., Johnsrude, I., et al. (2004). Cognitive Tasks for Driving a Brain-Computer Interfacing System: A Pilot Study. *IEEE Trans. Neural Syst. Rehabil. Eng.* 12, 48–54. doi:10.1109/TNSRE.2003.821372.

Dalgleish, T. (2004). The emotional brain. *Nat. Rev. Neurosci.* 5, 582–589. doi:10.1038/nrn1432.

Damasio, A. R., Grabowski, T. J., Bechara, A., Damasio, H., Ponto, L. L. B., Parvizi, J., et al. (2000). Subcortical and cortical brain activity during the feeling of self-generated emotions. *Nat. Neurosci.* 3, 1049–1056. doi:10.1038/79871.

Dan-Glauser, E. S., and Scherer, K. R. (2011). The Geneva affective picture database (GAPED): a new 730-picture database focusing on valence and normative significance. *Behav. Res. Methods* 43, 468–77. doi:10.3758/s13428-011-0064-1.

Darwin, C. (1956). THE EXPRESSION OF THE EMOTIONS IN MAN AND ANIMALS. *Am. J. Med. Sci.* 232, 477. doi:10.1097/00000441-195610000-00024.

Davidson, R. J. (1992). Anterior cerebral asymmetry and the nature of emotion. *Brain Cogn.* 20, 125–151. doi:10.1016/0278-2626(92)90065-T.

Davidson, R. J. (2002). Anxiety and affective style: Role of prefrontal cortex and amygdala. *Biol. Psychiatry* 51, 68–80. doi:10.1016/S0006-3223(01)01328-2.

Davidson, R. J., Ekman, P., Saron, C. D., Senulis, J. A., and Friesen, W. V (1990). Approach-withdrawal and cerebral asymmetry: emotional expression and brain physiology I. *J. Pers. Soc. Psychol.* 58, 330–341. doi:10.1037/0022-3514.58.2.330.

Davidson, R. J., Pizzagalli, D., Nitschke, J. B., and Kalin, N. H. (2003). "Parsing the subcomponents of emotion and disorders of emotion: Perspectives from affective neuroscience," in *Handbook of affective sciences* (Oxford University Press Oxford,, UK), 8–24.

Dayan, N., Bigirimana, A., Mccann, A., Stow, J., Mcelligott, J., Carroll, A., et al. (2019). Towards Answering Questions in Disorders of Consciousness and Locked-In Syndrome with a SMR-BCI. in *Proceedings of the 8th Graz Brain-Computer Interface Conference* doi:10.3217/978-3-85125-682-6-65.

de Jong, T. (2010). Cognitive load theory, educational research, and instructional design: Some food for thought. *Instr. Sci.* 38, 105–134. doi:10.1007/s11251-009-9110-0.

Delorme, a, Sejnowski, T., and Makeig, S. (2007). Enhanced detection of artifacts in EEG data using higher-order statistics and independent component analysis. *Neuroimage* 34, 1443–1449. doi:10.1016/j.neuroimage.2006.11.004.

Delorme, A., and Makeig, S. (2004). EEGLAB: An open source toolbox for analysis of single-trial EEG dynamics including independent component analysis. *J. Neurosci. Methods* 134, 9–21. doi:10.1016/j.jneumeth.2003.10.009.

Donchin, E., Spencer, K. M., and Wijesinghe, R. (2000). The mental prosthesis: Assessing the speed of a P300-based brain- computer interface. *IEEE Trans. Rehabil. Eng.* 8, 174–179. doi:10.1109/86.847808.

Donoho, D. L. (1993). Nonlinear Wavelet Methods for Recovery of Signals, Densities, and Spectra from Indirect and Noisy Data. in *Proceedings of Symposia in Applied Mathematics*, 173–205.

Durka, P. J., Ircha, D., Neuper, C., and Pfurtscheller, G. (2001). Time-frequency microstructure of event-related electro-encephalogram desynchronisation and synchronisation. *Med. Biol. Eng. Comput.* 39, 315–321. doi:10.1007/BF02345286.

Ekman, P. (1999). "Basic emotions," in *Handbook of cognition and emotion*, eds. T. Dalgleish and M. Power (New York: Wiley), 45–60. doi:10.1002/0470013494.ch3.

Erfanian, A., Oveisi, F., and Shadvar, A. (2011). "Feature Extraction by Mutual Information Based on Minimal-Redundancy-Maximal-Relevance Criterion and Its Application to Classifying EEG Signal for Brain-Computer Interfaces," in *Recent Advances in Brain-Computer Interface Systems*, 65. Available at: http://www.intechopen.com/books/recent-advances-in-brain- computer-interface-systems/feature-extraction-by-mutual-information-based-on-minimal-redundancy-maximal- relevance-criterion-and.

Eskandari, P., and Erfanian, A. (2008). Improving the performance of brain-computer interface through meditation practicing. in *2008 30th Annual International Conference of the IEEE Engineering in Medicine and Biology Society* (IEEE), 662–665. doi:10.1109/IEMBS.2008.4649239.

Estepp, J. R., and Christensen, J. C. (2015). Electrode replacement does not affect classification accuracy in dual- session use of a passive brain-computer interface for assessing cognitive workload. *Front. Neurosci.* 9, 1–20. doi:10.3389/fnins.2015.00054.

Fay, M. P., and Follmann, D. A. (2002). Designing Monte Carlo Implementations of Permutation or Bootstrap Hypothesis Tests. *Am. Stat.* 56, 63–70.

Felten, D. L., O'Banion, M. K., and Maida, M. S. (2016). *Netter's Atlas of Neuroscience*. 3rd ed. Elsevier Inc.

Fetz, E. E. (2007). Volitional control of neural activity: implications for brain-computer interfaces. *J. Physiol.* 579, 571–579. doi:10.1113/jphysiol.2006.127142.

Frantzidis, C. a., Bratsas, C., Papadelis, C. L., Konstantinidis, E., Pappas, C., and Bamidis, P. D.

(2010). Toward emotion aware computing: An integrated approach using multichannel neurophysiological recordings and affective visual stimuli. *IEEE Trans. Inf. Technol. Biomed.* 14, 589–597. doi:10.1109/TITB.2010.2041553.

Friedrich, E. V. C., Scherer, R., and Neuper, C. (2012). The effect of distinct mental strategies on classification performance for brain-computer interfaces. *Int. J. Psychophysiol.* 84, 86–94. doi:10.1016/j.ijpsycho.2012.01.014.

Gerloff, C., Richard, J., Hadley, J., Schulman, A. E., Honda, M., and Hallett, M. (1998). Functional coupling and regional activation of human cortical motor areas during simple, internally paced and externally paced finger movements. *Brain* 121, 1513–1531. doi:10.1093/brain/121.8.1513.

Giorgetta, C., Grecucci, A., Bonini, N., Coricelli, G., Demarchi, G., Braun, C., et al. (2013). Waves of regret: A meg study of emotion and decision-making. *Neuropsychologia* 51, 38–51. doi:10.1016/j.neuropsychologia.2012.10.015.

Goncharova, I. I., McFarland, D. J., Vaughan, T. M., and Wolpaw, J. R. (2003). EMG contamination of EEG: Spectral and topographical characteristics. *Clin. Neurophysiol.* 114, 1580–1593. doi:10.1016/S1388-2457(03)00093-2.

Gordon, R., and Rzempoluck, E. J. (2004). Introduction to Laplacian montages. *Am. J. Electroneurodiagnostic Technol.* 44, 98–102. doi:10.1080/1086508X.2004.11079469.

Gross, J. J. (2015). Emotion Regulation: Current Status and Future Prospects. *Psychol. Inq.* 26, 1–26. doi:10.1080/1047840X.2014.940781.

Gross, J. J., and Thompson, R. (2007). "Emotion regulation: Conceptual foundations," in *J. J. Gross (Eds.) Handbook of Emotion Regulation*, ed. Guilford (New York), 3–24.

Gu, J., Wang, Z., Kuen, J., Ma, L., Shahroudy, A., Shuai, B., et al. (2018). Recent advances in convolutional neural networks. *Pattern Recognit.* 77, 354–377. doi:10.1016/j.patcog.2017.10.013.

Guger, C., Daban, S., Sellers, E., Holzner, C., Krausz, G., Carabalona, R., et al. (2009). How many people are able to control a P300-based brain-computer interface (BCI)? *Neurosci. Lett.* 462, 94–98. doi:10.1016/j.neulet.2009.06.045.

Gupta, V., Chopda, M. D., and Pachori, R. B. (2019). Cross-Subject Emotion Recognition Using Flexible Analytic Wavelet Transform from EEG Signals. *IEEE Sens. J.* 19, 2266–2274. doi:10.1109/JSEN.2018.2883497.

Hamann, S. (2012). Mapping discrete and dimensional emotions onto the brain: Controversies and consensus. *Trends Cogn. Sci.* 16, 458. doi:10.1016/j.tics.2012.07.006.

Hamann, S., and Canli, T. (2004). Individual differences in emotion processing. *Curr. Opin. Neurobiol.* 14, 233–238. doi:10.1016/j.conb.2004.03.010.

Harlow, J. M. (1868). Recovery from the passage of an iron bar through the head. *Public Massachusetts Med. Soc.* 2, 327–334.

Headley, D. B., and Paré, D. (2013). In sync: gamma oscillations and emotional memory. *Front. Behav. Neurosci.* 7, 12. doi:10.3389/fnbeh.2013.00170.

Healey, J., and Picard, R. (1998). Digital processing of affective signals. *Proc. 1998 IEEE Int. Conf. Acoust. Speech Signal Process. ICASSP '98 (Cat. No.98CH36181)* 6, 3749–3752. doi:10.1109/ICASSP.1998.679699.

Hsu, W. Y., Lin, C. H., Hsu, H. J., Chen, P. H., and Chen, I. R. (2012). Wavelet-based envelope features with automatic EOG artifact removal: Application to single-trial EEG data. *Expert Syst. Appl.* 39, 2743–2749. doi:10.1016/j.eswa.2011.08.132.

Huang, C. L., and Wang, C. J. (2006). A GA-based feature selection and parameters optimizationfor support vector machines. *Expert Syst. Appl.* 31, 231–240. doi:10.1016/j.eswa.2005.09.024.

Huang, D., Zhang, H., Ang, K., Guan, C., Pan, Y., Wang, C., et al. (2012). Fast emotion detection from EEG using asymmetric spatial filtering. in *Acoustics, Speech and Signal Processing (ICASSP)*, 589–592. Available at: http://ieeexplore.ieee.org/xpls/abs_all.jsp?arnumber=6287952.

Iacoviello, D., Petracca, A., Spezialetti, M., and Placidi, G. (2015). A real-time classification algorithm for EEG-based BCI driven by self-induced emotions. *Comput. Methods Programs Biomed.* 122, 293–303. doi:10.1016/j.cmpb.2015.08.011.

Intriligator, J., and Polich, J. (1994). On the relationship between background EEG and the P300 event-related potential. *Biol. Psychol.* 37, 207–218. doi:10.1016/0301-0511(94)90003-5.

Jafarifarmand, A., and Badamchizadeh, M. A. (2013). Artifacts removal in EEG signal using a new neural network enhanced adaptive filter. *Neurocomputing* 103, 222–231. doi:10.1016/j.neucom.2012.09.024.

Jain, A. K., Duin, R. P. W., and Mao, J. (2000). Statistical pattern recognition: a review. *IEEE Trans. Pattern Anal. Mach. Intell.* 22, 4–37. doi:10.1109/34.824819.

Jenke, R., Peer, A., and Buss, M. (2014). Feature Extraction and Selection for Emotion Recognition

from EEG. *IEEE Trans. Affect. Comput.* 5, 327–339. doi:10.1109/TAFFC.2014.2339834.

Jeunet, C., Nkaoua, B., Subramanian, S., Hachet, M., and Lotte, F. (2015). Predicting Mental Imagery-Based BCI Performance from Personality, Cognitive Profile and Neurophysiological Patterns. *PLoS One* 10, 1–21. doi:10.1371/journal.pone.0143962.

Jodat, S., and Amirizadeh, K. (2017). Enhanced EEG-Based Emotion Detection Technique using Deep Belief Network and Wavelet Transform. 2, 56–67.

Johnston, S. J., Boehm, S. G., Healy, D., Goebel, R., and Linden, D. E. J. (2010). Neurofeedback: A promising tool for the self-regulation of emotion networks. *Neuroimage* 49, 1066–1072. doi:10.1016/j.neuroimage.2009.07.056.

Jung, T.-P. P., Makeig, S., Humphries, C., Lee, T.-W. W., McKeown, M. J., Iragui, V., et al. (2000). Removing electroencephalographic artifacts by blind source separation. *Psychophysiology* 37, 163–178. doi:10.1111/1469-8986.3720163.

Kai Keng Ang, Chai Quek, Ang, K. K., and Quek, C. (2006). Rough set-based neuro-fuzzy system. *2006 IEEE Int. Jt. Conf. Neural Netw. Proc.*, 742–749. doi:10.1109/IJCNN.2006.246758.

Kalcher, J., and Pfurtscheller, G. (1995). Discrimination between phase-locked and non-phase-locked event-related EEG activity. *Electroencephalogr. Clin. Neurophysiol.* 94, 381–384. doi:10.1016/0013-4694(95)00040-6.

Khosrowabadi, R., Member, S., Quek, C., Member, S., and Ang, K. K. (2011). ERNN : A biologically plausible feed-forward neural network to discriminate emotion from EEG signal.

Khosrowabadi, R., Quek, C., Ang, K. K., and Wahab, A. (2014). ERNN: A biologically inspired feedforward neural network to discriminate emotion from EEG signal. *IEEE Trans. Neural Networks Learn. Syst.* 25, 609–620. doi:10.1109/TNNLS.2013.2280271.

Khosrowabadi, R., Quek, H. C., Wahab, A., and Ang, K. K. (2010). EEG-based Emotion Recognition Using Self-Organizing Map for Boundary Detection. *2010 20th Int. Conf. Pattern Recognit.*, 4242–4245. doi:10.1109/ICPR.2010.1031.

Kiernan, M. C., Vucic, S., Cheah, B. C., Turner, M. R., Eisen, A., Hardiman, O., et al. (2011). Amyotrophic lateral sclerosis. *Lancet* 377, 942–955. doi:10.1016/S0140-6736(10)61156-7.

Kim, M.-K. M., Kim, M.-K. M., Oh, E., and Kim, S.-P. (2013). A Review on the Computational Methods for Emotional State Estimation from the Human EEG. *Comput. Math. Methods Med.* 2013, 1–13. doi:10.1155/2013/573734.

Klados, M. A., Frantzidis, C., Vivas, A. B., Papadelis, C., Lithari, C., Pappas, C., et al. (2009). A framework combining delta event-related oscillations (EROs) and synchronisation effects (ERD/ERS) to study emotional processing. *Comput. Intell. Neurosci.* 2009, 306. doi:10.1155/2009/549419.

Klimesch, W., Sauseng, P., and Hanslmayr, S. (2007). EEG alpha oscillations: The inhibition–timing hypothesis. *Brain Res. Rev.* 53, 63–88. doi:10.1016/j.brainresrev.2006.06.003.

Knerr, S., Personnaz, L., and Dreyfus, G. (1990). "Single-layer learning revisited: a stepwise procedure for building and training a neural network," in *Neurocomputing* (Berlin, Heidelberg: Springer Berlin Heidelberg), 41–50. doi:10.1007/978-3-642-76153-9_5.

Koelstra, S., Mühl, C., Soleymani, M., Lee, J. S., Yazdani, A., Ebrahimi, T., et al. (2012). DEAP: A database for emotion analysis; Using physiological signals. *IEEE Trans. Affect. Comput.* 3, 18–31. doi:10.1109/T-AFFC.2011.15.

Kohn, N., Eickhoff, S. B., Scheller, M., Laird, A. R., Fox, P. T., and Habel, U. (2014). Neural network of cognitive emotion regulation - An ALE meta-analysis and MACM analysis. *Neuroimage* 87, 345–355. doi:10.1016/j.neuroimage.2013.11.001.

Korik, A., Hay, L., Choo, P. L., Gilbert, S. J., Grealy, M., Duffy, A. H. B., et al. (2018). Primitive shape imagery classification from electroencephalography. *7th Int. BCI Meet.*, 2–3. Available at: https://strathprints.strath.ac.uk/id/eprint/66654.

Kothe, C. A., Makeig, S., and Onton, J. A. (2013). Emotion Recognition from EEG during Self-Paced Emotional Imagery. in *2013 Humaine Association Conference on Affective Computing and Intelligent Interaction* (IEEE), 855–858. doi:10.1109/ACII.2013.160.

Koutroumanidis, M., Martin-Miguel, C., Hennessy, M. J., Akanuma, N., Valentin, A., Alarcón, G., et al. (2004). Interictal temporal delta activity in temporal lobe epilepsy: Correlations with pathology and outcome. *Epilepsia* 45, 1351–1367. doi:10.1111/j.0013-9580.2004.61203.x.

Kroupi, E., Yazdani, A., and Ebrahimi, T. (2011). "EEG Correlates of Different Emotional States Elicited during Watching Music Videos," in *Affective Computing and Intelligent Interaction*, 457–466. doi:10.1007/978-3-642-24571-8_58.

Krusienski, D. J., Sellers, E. W., McFarland, D. J., Vaughan, T. M., and Wolpaw, J. R. (2008). Toward enhanced P300 speller performance. *J. Neurosci. Methods* 167, 15–21. doi:10.1016/j.jneumeth.2007.07.017.

Lang, P. J., Bradley, M. M., and Cuthbert, B. N. (2008). International affective picture system (IAPS): Affective ratings of pictures and instruction manual. *Tech. Rep. A-8, Univ. Florida*.

Li, X., Song, D., Zhang, P., Zhang, Y., Hou, Y., and Hu, B. (2018). Exploring EEG features in cross-subject emotion recognition. *Front. Neurosci.* 12. doi:10.3389/fnins.2018.00162.

Liang, L., and Shastri, D. J. (2018). Meditation: A Performance Booster for BCI Applications. in *Extended Abstracts of the 2018 CHI Conference on Human Factors in Computing Systems - CHI '18* (New York, New York, USA: ACM Press), 1–5. doi:10.1145/3170427.3174354.

Lin, K., Cinetto, A., Wang, Y., Chen, X., Gao, S., and Gao, X. (2016). An online hybrid BCI system based on SSVEP and EMG. *J. Neural Eng.* 13. doi:10.1088/1741-2560/13/2/026020.

Lin, Y.-P., Duann, J.-R., Chen, J.-H., and Jung, T.-P. (2010a). Electroencephalographic dynamics of musical emotion perception revealed by independent spectral components. *Neuroreport* 21, 410–415. doi:10.1097/WNR.0b013e32833774de.

Lin, Y. P., Wang, C. H., Jung, T. P., Wu, T. L., Jeng, S. K., Duann, J. R., et al. (2010b). EEG-based emotion recognition in music listening. *IEEE Trans. Biomed. Eng.* 57, 1798–1806. doi:10.1109/TBME.2010.2048568.

Liu, Y. J., Yu, M., Zhao, G., Song, J., Ge, Y., and Shi, Y. (2018a). Real-time movie-induced discrete emotion recognition from EEG signals. *IEEE Trans. Affect. Comput.* 9, 550–562. doi:10.1109/TAFFC.2017.2660485.

Liu, Y., Wei, Q., and Lu, Z. (2018b). A multi-target brain-computer interface based on code modulated visual evoked potentials. *PLoS One* 13, 1–17. doi:10.1371/journal.pone.0202478.

Lotte, F., Bougrain, L., Cichocki, A., Clerc, M., Congedo, M., Rakotomamonjy, A., et al. (2018). A review of classification algorithms for EEG-based brain-computer interfaces: A 10 year update. *J. Neural Eng.* 15. doi:10.1088/1741-2552/aab2f2.

Lotte, F., Congedo, M., Lécuyer, A., Lamarche, F., Arnaldi, B., Anatole, L., et al. (2007). A review of classification algorithms for EEG-based brain–computer interfaces. *J. Neural Eng.* 4, R1–R13. doi:10.1088/1741-2560/4/2/R01.

Lotte, F., and Cuntai, G. (2011). Regularizing Common Spatial Patterns to Improve BCI Designs: Unified Theory and New Algorithms. *IEEE Trans. Biomed. Eng.* 58, 355–362. doi:10.1109/TBME.2010.2082539.

Luck, S. J. (2005). "Event-Related Potentials," in *APA Handbook of Research Methods in Psychology*,

1–50. doi:10.1037/13619-028.

Makeig, S. (1993). Auditory event-related dynamics of the EEG spectrum and effects of exposure to tones. *Electroencephalogr. Clin. Neurophysiol.* 86, 283–293. doi:10.1016/0013-4694(93)90110-H.

Makeig, S., Leslie, G., Mullen, T., Sarma, D., Bigdely-Shamlo, N., and Kothe, C. (2011). First Demonstration of a Musical Emotion BCI. in *Affective Computing and Intelligent Interaction*, 487–496. doi:10.1007/978-3-642-24571-8_61.

Maris, E., and Oostenveld, R. (2007). Nonparametric statistical testing of EEG- and MEG-data. *J. Neurosci. Methods* 164, 177–190. doi:10.1016/j.jneumeth.2007.03.024.

Marshall, D., Beveridge, R., Wilson, S., and Coyle, D. (2015a). Interacting with multiple game genres using Motion Onset Visual Evoked Potentials. in *2015 Computer Games: AI, Animation, Mobile, Multimedia, Educational and Serious Games (CGAMES)* (IEEE), 18–27. doi:10.1109/CGames.2015.7272957.

Marshall, D., Coyle, D., Wilson, Shane, and Callaghan, M. (2013). Games, gameplay, and BCI: The state of the art. *IEEE Trans. Comput. Intell. AI Games* 5, 82–99. doi:10.1109/TCIAIG.2013.2263555.

Marshall, D., Wilson, S., and Coyle, D. (2015b). Motion-Onset Visual Evoked Potentials for Gaming. in *8th Annual International Conference on Computer Games, Multimedia and Allied Technology (CGAT 2015)* (Global Science & Technology Forum (GSTF)), 155–164. doi:10.5176/2251-1679_CGAT15.41.

Mauss, I. B., and Robinson, M. D. (2009). Measures of emotion: A review. *Cogn. Emot.* 23, 209–237. doi:10.1080/02699930802204677.

Mert, A., and Akan, A. (2018). Emotion recognition from EEG signals by using multivariate empirical mode decomposition. *Pattern Anal. Appl.* 21, 81–89. doi:10.1007/s10044-016-0567-6.

Mognon, A., Jovicich, J., Bruzzone, L., and Buiatti, M. (2011). ADJUST: An automatic EEG artifact detector based on the joint use of spatial and temporal features. *Psychophysiology* 48, 229–240. doi:10.1111/j.1469-8986.2010.01061.x.

Morozov, V. A. (1966). Regularization of incorrectly posed problems and the choice of regularization parameter. *USSR Comput. Math. Math. Phys.* 6, 242–251. doi:10.1016/0041-5553(66)90046-2.

Müller-putz, G. R., Scherer, R., Brunner, C., Leeb, R., and Pfurtscheller, G. (2008). Better than

random ? A closer look on BCI results. *Int. Jouranl Bioelectromagn.* 10, 52–55.

Murugappan, M., Juhari, M. R. B. M., Nagarajan, R., and Yaacob, S. (2009a). An investigation on visual and audiovisual stimulus based emotion recognition using EEG. *Int. J. Med. Eng. Inform.* 1, 342. doi:10.1504/ijmei.2009.022645.

Murugappan, M., Nagarajan, R., and Yaacob, S. (2009b). Comparison of different wavelet features from EEG signals for classifying human emotions. in *2009 IEEE Symposium on Industrial Electronics and Applications, ISIEA 2009 - Proceedings*, 836–841.

Murugappan, M., Nagarajan, R., and Yaacob, S. (2011). Combining spatial filtering and wavelet transform for classifying human emotions using EEG Signals. *J. Med. Biol. Eng.* 31, 45–51. doi:10.5405/jmbe.710.

Murugappan, M., Ramachandran, N., and Sazali, Y. (2010). Classification of human emotion from EEG using discrete wavelet transform. *J. Biomed. Sci. Eng.* 03, 390–396. doi:10.4236/jbise.2010.34054.

Myrden, A., and Chau, T. (2015). Effects of user mental state on EEG-BCI performance. *Front. Hum. Neurosci.* 9, 308. doi:10.3389/fnhum.2015.00308.

Näätänen, R., Pakarinen, S., Rinne, T., and Takegata, R. (2004). The mismatch negativity (MMN): Towards the optimal paradigm. *Clin. Neurophysiol.* 115, 140–144. doi:10.1016/j.clinph.2003.04.001.

Nagel, S., and Spüler, M. (2019). Asynchronous non-invasive high-speed BCI speller with robust non-control state detection. *Sci. Rep.* 9, 1–9. doi:10.1038/s41598-019-44645-x.

Nakisa, B., Rastgoo, M. N., Tjondronegoro, D., and Chandran, V. (2018). Evolutionary computation algorithms for feature selection of EEG-based emotion recognition using mobile sensors. *Expert Syst. Appl.* 93, 143–155. doi:10.1016/j.eswa.2017.09.062.

Nguyen, T. H., Yang, D. L., and Chung, W. Y. (2018). A high-rate BCI speller based on eye-closed EEG Signal. *IEEE Access* 6, 33995–34003. doi:10.1109/ACCESS.2018.2849358.

Nicolas-Alonso, L. F., and Gomez-Gil, J. (2012). Brain computer interfaces, a review. *Sensors* 12, 1211–1279. doi:10.3390/s120201211.

Numminen-Kontti, T. (2014). Personality affects musical emotion processing: an fMRI study.

Ojala, M., and Garriga, G. C. (2010). Permutation Tests for Studying Classifier Performance. *J. Mach. Learn. Res.* 11, 1833–1863.

Olofsson, J. K., Nordin, S., Sequeira, H., and Polich, J. (2008). Affective picture processing: An integrative review of ERP findings. *Biol. Psychol.* 77, 247–265. doi:10.1016/j.biopsycho.2007.11.006.

Paek, A. Y., Agashe, H. A., and Contreras-Vidal, J. L. (2014). Decoding repetitive finger movements with brain activity acquired via non-invasive electroencephalography. *Front. Neuroeng.* 7, 1–18. doi:10.3389/fneng.2014.00003.

Pakarinen, S., Takegata, R., Rinne, T., Huotilainen, M., and Näätänen, R. (2007). Measurement of extensive auditory discrimination profiles using the mismatch negativity (MMN) of the auditory event-related potential (ERP). *Clin. Neurophysiol.* 118, 177–185. doi:10.1016/j.clinph.2006.09.001.

Palaniappan, R. (2010). *Biological Signal Analysis*. 3rd ed. Ramaswamy Palaniappan & Ventus Publishing ApS Available at: http://www.fulviofrisone.com/attachments/article/415/introduction-to-biological-signal-analysis.pdf.

Palmer, C. A., and Alfano, C. A. (2017). Sleep and emotion regulation: An organizing, integrative review. *Sleep Med. Rev.* 31, 6–16. doi:10.1016/j.smrv.2015.12.006.

Parvizi, J., and Kastner, S. (2018). Human Intracranial EEG: Promises and Limitations. *Nat. Neurosci.* 21, 474–483. doi:10.1038/s41593-018-0108-2.

Peker, M., Arslan, A., Sen, B., Celebi, F. V, and But, A. (2015). A novel hybrid method for determining the depth of anesthesia level: Combining ReliefF feature selection and random forest algorithm (ReliefF+RF). in *Innovations in Intelligent SysTems and Applications (INISTA), 2015 International Symposium on*, 1–8.

Peng, H. C., Long, F. H., and Ding, C. (2005). Feature selection based on mutual information: Criteria of max-dependency, max-relevance, and min-redundancy. *IEEE Trans. Pattern Anal. Mach. Intell.* 27, 1226–1238. doi:10.1109/TPAMI.2005.159.

Petrantonakis, P. C., and Hadjileontiadis, L. J. (2010). Emotion recognition from EEG using higher order crossings. *IEEE Trans. Inf. Technol. Biomed.* 14, 186–197. doi:10.1109/TITB.2009.2034649.

Petrantonakis, P. C., and Hadjileontiadis, L. J. (2012). Adaptive emotional information retrieval from EEG signals in the time-frequency domain. *IEEE Trans. Signal Process.* 60, 2604–2616.

doi:10.1109/TSP.2012.2187647.

Pfurtscheller, G. (1992). Event-related synchronization (ERS): an electrophysiological correlate of cortical areas at rest. *Electroencephalogr. Clin. Neurophysiol.* 83, 62–69. doi:10.1016/0013-4694(92)90133-3.

Pfurtscheller, G., and Aranibar, A. (1977). Event-related cortical desynchronization detected by power measurements of scalp EEG. *Electroencephalogr. Clin. Neurophysiol.* 42, 817–826. doi:10.1016/0013-4694(77)90235-8.

Pfurtscheller, G., C. Neuper, Schlögl, A., Lugger, K., Neuper, C., Schlogl, A., et al. (1998). Separability of EEG signals recorded during right and left motor imagery using adaptive autorregresive parameters. *IEEE Trans. Rehabil. Eng.* 6, 316–324. doi:10.1109/86.712230.

Pfurtscheller, G., and Lopes Da Silva, F. H. H. (1999). Event-related EEG/MEG synchronization and desynchronization: basic principles. *Clin. Neurophysiol.* 110, 1842–1857. doi:10.1016/S1388-2457(99)00141-8.

Pfurtscheller, G., and Neuper, C. (1997). Motor imagery activates primary sensorimotor area in humans. *Neurosci. Lett.* 239, 65–68. doi:10.1016/S0304-3940(97)00889-6.

Pfurtscheller, G., Neuper, C., Guger, C., Harkam, W., Ramoser, H., Schlögl, A., et al. (2000). Current trends in Graz Brain-Computer Interface (BCI) research. *IEEE Trans. Rehabil. Eng.* 8, 216–219. doi:10.1109/86.847821.

Phillips, M. L., Drevets, W. C., Rauch, S. L., and Lane, R. (2003). Neurobiology of emotion perception I: The neural basis of normal emotion perception. *Biol. Psychiatry* 54, 504–514. doi:10.1016/S0006-3223(03)00168-9.

Posner, J., Russell, J. a, and Peterson, B. S. (2005). The circumplex model of affect: an integrative approach to affective neuroscience, cognitive development, and psychopathology. *Dev. Psychopathol.* 17, 715–734. doi:10.1017/S0954579405050340.

Power, S. D., Kushki, A., and Chau, T. (2011). Towards a system-paced near-infrared spectroscopy brain–computer interface: differentiating prefrontal activity due to mental arithmetic and mental singing from the no-control state. *J. Neural Eng.* 8, 066004. doi:10.1088/1741-2560/8/6/066004.

Prasad, G., Herman, P., Coyle, D., McDonough, S., and Crosbie, J. (2010). Applying a brain-computer interface to support motor imagery practice in people with stroke for upper limb recovery: a feasibility study. *J. Neuroeng. Rehabil.* 7, 60. doi:10.1186/1743-0003-7-60.

Proudfoot, M., Woolrich, M. W., Nobre, a. C., and Turner, M. R. (2014). Magnetoencephalography. *Pract. Neurol.* 14, 336–343. doi:10.1136/practneurol-2013-000768.

Rathee, D., Chowdhury, A., Meena, Y. K., Dutta, A., McDonough, S., and Prasad, G. (2019). Brain-Machine Interface-Driven Post-Stroke Upper-Limb Functional Recovery Correlates with Beta-Band Mediated Cortical Networks. *IEEE Trans. Neural Syst. Rehabil. Eng.* 27, 1020–1031. doi:10.1109/TNSRE.2019.2908125.

Reid, S. M., Meehan, E., McIntyre, S., Goldsmith, S., Badawi, N., and Reddihough, D. S. (2016). Temporal trends in cerebral palsy by impairment severity and birth gestation. *Dev. Med. Child Neurol.* 58, 25–35. doi:10.1111/dmcn.13001.

Reznik, S. J., and Allen, J. J. B. (2018). Frontal asymmetry as a mediator and moderator of emotion: An updated review. *Psychophysiology* 55. doi:10.1111/psyp.12965.

Robinson, R. G., Starr, L. B., Lipsey, J. R., Rao, K., and Price, T. R. (1984). A two-year longitudinal study of post-stroke mood disorders: dynamic changes in associated variables over the first six months of follow-up. *Stroke.* 15, 510–517. doi:10.1161/01.STR.15.3.510.

Russell, J. A. (1980). A circumplex model of affect. *J. Pers. Soc. Psychol.* 39, 1161–1178. doi:10.1037/h0077714.

Salmelin, R., Hámáaláinen, M., Kajola, M., and Hari, R. (1995). Functional Segregation of Movement-Related Rhythmic Activity in the Human Brain. *Neuroimage* 2, 237–243. doi:10.1006/nimg.1995.1031.

Sanei, S., and Chambers, J. A. (2007). *EEG Signal Processing*. John Wiley & Sons, Ltd doi:10.1002/9780470511923.

Scherer, K. R. (2005). What are emotions? And how can they be measured? *Soc. Sci. Inf.* 44, 695–729. doi:10.1177/0539018405058216.

Schlögl, A., Neuper, C., and Pfurtscheller, G. (2002). Estimating the Mutual Information of an EEG-based Brain-Computer Interface. *Biomed. Tech. Eng.* 47, 3–8. doi:10.1515/bmte.2002.47.1-2.3.

Shu, L., Xie, J., Yang, M., Li, Z., Li, Z., Liao, D., et al. (2018). A Review of Emotion Recognition Using Physiological Signals. *Sensors* 18, 2074. doi:10.3390/s18072074.

Sitaram, R., Lee, S., Ruiz, S., Rana, M., Veit, R., and Birbaumer, N. (2011). Real-time support vector classification and feedback of multiple emotional brain states. *Neuroimage* 56, 753–765. doi:10.1016/j.neuroimage.2010.08.007.

Smith, A. P. R., Stephan, K. E., Rugg, M. D., and Dolan, R. J. (2006). Task and content modulate amygdala-hippocampal connectivity in emotional retrieval. *Neuron* 49, 631–638. doi:10.1016/j.neuron.2005.12.025.

Soleymani, M., Pantic, M., and Pun, T. (2012). Multimodal emotion recognition in response to videos. *IEEE Trans. Affect. Comput.* 3, 211–223. doi:10.1109/T-AFFC.2011.37.

Sourina, O., Liu, Y., and Nguyen, M. K. (2012). Real-time EEG-based emotion recognition for music therapy. *J. Multimodal User Interfaces* 5, 27–35. doi:10.1007/s12193-011-0080-6.

Speier, W., Chandravadia, N., Roberts, D., Pendekanti, S., and Pouratian, N. (2017). Online BCI typing using language model classifiers by ALS patients in their homes. *Brain-Computer Interfaces* 4, 114–121. doi:10.1080/2326263X.2016.1252143.

Speller, I. B. C. I. (2015). A Dynamically Optimized SSVEP Brain – Computer. *IEEE Trans. Biomed. Eng.* 62, 1447–1456. doi:10.1109/TBME.2014.2320948.

Stangl, M., Bauernfeind, G., Kurzmann, J., Scherer, R., and Neuper, C. (2013). A haemodynamic brain-computer interface based on real-time classification of near infrared spectroscopy signals during motor imagery and mental arithmetic. *J. Near Infrared Spectrosc.* 21, 157–171. doi:10.1255/jnirs.1048.

Stawicki, P., Gembler, F., and Volosyak, I. (2016). Driving a Semiautonomous Mobile Robotic Car Controlled by an SSVEP-Based BCI. *Comput. Intell. Neurosci.* 2016. doi:10.1155/2016/4909685.

Sutter, E. E. (1992). The brain response interface: communication through visually-induced electrical brain responses. *J. Microcomput. Appl.* 15, 31–45. doi:10.1016/0745-7138(92)90045-7.

Takahashi, K. (2004). Remarks on emotion recognition from multi-modal bio-potential signals. *2004 IEEE Int. Conf. Ind. Technol. 2004. IEEE ICIT '04.* 3, 95–100. doi:10.1109/ICIT.2004.1490720.

Tan, L.-F., Dienes, Z., Jansari, A., and Goh, S.-Y. (2014a). Effect of mindfulness meditation on brain–computer interface performance. *Conscious. Cogn.* 23, 12–21. doi:10.1016/j.concog.2013.10.010.

Tan, L.-F., Dienes, Z., Jansari, A., and Goh, S.-Y. (2019). Effect of mindfulness meditation on brain–computer interface performance: fMRI perspective. *Neurol. Asia* 24, 343–353. Available at: https://linkinghub.elsevier.com/retrieve/pii/S1053810013001499.

Tan, L. F., Dienes, Z., Jansari, A., and Goh, S. Y. (2014b). Effect of mindfulness meditation on brain-computer interface performance. *Conscious. Cogn.* 23, 12–21.

doi:10.1016/j.concog.2013.10.010.

Tang, J., Liu, Y., Hu, D., and Zhou, Z. T. (2018). Towards BCI-actuated smart wheelchair system. *Biomed. Eng. Online* 17, 1–22. doi:10.1186/s12938-018-0545-x.

Tang, Z., Li, C., and Sun, S. (2017). Single-trial EEG classification of motor imagery using deep convolutional neural networks. *Optik (Stuttg).* 130, 11–18. doi:10.1016/j.ijleo.2016.10.117.

Tariq, M., Trivailo, P. M., and Simic, M. (2018). EEG-Based BCI Control Schemes for Lower-Limb Assistive-Robots. *Front. Hum. Neurosci.* 12. doi:10.3389/fnhum.2018.00312.

Valenzi, S., Islam, T., Jurica, P., and Cichocki, A. (2014). Individual Classification of Emotions Using EEG. *J. Biomed. Sci.*, 604–620. Available at: http://file.scirp.org/Html/16-9101984_47360.htm.

van Boxtel, A. (2001). Optimal signal bandwidth for the recording of surface EMG activity of facial, jaw, oral, and neck muscles. *Psychophysiology* 38, S004857720199016X. doi:10.1017/S004857720199016X.

Vidaurre, C., and Blankertz, B. (2010). Towards a cure for BCI illiteracy. *Brain Topogr.* 23, 194–198. doi:10.1007/s10548-009-0121-6.

Vidaurre, C., Klauer, C., Schauer, T., Ramos-Murguialday, A., and Müller, K. R. (2016). EEG-based BCI for the linear control of an upper-limb neuroprosthesis. *Med. Eng. Phys.* 38, 1195–1204. doi:10.1016/j.medengphy.2016.06.010.

Vidaurre, C., Sannelli, C., Müller, K.-R., and Blankertz, B. (2011). Co-adaptive calibration to improve BCI efficiency. *J. Neural Eng.* 8, 025009. doi:10.1088/1741-2560/8/2/025009.

Wang, F., He, Y., Qu, J., Xie, Q., Lin, Q., Ni, X., et al. (2017). Enhancing clinical communication assessments using an audiovisual BCI for patients with disorders of consciousness. *J. Neural Eng.* 14. doi:10.1088/1741-2552/aa6c31.

Wang, X.-W., Nie, D., and Lu, B.-L. (2011). "EEG-Based Emotion Recognition Using Frequency Domain Features and Support Vector Machines," in *Science*, 734–743. doi:10.1007/978-3-642-24955-6_87.

Whitham, Emma M. Pope, Kenneth J. Fitzgibbon, Sean P. Lewis, Trent Clark, C. Richard Loveless, Stephen Broberg, Marita Wallace, Angus DeLosAngeles, Dylan Lillie, Peter Hardy, Andrew Fronsko, Rik Pulbrook, Alyson Willoughby, J. O. (2007). Scalp electrical recording during paralysis: Quantitative evidence that EEG frequencies above 20 Hz are contaminated by EMG. *Clin. Neurophysiol.* 118, 1877–1888. doi:10.1016/j.clinph.2007.04.027.

Wolpaw, J. R., Birbaumer, N., Heetderks, W. J., McFarland, D. J., Peckham, P. H., Schalk, G., et al. (2000). Brain-computer interface technology: a review of the first international meeting. *IEEE Trans. Rehabil. Eng.* 8, 164–173. doi:10.1109/TRE.2000.847807.

Wolpaw, J. R., Birbaumer, N., McFarland, D. J., Pfurtscheller, G., and Vaughan, T. M. (2002). Brain Computer Interfaces for communication and control. *Front. Neurosci.* 4, 767–791. doi:10.3389/conf.fnins.2010.05.00007.

Wolpaw, J. R., Ramoser, H., McFarland, D. J., and Pfurtscheller, G. (1998). EEG-based communication: Improved accuracy by response verification. *IEEE Trans. Rehabil. Eng.* 6, 326–333. doi:10.1109/86.712231.

Wolpaw, J. R., and Winter Wolpaw, E. (2012). "Brain–Computer Interfaces: Something New under the Sun," in *Brain–Computer InterfacesPrinciples and Practice* (Oxford University Press), 3–12. doi:10.1093/acprof:oso/9780195388855.003.0001.

Yger, F., Berar, M., and Lotte, F. (2017). Riemannian Approaches in Brain-Computer Interfaces: A Review. *IEEE Trans. Neural Syst. Rehabil. Eng.* 25, 1753–1762. doi:10.1109/TNSRE.2016.2627016.

Yohanes, R. E. J., Wee Ser, and Guang-bin Huang (2012). Discrete Wavelet Transform coefficients for emotion recognition from EEG signals. in *2012 Annual International Conference of the IEEE Engineering in Medicine and Biology Society* (IEEE), 2251–2254. doi:10.1109/EMBC.2012.6346410.

Zheng, W., Guo, H., and Lu, B.-L. (2015). Revealing critical channels and frequency bands for emotion recognition from EEG with deep belief network. in *2015 7th International IEEE/EMBS Conference on Neural Engineering (NER)* (IEEE), 154–157. doi:10.1109/NER.2015.7146583.

Zheng, W. L., and Lu, B. L. (2015). Investigating Critical Frequency Bands and Channels for EEG-Based Emotion Recognition with Deep Neural Networks. *IEEE Trans. Auton. Ment. Dev.* 7, 162–175. doi:10.1109/TAMD.2015.2431497.

Zhou, F., Qu, X., Jiao, J., and Helander, M. G. (2014). Emotion prediction from physiological signals: A comparison study between visual and auditory elicitors. *Interact. Comput.* 26, 285–302. doi:10.1093/iwc/iwt039.

Zhu, D., Bieger, J., Garcia Molina, G., and Aarts, R. M. (2010). A survey of stimulation methods used in SSVEP-based BCIs. *Comput. Intell. Neurosci.* 2010. doi:10.1155/2010/702357.

Zumsteg, D., and Wieser, H. G. (2000). Presurgical Evaluation: Current Role of Invasive EEG. *Epilepsia* 41, S55–S60. doi:10.1111/j.1528-1157.2000.tb01535.x.

APPENDIX A: PUBLISHED PAPERS

Conference papers

Dayan N, Bigirimana A, McCann A, Stow J, McElligott J, and Carroll A. (2019). Towards Answering Questions in Disorders of Consciousness and Locked-In Syndrome with a SMR-BCI. In: *8th Graz Brain-Computer Interface Conference (GBCIC)* (Graz, Austria: Verlag der TU Graz, Graz University of Technology), doi:10.3217/978-3-85125-682-6-65.

Bigirimana, A. D., Siddique, N., and Coyle, D. (2018). Emotion-inducing imagery versus motor imagery based BCI: participants' performance, perceived control and imagery preference. In: *Proceedings of the 7th International Brain-Computer Interface Meeting* (California, USA , May 21-15, 2018).

Bigirimana, A. D., Siddique, N., and Coyle, D. (2017). Brain-Computer Interfacing with Emotion-Inducing Imagery: A Pilot Study. In: *7th Graz Brain-Computer Interface Conference (GBCIC)* (Graz, Austria: Verlag der TU Graz, Graz University of Technology), 26–31. doi:10.3217/978-3-85125-533-1-06.

Bigirimana, A. D., Siddique, N., and Coyle, D. (2016a). A hybrid ICA-wavelet transform for automated artefact removal in EEG-based emotion recognition. In: *2016 IEEE International Conference on Systems, Man, and Cybernetics (SMC)* (Budapest, Hungary: IEEE), 004429–004434. doi:10.1109/SMC.2016.7844928.

Bigirimana, A. D., Siddique, N., and Coyle, D. (2016b). Emotion Imagery BCI. In: *Proceedings of the 6th International Brain-Computer Interface Meeting* (California, USA: Verlag der TU Graz), 125–125. doi:10.3217/978-3-85125-467-9-125.

Journal Papers

Bigirimana, A.D., Siddique, N. & Coyle, D. (2020). Emotion-inducing imagery versus motor imagery for a brain-computer interface. In: *IEEE Transactions on Neural Systems and Rehabilitation Engineering. 28, 4, p. 850-859 10 p., 9026750.*

Papers in Preparation

Bigirimana, A.D., Siddique, N. & Coyle, D. (2020). Detecting changes in affective states self-induced by emotion related imagery using MEG/EEG. (To be submitted in: *IEEE Transactions on*

Affective Computing)